DISS. ETH NO. 16932

EVIDENCE FOR A MAJOR PALEOCEANOGRAPHIC REORGANIZATION DURING THE LATE JURASSIC; INSIGHTS FROM SEDIMENTOLOGY AND GEOCHEMISTRY.

A dissertation submitted to

ETH ZURICH

for the degree of

Doctor of Natural Sciences

presented by

PAULINE SOPHIE CLAUDINE RAIS

Dipl. Sciences de la Terre BENEFRI, Université de Neuchâtel

born 25.03.1977

citizen of Delémont, Jura

accepted on the recommendation of

Prof. Dr. Helmut Weissert, ETH Zurich, examiner
PD Dr. Stefano M. Bernasconi, ETH Zurich, co-examiner
Prof. Dr. Judith A. McKenzie, ETH Zurich, co-examiner
Dr. Peter Stille, Université Louis Pasteur, Strasbourg, co-examiner

2007

Table of contents

Abstract

The Late Jurassic (160-145 Ma) was a time of major change in terms of climate and oceanography, reflected by a distinct transition from carbonate-poor to carbonate-rich sediments and by important geochemical variations. These changes are observed primarily within Oxfordian sediment successions. To better constrain the origin and timing of this turning point in the Late Jurassic, Oxfordian deposits were investigated through a combination of sedimentologic analyses and isotope geochemistry. The Alpine Tethys, a sensible seaway situated close to the opening Hispanic Corridor, was chosen for investigation. A composite carbon isotope curve, compiled from Tethyan sections, was established for the Late Jurassic and used as a correlation tool between the sections. Carbon-isotope and ammonite stratigraphy precisely locate the transition from carbonate-poor to carbonate-rich sediments in the upper part of the Plicatilis ammonite zone (Middle Oxfordian). The Early Oxfordian was characterized by the deposition of carbonate-poor ooze and radiolarian ooze in deep basins, and by a strongly condensed sedimentation in shallower environments. Carbonate accumulation rates increased during the Middle Oxfordian and developed progressively to a carbonate-dominated sedimentation at the end of the Jurassic.

Detailed sedimentologic analyses reveal that the Callovian and Early Oxfordian hardgrounds of the Northern Tethyan shelf formed under intense current activity. Additionally, strongly condensed sedimentation on the Trento Plateau supports vigorous ocean circulation during that time. The reorganization of oceanic current patterns, during the Middle Oxfordian, resulted in an apparent decrease in current strength on both margins. To document this change in ocean circulation, neodymium isotopes were measured on belemnites and shark teeth. The results obtained are insufficient for a reconstruction of paleocurrents, but they are promising for further work.

Oxygen isotope measurements, performed on belemnites of the northern Tethyan shelf, record a small temperature increase of 2°C during the Oxfordian, which contrasts with the temperature increase of at least 7°C at higher latitudes, documented in previous works. These results are in agreement with climate models for the Late Jurassic, which report the onset of new climatic conditions characterized by low latitudinal thermal gradients.

Important changes in strontium isotopes occurred during the Oxfordian. Data obtained from well-dated belemnites reveal a turning point in $^{87}Sr/^{86}Sr$ during the Plicatilis ammonite zone. The lowest values ($^{87}Sr/^{86}Sr$ =0.70682) correspond to the minimum Mesozoic values and indicate a period of increased hydrothermal activity associated with the fragmentation of Pangea.

Our data show that a major reorganization of oceanographic and climatic conditions occurred during the Middle Oxfordian. Based on our results and existing work on climate modeling and fauna migrations, we conclude that this reorganization was linked to the opening of the Hispanic Corridor between Gondwana and Eurasia. During the Middle Oxfordian, this seaway was both wide and deep enough to allow significant water mass exchanges at low latitudes. This new configuration modified the global ocean circulation and the latitudinal heat exchange. The oceanographic and climatic conditions became favorable for the development of calcareous producers, which proliferated in shallow and pelagic environments following the Middle Oxfordian reorganization.

In addition to this study, we report the discovery of a new occurrence of authigenic albites in Oxfordian sediments from the Helvetic Domain of eastern Switzerland. The euhedral shape and chemical purity of these albites are evidence for their authigenic origin. The crystals are irregularly distributed in the sediment, highlighting the importance of host rock composition for albite authigenesis. We conclude that these albites formed under deep burial diagenesis conditions, in association with other diagenetic processes.

Résumé

Le Jurassique supérieur (160-145 Ma) fut une période marquée par des changements climatiques et océanographiques majeurs, se reflétant principalement dans la séquence sédimentaire de l'Oxfordien. Ces changements se traduisent par un net enrichissement de la teneur en carbonate dans les sédiments ainsi que par des variations géochimiques importantes. Afin de mieux caractériser l'origine et l'évolution temporelle des évènements du Jurassique supérieur, une étude sédimentologique accompagnée d'analyses isotopiques, radiogéniques et stables, a été conduite sur des dépôts d'âge Oxfordien. La Téthys alpine, une voie maritime étroite située à proximité du corridor hispanique a été choisie comme zone d'étude. Durant l'Oxfordien inférieur, des boues argileuses pauvres en carbonate et des boues siliceuses se déposent dans les bassins profonds, alors que la sédimentation des environnements peu profonds est fortement condensée. Le taux d'accumulation des carbonates augmente lors de l'Oxfordien pour atteindre une sédimentation principalement carbonatée à la fin du Jurassique. Une courbe des compositions isotopiques du carbone, compilée à partir de sections téthysiennes, a été établie pour le Jurassique supérieur et a été utilisée comme outil de corrélation entre les différentes sections. La stratigraphie basée sur les isotopes du carbone associée à la biostratigraphie ont permis de placer la principale transition sédimentaire dans la partie supérieure de la Zone d'ammonite à Plicatilis (Oxfordien moyen).

Des analyses sédimentologiques détaillées indiquent que les hardgrounds du Callovien et de l'Oxfordien inférieur, de la plateforme nord-téthysienne se sont formés sous l'actions de courants océaniques intenses. De plus, la sédimentation fortement condensée sur le Plateau de Trento (marge sud de la Téthys Alpine) confirme la présence d'une circulation océanique vigoureuse durant cette période. Durant l'Oxfordien moyen, une diminution de l'intensité des courants océaniques est observée sur les deux marges de la Téthys Alpine. Afin de documenter ces variations de courants océaniques, des analyses isotopiques du néodyme ont été effectuées sur des bélemnites et des dents de requin. Les résultats préliminaires ne sont, pour le moment, pas suffisants pour une reconstruction de la circulation des paléo-courants, mais sont prometteurs pour de futures recherches.

Les isotopes de l'oxygène mesurés sur des bélemnites de la marge nord-téthysienne montrent une augmentation de la température de seulement 2°C pendant l'Oxfordien, alors que pour des latitudes plus élevées, une augmentation d'au moins 7°C a été documentée dans de récents travaux.

Des rapports isotopiques du strontium mesurés sur des bélemnites d'âges connus révèlent une modification majeure affectant la composition isotopique de l'eau de mer durant l'Oxfordien. En effet, l'Oxfordien moyen (zone à Plicatilis) est caractérisé par les plus faibles rapports

isotopiques du strontium du Mésozoïque ($^{87}Sr/^{86}Sr$ =0.70682), reflétant une augmentation de l'activité hydrothermale associée à la fragmentation de la Pangée.
Nos résultats démontrent que l'Oxfordien moyen témoigne d'une réorganisation majeure des conditions océanographiques et climatiques. Grâce à ces résultats, combinés à de récent travaux de modélisations climatiques et de migrations des faunes, nous démontrons que cette réorganisation est liée à l'ouverture du corridor hispanique entre le Gondwana et l'Eurasie. Lors de l'Oxfordien moyen, cette voie maritime était suffisamment large et profonde pour permettre le transfert d'importantes masses d'eau à basses latitudes. Cette nouvelle configuration océanique et continentale modifia la circulation océanique globale et les échanges latitudinaux de température. Les conditions océaniques et climatiques résultant de la réorganisation Oxfordienne sont favorables au développement des producteurs de carbonates, qui prolifèrent dans les environnements peu profonds et pélagiques.

Parallèlement à cette étude paléo-océanographique, nous documentons un nouvel affleurement d'albites authigènes dans des sédiments Oxfordiens du domaine Helvétique de l'Est de la Suisse. La forme automorphe et la pureté chimique de ces albites attestent d'une origine authigène. Les cristaux sont répartis de manière irrégulière dans le sédiment, soulignant l'importance de la composition chimique de la roche hôte pour l'authigenèse des cristaux d'albite. En conclusion, nous proposons que ces albites se sont formées sous des conditions de diagenèse d'enfouissement profonde, en association avec d'autres procédés diagénétiques.

Zusammenfassung

Während der älteren Jura-Zeit (160-145 Ma) änderten sich Klima und Ozeanographie signifikant, angezeigt durch einen auffälligen Wechsel von Karbonat-armen zu Karbonat-reichen Sedimenten und durch grosse Schwankungen in geochemischen Parametern. Diese Änderungen geschehen vornehmlich während des Oxfordien. Um diesen Wendepunkt im älteren Jura besser zu charakterisieren, wurden Meeresablagerungen aus dem Oxfordien mittels sedimentologischen und Isotopen-geochemischen Methoden untersucht. Als Untersuchungsgebiet wurde die Alpine Tethys gewählt, ein Ozean in der Nähe des sich öffnenden Hispanic Corridors. Eine Kohlenstoff-Isotopenkurve für den späten Jura wurde aus mehreren Profilen der Tethys zusammen gesetzt und zur Korrelation von schlecht datierten Profilen benutzt. Kohlenstoff-Isotopenstratigraphie kombiniert mit Ammonitenstratigraphie erlaubten es in der Folge, den Übergang von Karbonat-armen zu Karbonat-reichen Sedimenten präzis zu datieren und dem oberen Teil der Plicatilis Ammonitenzone des mittleren Oxfordien zu zu ordnen. Das frühe Oxfordien ist gekennzeichnet durch die Ablagerung von Karbonat-armem und Radiolarien-reichem Schlamm in tiefen Becken, und durch eine stark reduzierte Sedimentation in Becken mit geringerer Meerestiefe. Die Karbonat-Ablagerungsrate nahm anschliessend während des mittleren Oxfordien zu – es entwickelte sich gegen Ende der Jurazeit eine Karbonat-dominierte Sedimentation.

Detaillierte sedimentologische Analysen zeigen, dass die Bildung von marinen Hartgründen im Callovien und frühen Oxfordien durch die Einwirkung intensiver Strömungen zu erklären ist. Auch die stark reduzierte Sedimentation auf dem Trento Plateau deutet auf eine starke ozeanische Zirkulation während dieser Zeit hin. Eine Reorganisation der globalen Strömungsverhältnisse im mittleren Oxfordien bewirkte dann offenbar eine Abnahme der Strömungsstärke sowohl auf dem nördlichen wie auf dem südlichen Kontinentalrand der alpinen Tethys. Um diese Veränderung der Meeresströmungen zu dokumentieren, wurden Neodymium-Isotopen an Belemniten und Haifisch-Zähnen gemessen. Die Resultate sind vielversprechend für weitere Untersuchungen, lassen gegenwärtig aber keine Rekonstruktion der Ozeanströmungen zu.

Sauerstoff-Isotopendaten, gemessen an Belemniten des nördlichen Kontinentalabhangs der Tethys, zeigen einen geringfügigen Temperaturanstieg von 2°C während des Oxfordien an. Dieses Resultat kontrastiert mit den 7°C Temperaturanstieg angezeigt durch frühere Studien, stimmt aber mit Klima-Simulationen des späten Juras überein, welche ein Klimaregime mit einem geringen Temperaturgradienten zwischen Aequator und Polen andeuten.

Während des Oxfordien verändert sich der Strontium-Isotopenwert des Meerwassers stark. Neue Daten aus sehr gut datierten Belemniten zeigen, dass ein Tiefpunkt im $^{87}Sr/^{86}Sr$-Verhältnis

($^{87}Sr/^{86}Sr = 0.70682$) während der Plicatilis Ammonitenzone erreicht wird. Es sind die tiefsten Werte während des ganzen Mesozoikums. Sie deuten an, dass das mittlere Oxfordien durch erhöhte hydrothermale Aktivität gekennzeichnet ist, welche im Zusammenhang mit dem Aufbrechen des Riesenkontinentes Pangäa steht.
Alle diese neuen Daten zeigen, dass eine wichtige Reorganisation der ozeanographischen und klimatischen Bedingungen während des mittleren Oxfordien stattfand. Basierend auf unseren Resultaten und früheren Studien über das Klima und die Faunenverteilung im Oxfordien schliessen wir dass diese Reorganisation im Zusammenhang mit der Öffnung des Hispanic Corridors zwischen Gondwana und Laurasia steht. Dieser Seeweg nahm während des mittleren Oxfordien an Tiefe und Breite zu, so dass grosse Wassermassen hindurch fliessen konnten. Diese neue Konfiguration der Kontinente und Ozeane beeinflusste die globale Ozeanzirkulation und den Energieaustausch zwischen tiefen und hohen Breiten. Die neuen ozeanographischen und klimatischen Bedingungen begünstigten die Entwicklung von karbonatproduzierenden Organismen, welche in Flachmeeren und im offenen Ozean nach der Reorganisation der Ozeane im mittleren Oxfordien aufblühten.

Zusätzlich zu diesen Resultaten beschreiben wir ein bisher unbekanntes Vorkommen von authigenem Albit in Oxfordien-Sedimentabfolgen des östlichen Helvetikums. Die euhedrale Form und die chemische Reinheit dieser Albite bezeugen ihre authigene Herkunft. Die Kristalle sind in den Sedimenten ungleichmässig verteilt, was der Zusammensetzung des Wirtgesteins eine wichtige Rolle bei der Entstehung der Albite zuweist. Gemäss unseren Untersuchungen entstanden die Albite unter den Bedingungen einer tiefen Vergrabungsdiagenese, und unter der Einwirkung weiterer diagenetischer Prozesse.

CHAPTER 1

Introduction

Linking paleoceanography, climate and plate tectonics

The Jurassic was a time of important changes in ocean/continent configuration (Fig 1). Hydrothermal activity associated to the fragmentation of Pangea was accelerated during that time, as mirrored by the decrease of strontium isotope ratio, reaching the lowest values of the Mesozoic during the Oxfordian (Jones et al., 1994; McArthur et al., 2001). The separation of Eurasia and Gondwana triggered the opening of the Hispanic Corridor, a seaway connecting western Tethys and Pacific (Fig. 1). The first oceanic connection through the Hispanic Corridor is dated as Early Jurassic by bivalve and ammonite migration (Riccardi, 1991; Aberhan, 2001). The oceanic circulation was superficial at that time, allowing only intermittent fauna exchange. The gradual widening and deepening of the Hispanic Corridor,

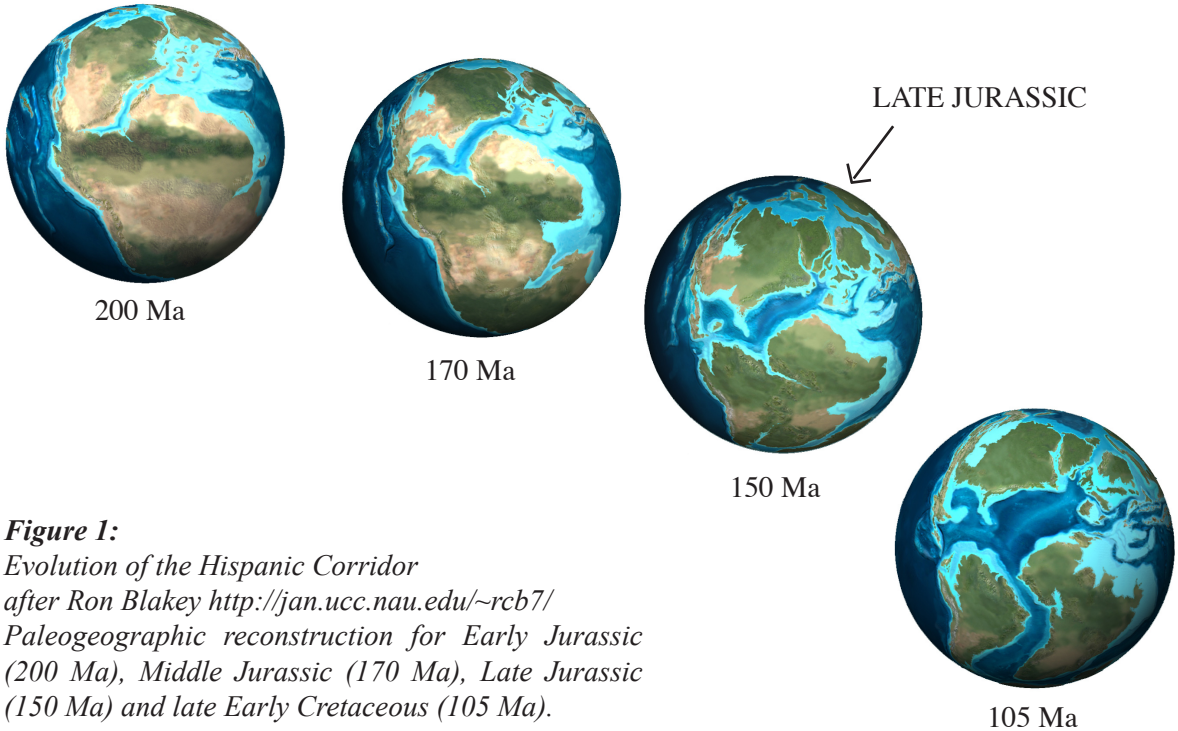

Figure 1:
Evolution of the Hispanic Corridor after Ron Blakey http://jan.ucc.nau.edu/~rcb7/ Paleogeographic reconstruction for Early Jurassic (200 Ma), Middle Jurassic (170 Ma), Late Jurassic (150 Ma) and late Early Cretaceous (105 Ma).

associated with a first order sea-level rise (Haq et al., 1988), allowed significant water mass exchange between western Tethys and Pacific during the Late Jurassic (Winterer, 1991; Hotinski and Toggweiler, 2003). Studies on reef development (Leinfelder et al., 2002) and brachiopod migration (Voros, 1993; Voros, 2005) confirm the establishment of a first true seaway at the beginning of the Late Jurassic. The seaway further enlarged and reached its acme in the Late Cretaceous (Fig. 1). It has been shown that modifications of the oceanic connections between oceanic basins have a strong influence on ocean circulation and global climate (e.g. Smith and Pickering, 2003). Hotinsky & Toggweiler (2003), based on model simulations, showed that the opening of the Hispanic Corridor triggered an improvement of latitudinal heat exchange due to a large-scale change in ocean current pattern. Therefore, the Late Jurassic offers a good opportunity to study the interaction between paleoceanography, climate and plate tectonics.

The Late Jurassic, a time of global change

The study of Late Jurassic sediments provides evidence for an important reorganization of oceanographic and climatic conditions. Most remarkable is the widespread shift from carbonate-poor to carbonate-rich sediments. The beginning of the Late Jurassic was a time of exceptionally low carbonate accumulation rates. Around the Middle-Late Jurassic transition, epiric seas were almost free of carbonate-rich sediments on a global-scale (Dromart et al., 2003a). Pelagic sedimentation was dominated by radiolarian ooze and clayey carbonate-poor ooze, and hardgrounds formed along shallow shelf environments and on submarine highs (Baumgartner, 1987; Dromart et al., 2003a). A drastic change in sediment production occurred during the Middle Oxfordian with the development of new reef sites and the expansion of calcareous nannofossils (Leinfelder et al., 2002; Cecca et al., 2005).
Facies changes coincided with important climatic variations. The cool and humid climate of the early Late Jurassic was replaced within the Oxfordian by an increasingly warmer and drier climate (Hallam, 1985; Dromart et al., 2003a; Dromart et al., 2003b). The Oxfordian warming is well documented in high latitude environments: in oxygen isotope composition of belemnites from the Russian platform (Riboulleau et al., 1998), in sporomorph data from the North Sea (Abbink et al., 2001) and in the migration of Tethyan ammonites to higher latitudes (Enay, 1980). Oxygen isotopes measured on Russian belemnites indicate a temperature increase of 7–15°C (Riboulleau et al., 1998; Dromart et al., 2003a). Interestingly, tropical sea-surface temperature proxy indicate a relatively small temperature increase in the order of 3°C during that time (Lécuyer et al., 2003).

The Late Jurassic global changes are recorded in the carbon-isotope record. The Oxfordian is marked by a distinct positive excursion in $\delta^{13}C_{carb}$ (Jenkyns, 1996; Louis-Schmid, 2006), comparable in terms of amplitude to the prominent positive anomalies of the Valanginian and the Aptian event (Weissert and Erba, 2004). During the main increase in $\delta^{13}C$ in carbonates, $\delta^{13}C$ in organic matter decreases (Louis-Schmid, 2006). Model simulations indicate that an increase in pCO_2 may be the cause of these contrasting trends (see Louis-Schmid, 2006 for extensive discussion).

Main objectives and general outline of the thesis

The purpose of this study is to investigate the origin, the timing and the consequences of the Oxfordian climatic and oceanographic reorganization, and to consider the possible influence of tectonic plate motion on the observed changes. Sedimentary deposits from Switzerland, southeastern France and northern Italy were chosen as archives for the past perturbations, which are studied using sedimentological and geochemical methods. This thesis is closely connected to the study carried out by Beat Louis at the Geological Institute of ETH Zurich, focusing on the Oxfordian carbon cycle. The aims of the present thesis are:

1) To document the Late Jurassic changes in oceanography and climate
2) To investigate the transition from carbonate-poor to carbonate-rich sediments, and to determine how these facies changes were linked to the Oxfordian oceanic and climatic reorganization
3) To test if the distribution patterns of hardgrounds in Oxfordian shelf seas can be used as proxy for shelf current activity
4) Investigating if these changes coincided with a reorganization of ocean current patterns possibly triggered by the opening of the Hispanic Corridor
5) To highlight the role of tectonics in past paleoceanographical changes

Bulk carbonate carbon-isotope stratigraphy provided detailed information on the age of the main transitions.

In chapter 2, sedimentological and geochemical methods are used to reconstruct the Oxfordian sedimentation history of the northern Tethyan Shelf, with a focus on condensed sediments. Jurassic hardgrounds and nodular limestones are compared to recent condensed sediments forming under strong oceanic currents. Carbon-isotope stratigraphy was used in addition to biostratigraphy to date the end of the sediment condensation. A model for Oxfordian paleoceanographic and climatic changes is proposed.

In chapter 3, the Late Jurassic sediment succession of the southern Alpine Tethys is revisited and compared to the sedimentation patterns of the northern Tethyan margin. Five paleoenvironments are investigated: The Lombardian Basin, the Trento Plateau, the Belluno Trough, the Helvetic Shelf and the Subalpine Basin. Two characteristics recorded in the sediment succession of both margins are highlighted: the increase of carbonate accumulation rates during the Late Jurassic and the strong condensation of Callovian and Early Oxfordian sediments on parts of the shallower environments.

Chapter 4 documents the Late Jurassic climatic and oceanographic reorganization by combining sedimentological analyses and isotopic geochemistry. The hypothesis of the onset of a circumequatorial ocean circulation during the Late Jurassic is tested.

In chapter 5 a new occurrence of authigenic albites is investigated. The chemical composition of the albites was determined by using electron microprobe analyses. Albite crystal distribution is described from a regional to a thin section scale, and a possible diagenetic or hydrothermal origin of these albites is discussed.

References:

Abbink, O., Targarona, J., Brinkhuis, H. and Visscher, H., 2001. Late Jurassic to earliest Cretaceous palaeoclimatic evolution of the southern North Sea. Global and Planet. Change, 30(3-4): 231-256.

Aberhan, M., 2001. Bivalve palaeobiogeography and the Hispanic Corridor; time of opening and effectiveness of a proto-Atlantic seaway. Palaeogeogr., Palaeoclimatol., Palaeoecol., 165(3-4): 375-394.

Baumgartner, P.O., 1987. Age and genesis of Tethyan Jurassic radiolarites. Eclogae Geol. Helv., 80(3): 831-879.

Cecca, F., Martin Garin, B., Marchand, D., Lathuiliere, B. and Bartolini, A., 2005. Paleoclimatic control of biogeographic and sedimentary events in Tethyan and peri-Tethyan areas during the Oxfordian (Late Jurassic). Palaeogeogr., Palaeoclimatol., Palaeoecol., 222(1-2): 10-32.

Dromart, G. et al., 2003a. Perturbation of the carbon cycle at the Middle/ Late Jurassic transition; geological and geochemical evidence. Am. J. Sci., 303(8): 667-707.

Dromart, G. et al., 2003b. Ice age at the Middle-Late Jurassic transition? Earth Planet. Sci. Lett., 213: 205-220.

Enay, R., 1980. Paleobiogeographie et Ammonites jurassiques; “rythmes fauniques” et variations du niveau marin; voies d’echanges, migrations et domaines biogeographiques, Livre jubilaire du cent cinquantenaire 1830-1980. Memoire Hors Serie - Societe Geologique de France, pp. 261-281.

Hallam, A., 1985. A review of Mesozoic climate. J. Geol. Soc. London, 142(3): 433-445.

Haq, B.U., Hardenbol, J. and Vail, P.R., 1988. Mesozoic and Cenozoic chronostratigraphy and cycles of sea-level change. In: K. Wilgus Cheryl et al. (Editors), Sea-level changes; an integrated approach. Soc. Econ. Paleonto. Mineralo., Special Publication. SEPM (Society for Sedimentary Geology), Tulsa, OK, United States, pp. 72-108.

Hotinski, R.M. and Toggweiler, J.R., 2003. Impact of a Tethyan circumglobal passage on ocean heat transport and “equable” climates. Paleoceanography, 18(1): 7.

Jenkyns, H.C., 1996. Relative sea-level change and carbon isotopes; data from the Upper Jurassic (Oxfordian) of central and southern Europe. Terra Nova, 8(1): 75-85.

Jones, C.E., Jenkyns, H.C., Coe, A.L. and Hesselbo, S.P., 1994. Strontium isotopic variations in Jurassic and Cretaceous seawater. Geochim. Cosmochim. Acta, 58(14): 3061-3074.

Leinfelder, R.R., Schmid, D.U., Nose, M. and Werner, W., 2002. Jurassic reef patterns; the expression of a changing globe. In: W. Kiessling, E. Fluegel and J. Golonka (Editors), Phanerozoic reef patterns. Soc. Sediment. Geol. (SEPM). Tulsa, US.

Louis-Schmid, B., 2006. Feedback mechanisms between carbon cycling, climate and oceanography: a combined geochemical, sedimentological and modeling approach. Ph. D. thesis Thesis, ETH Zurich, Zurich.

Lécuyer, C. et al., 2003. Thermal evolution of Tethyan surface waters during the Middle-Late Jurassic: Evidence from ∂18O values of marine fish teeth. Paleoceanography, 18(3): 1076.

McArthur, J.M., Howarth, R.J. and Bailey, T.R., 2001. Strontium isotope stratigraphy; LOWESS Version 3; best fit to the marine Sr-isotope curve for 0-509 Ma and accompanying look-up table for deriving numerical age. J. Geol., 109(2): 155-170.

Riboulleau, A. et al., 1998. Evolution de la paleotemperature des eaux de la plate-forme russe au cours du Jurassique superieur. C.R. Acad. Sci., Ser II, 326(4): 239-246.

Riccardi, A.C., 1991. Jurassic and Cretaceous marine connections between the Southeast Pacific and Tethys. In: E.T. Channell James, L. Winterer Edward and F. Jansa Lubomir (Editors), Palaeogeography and paleoceanography of Tethys. Palaeogeogr., Palaeoclimatol., Palaeoecol., pp. 155-189.

Smith, A.G. and Pickering, K.T., 2003. Oceanic gateways as a critical factor to initiate icehouse Earth. J. Geol. Soc. London, 160(3): 337-340.

Voros, A., 1993. Jurassic microplate movements and brachiopod migrations in the western part of the Tethys. In: M.O. Mancenido (Editor), Brachiopod and molluscan biogeography, palaeoecology and stratigraphy; a tribute to Derek Ager. Palaeogeogr., Palaeoclimatol., Palaeoecol. Elsevier, Amsterdam, Netherlands, pp. 125-145.

Voros, A., 2005. The smooth brachiopods of the Mediterranean Jurassic; refugees or invaders? Palaeogeogr., Palaeoclimatol., Palaeoecol., 223(3-4): 222-242.

Weissert, H. and Erba, E., 2004. Volcanism, CO (sub 2) and palaeoclimate; a Late Jurassic-Early Cretaceous carbon and oxygen isotope record. In: S. Morgans Bell Helen and S. Cohen Anthony (Editors), Organic-carbon burial, climate change and ocean chemistry (Mesozoic-Palaeogene). Geological Society of London. London, UK. 2004.

Winterer, E.L., 1991. The Tethyan Pacific during Late Jurassic and Cretaceous times. In: E.T. Channell James, L. Winterer Edward and F. Jansa Lubomir (Editors), Palaeogeography and paleoceanography of Tethys. Palaeogeogr., Palaeoclimatol., Palaeoecol. Elsevier, Amsterdam, Netherlands, pp. 253-265.

CHAPTER 2

Paleoceanographic and paleoclimatic reorganization around the Middle-Late Jurassic transition.

Abstract

A Middle to Upper Jurassic succession of submarine hardgrounds overlain by nodular limestones is exposed in the Jura mountains and in the Helvetic of the Swiss Alps. These sediments were accumulated along the northern shelf of the east-west trending Tethys seaway. Submarine hardgrounds and nodular limestones were also formed on the Briançonnais High, today outcropping in the middle Penninic nappe pile of the Alps. Hardgrounds record strong and persistent current activity along the northern Tethys shelf and on the Briançonnais High during the Callovian and Early Oxfordian. The transition from hardgrounds to nodular limestones corresponds to a major reorganization of Tethys oceanography. The change occurred in Plicatilis ammonite Zone (Middle Oxfordian). Carbon isotope stratigraphy, calibrated against an ammonite-dated reference section in the French Subalpine Basin, serves as a correlation tool between ammonite-dated sections and successions with poor biostratigraphic resolution. Correlation demonstrates that the end of hardground formation was synchronous over wide parts of the northern Tethys. The change in shelf sedimentation coincides with a positive carbon isotope excursion with an amplitude of 1.5‰. The change in C-isotope stratigraphy indicates that observed reorganization of current patterns along the northern Tethys shelf was coupled with global change in oceanography and climate. We propose that the change in northern Tethys sedimentation was caused by opening of new seaways at a time of progressive collapse of Pangaea.

Keywords:

Paleoceanography; Tethys; Oxfordian; Hardgrounds; Chemostratigraphy; Paleocirculation

Submitted to Palaeogeography, Palaeoclimatology, Palaeoecology as: P. Rais, B. Louis-Schmid, S. M. Bernasconi and H. Weissert. Paleoceanographic and paleoclimatic reorganization around the Middle-Late Jurassic transition.

1. Introduction

Middle to Late Jurassic sediments presently outcropping in the Jura mountains and in the Helvetic and Penninic nappe pile of the Alps provide an archive of significant changes in oceanography and climate (Sandy, 1991; Norris and Hallam, 1995; Jenkyns, 1996; Pellenard et al., 1999; Abbink et al., 2001; Dromart et al., 2003a; Dromart et al., 2003b). Submarine hardgrounds formed during the Callovian and Early Oxfordian over wide areas of the northern Tethys shelf and on the Briançonnais High (Furrer, 1979; Norris and Hallam, 1995; Collin et al., 2005). Low sediment accumulation rates on outer-shelf to upper slope environments coincided with the deposition of organic-carbon enriched hemipelagic marlstones in basins along the northern Tethys and with radiolarites in deep pelagic settings (Baumgartner, 1987; Tribovillard, 1988; Norris and Hallam, 1995; Dromart et al., 2003a). A change in the sedimentation pattern occurred in the Middle Oxfordian. Carbonate sedimentation became dominant over wide parts of the northern Tethys, with the development of new reef sites and the expansion of calcareous nannofossils (Bartolini et al., 1996; Leinfelder et al., 2002; Cecca et al., 2005).

The observed change in Tethys sedimentation occurred at a time of progressive fragmentation of Pangaea (Dercourt et al., 1994). New oceanic gateways were formed with, in particular, the opening of the Hispanic Corridor, connecting the Pacific to the western Tethys Ocean (Ziegler, 1988; Scotese, 2001). Ocean floor spreading rates were especially high during the Callovian and the Oxfordian (Jones et al., 1994; Corbin et al., 2000; Cogne and Humler, 2004).

The Callovian-Oxfordian is also marked by a significant temperature increase which is well documented at high latitudes (Riboulleau et al., 1998). Oxygen isotope composition of belemnites from the Russian platform, sporomorph data from the North Sea (Abbink et al., 2001) and the migration of Tethyan ammonites to higher latitudes (Enay, 1980) all provide evidence for substantial warming during the Oxfordian. The temperature increase was accompanied by an extension of the arid climate belt in the northern hemisphere documented by studies on palynology and clay mineralogy, and by the distribution of evaporites and coal (Hallam, 1985; Rioult et al., 1991; Abbink et al., 2001; Hautevelle, 2005).

For this study we traced the Callovian-Oxfordian evolution of the Tethys Ocean in sedimentary archives from the northern Tethys. The northern Tethyan margin is an appropriate area to investigate palaeoceanographic changes, as it is situated along a sensible west-east trending seaway connecting the opening Atlantic Ocean with the eastern Tethys. Biostratigraphy and carbon-isotope stratigraphy were used as a correlation tool to establish a chronology of oceanic changes in the northwestern Tethys. We propose that observed changes in Tethys

sedimentation were triggered by a reorganization of Tethys-Atlantic oceanography triggered by the opening and deepening of the Hispanic corridor.

2. Study sites

In this study we investigated four sections situated in Switzerland. The section "Weiach", a drill hole section, is situated north of Zurich. The Auenstein section is located in the Jura

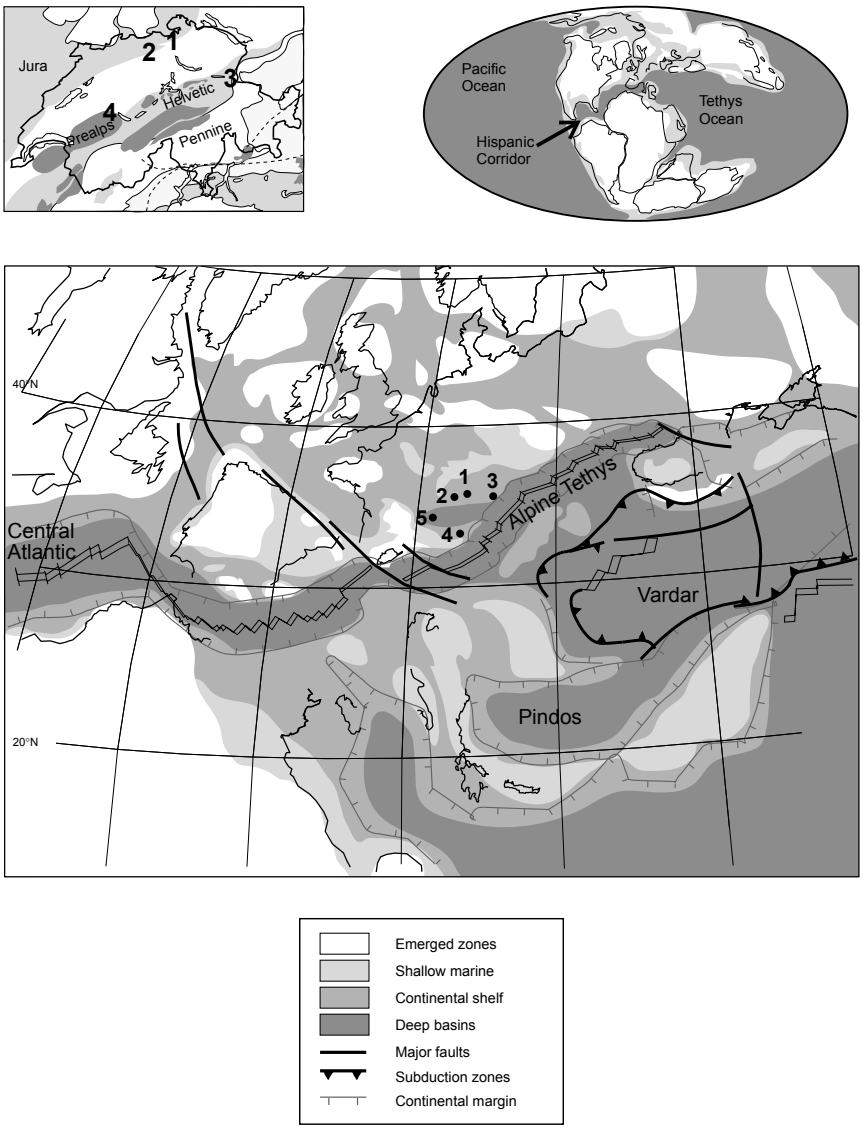

Figure 1: *Position of the sections on paleogeographic and tectonic maps. 1: Weiach; 2: Auenstein; 3: Nissibach; 4: Gantrisch; 5: Subalpine Basin. World map of the Late Jurassic, modified after Scotese (2001). Western Tethys map of the Oxfordian, compiled and modified after Stampfli and Borel (2002) (for tectonic & continent position), Ziegler (1988) and Thierry et al. (2000a; 2000b) (for depositional environments).*

mountains of Northern Switzerland. The Nissibach section in northeastern Switzerland geologically belongs to the Helvetic nappe pile. The middle Penninic Gantrisch section is located in the Prealps in western Switzerland (Fig. 1). The studied sediments were deposited on the northern continental shelf of the Alpine Tethys at palaeolatitudes of approximately 35°N (Smith et al., 1994; Stampfli and Borel, 2002) (Fig. 1). The chosen localities provide a good overall picture of the depositional environment prevailing along the northern Tethyan shelf during the Callovian-Oxfordian.

Weiach

The Weiach section (Fig. 2) is from a borehole situated near the village of Glattfelden that was drilled in 1983 by the NAGRA (Swiss National Cooperative for the Storage of Radioactive Waste). The Middle-Upper Jurassic sediments were formed in a shelf-trough of up to a few hundred meters depth influenced by detrital input (Allenbach, 2001). The sediments consist predominantly of limestone and claystone, and contain some detrital quartz (Matter et al., 1988). The fauna is mainly pelagic, dominated by cephalopods and thin-shelled bivalves. Biostratigraphic control was obtained by lithological correlation with biostratigraphically dated sections and by the ammonites found within the core (Matter et al., 1988). The Middle Callovian is not represented in the core, reflecting a stratigraphic gap. The Upper Callovian Anceps-Athleta Beds consist of a 1.6 m-thick unit characterized by the presence of incrusted ammonites and belemnites and the abundance of polynucleus iron ooids. The Anceps-Athleta Beds are overlain by 70 cm of Lower Oxfordian glauconitic marls followed by the Birmensdorf Member. We identified the Birmensdorf Member as a 2.8 m thick bed that consists of marlstones with small carbonate lenses and bioclasts. The studied part of the core ends within the lower part of the Effinger Member, a limestone-marl alternation containing belemnites and ammonites.

Auenstein

The section is exposed in a quarry near the village of Auenstein (Aargau) (Fig. 3). The sediments were deposited on a open-marine shelf, at an estimated depth of approximately 100 m (Gygi and Persoz, 1986). The large amount of bioclasts and the detrital quartz testify the proximity of a platform and of emerged land (Allenbach, 2001). Ammonite stratigraphy indicates very low sedimentation rates and only intermittent sedimentation from the Middle Bathonian to the Late Callovian (Gygi and Marchand, 1982). The Early Oxfordian is represented by the 50 cm-thick Schellenbrücke Bed, which consists of an iron-impregnated

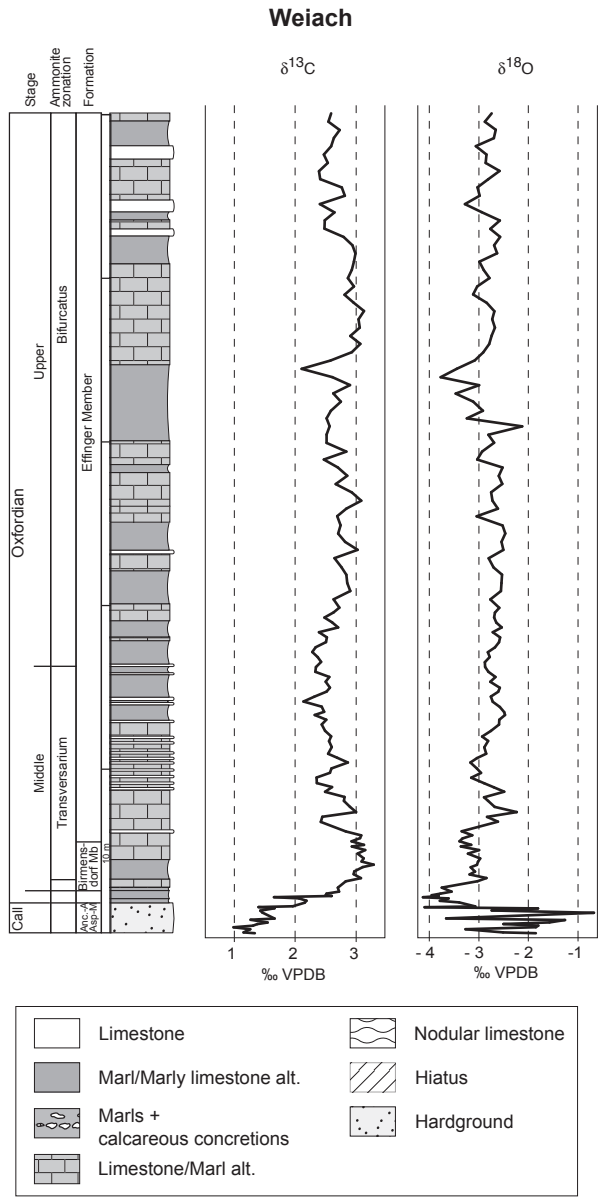

Figure 2:
Lithology, stratigraphy and carbon and oxygen stable isotopes of the Weiach section. Biostratigraphy based on Matter et al. (1988).
Key to lithological patterns used in this paper.

limestone bed containing iron ooids and numerous fossils, and topped by a hardground (Gygi and Persoz, 1986). More than 80% of the fauna consists of cephalopods, other fossils consisting of echinoderms, bryozoans, bivalves, sponges and serpulids. The top of the bed is covered by a stromatolitic crust. Thin-bedded micritic limestones and marlstones of the overlying Birmensdorf Member contain micritic limestone nodules, algae, sponges and pelagic fauna (mainly ammonites). The first 50 cm of this Member are rich in fossil shells and glauconitic pebbles. The Effinger Member with its thin-bedded succession of alternating marlstones and limestones is similar to the Effinger Member in Weiach. According to Gygi (1986), the boundary between the Birmensdorf and Effinger Members corresponds to the transition from the Transversarium to the Plicatilis ammonite Zone. The correlation

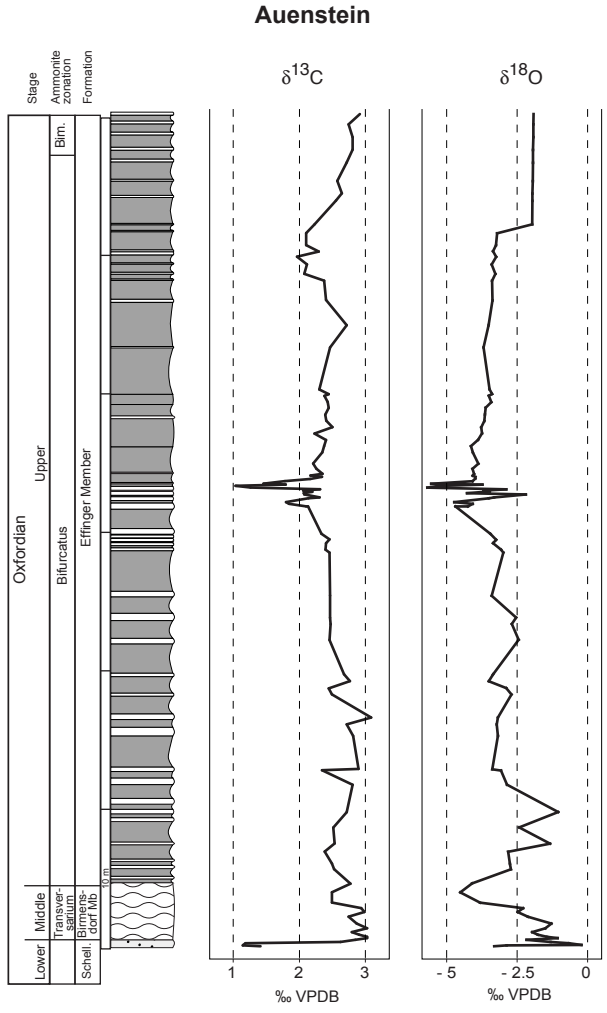

Figure 3:
Lithology, stratigraphy and carbon and oxygen stable isotopes of the Auenstein section. Biostratigraphy based on Gygi (2000). The isotopic curve is a compilation of Padden et al. (2002) and our own measurements.

between the regional biostratigraphy (Gygi and Persoz, 1986; Gygi, 2000) and the usual Tethyan zonation was established by Louis-Schmid et al. (in press), by using carbon-isotope stratigraphy. In this paper, all ammonite zones refer to the Tethyan zonation.

Nissibach

Nissibach is located in the Helvetic tectonic unit near Walenstadt. This section is composed of sediments accumulated along a more distal part of the northern Tethyan shelf (Fig. 4). The studied succession starts with a 100 cm-thick bed described as Blegi-Oolith, which consist of a limestone rich in iron ooids and fossils, and covered by a hardground (Dollfus, 1961; Kugler, 1987; Burkhalter, 1995). The overlying lithology, the Schilt Limestone, is a micritic nodular limestone containing planktonic foraminifera, ammonites and belemnites. The end of the Blegi-Oolith is dated as Early Callovian, and the onset of the Schilt Limestone as Middle Oxfordian (Transversarium Zone). The sedimentation gap between the two formations

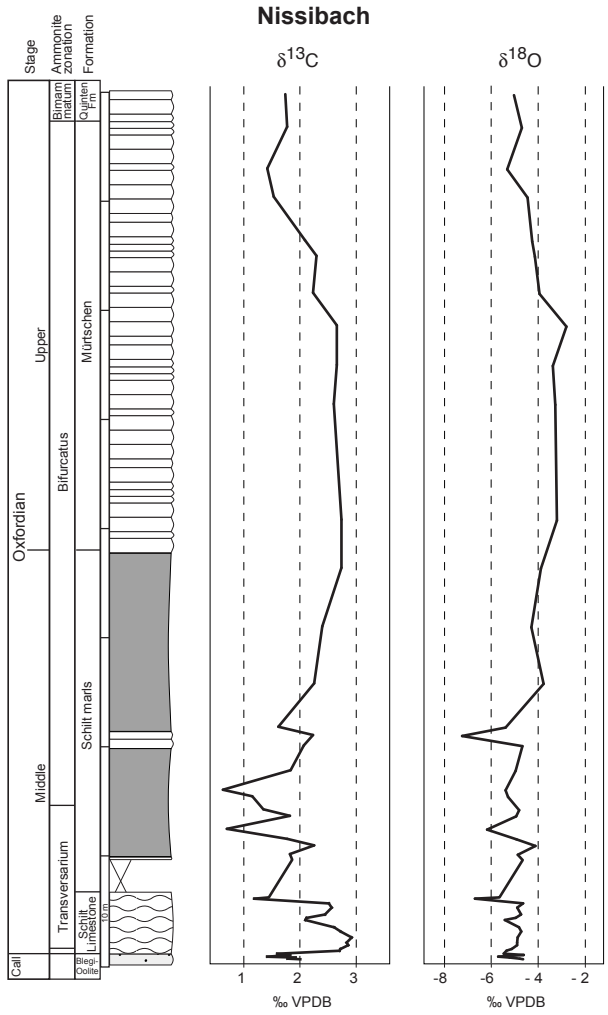

Figure 4:
Lithology, stratigraphy and carbon and oxygen stable isotopes of the Nissibach section. Biostratigraphy based on Kugler (1987). The isotopic curve is a compilation of Padden et al. (2002) and our own measurements.

covers several ammonite zones (Dollfus, 1961; Kugler, 1987). The last part of the Oxfordian is represented by the dark-grey Schilt Marls, followed by the Mürtschen Member, a well-bedded grey limestone.

Gantrisch

The Gantrisch section (Fig. 5) is located in the Middle Penninic "Prealpes Medianes" tectonic unit. Palaeogeographically this area was part of the Briançonnais, a submarine high located southeast of the Iberian microplate during the Jurassic. Based on the description of Furrer (1979), Homewood and Winkler (1977), and Winkler (1977), we have divided the Gantrisch section in three parts: the Formation Calcaréo-argileuse, the Knollenkalk and the Malmkalk. The Formation Calcaréo-argileuse is a monotonous marl with thin-shelled bivalves and scarce echinoderm debris. The Knollenkalk is a micritic nodular limestone that contains planktonic foraminifera, calcispheres and thin-shelled bivalves. Furrer (1979) defined the

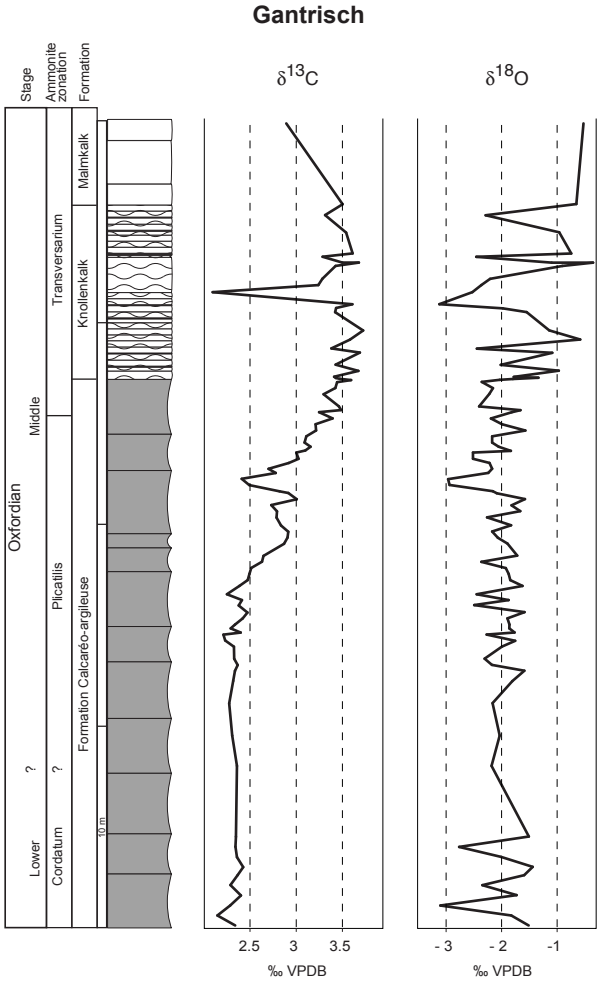

Figure 5:
Lithology, stratigraphy and carbon and oxygen stable isotopes of the Gantrisch section. Biostratigraphy based on Furrer (1979).

Knollenkalk as Middle Oxfordian in age, whereas the remainder of the Upper Jurassic is represented by the Malmkalk, a thick succession of white micritic limestones.

3. Materials and methods

Sediment description is based on field observation combined with thin section analyses. Further investigations were done by cathodoluminescence microscopy. Samples for carbon isotope analysis were taken at intervals ranging from 5 cm in the hardgrounds to 50 cm in the non-condensed parts. Powders were produced by using a micro-drill to avoid crack fillings, fossils or irregularities especially in hardgrounds. In nodular limestones, samples were obtained from the nodules rather than from the matrix, because they are less diagenetically altered (for more details, see below).

The oxygen and carbon isotope composition of bulk-rock was analyzed with a VG-Prism mass spectrometer fitted with an automated Isocarb common acid bath preparation system. The mass spectrometer was calibrated with NBS 19, NBS18 and NBS20. The isotopic

compositions are reported in the conventional delta-notation with respect to VPDB. Analytical reproducibility is better than ±0.1‰ for both carbon and oxygen.
Inorganic carbon and total carbon contents were measured on a UIC CM5012 Coulometer. Organic carbon contents were calculated by difference. Organic and inorganic carbon contents are expressed in weight percent carbonate. Analytical precision is ±0.1 wt-% for carbonate carbon and ±0.3 wt-% for organic carbon.

4. Lithological and geochemical characteristics of Callovian and Oxfordian sediments

The "Anceps-Athleta Bed", the "Schellenbrücke bed", and the "Blegi-Oolith".

The Callovian and the Lower Oxfordian in Weiach, Auenstein and Nissibach are characterized by intermittent sedimentation and long sedimentary gaps (Dollfus, 1961; Gygi and Persoz, 1986; Kugler, 1987; Matter et al., 1988). The sediments deposited during this period show a variety of unusual sedimentologic features related to low accumulation rates and characteristic of hardgrounds and condensed sediments (Gygi, 1981; Gehring, 1986; Kugler, 1987; Burkhalter, 1995), such as thorough bioturbation, reworked intraclasts, concentration of fossils, encrusting organisms, enrichment with glauconite and iron mineralization.
In Weiach, the "Anceps-Athleta Bed" is a 1.6 m thick alternation of dark grey marls and grey limestones. The limestone beds are 5 to 20 cm thick and consist of a bioturbated wackestone to packstone, with around 70 wt-% carbonate. The dark grey marls have the same range of bed thickness. Their carbonate content is around 20 wt-%, and the organic carbon content is up to 0.7 wt-%. The extraclasts embedded in the carbonate matrix consist mainly of iron ooids and pelagic fossils, which are irregularly distributed in a micritic matrix. The iron ooids are abundant and are generally composed of a nucleus of quartz, bioclast or a broken-piece of iron-ooid, surrounded by circular layers, which mainly consist of chamosite (Matter et al., 1988) (Fig. 6A). Their diameter is usually around 0.5 mm, but can reach up to 1.5 mm, especially when the center consists of an assemblage of several smaller ooids. Macrofossils consist exclusively of ammonites and belemnites. They are occasionally covered by a limonitic crust or have microboring features. Belemnites are sometimes enriched in pockets. In the Weiach core, a cluster of eight belemnites was found (Fig. 6A). The microfossils are represented by a few planktonic foraminifera, calcareous thin-shelled bivalves and echinoderm fragments. Quartz grains, glauconite and cavities filled with calcite crystals were also observed.
In Auenstein, the "Schellenbrücke bed" is a 50 cm-thick limestone bed, of red, yellow or green color (Fig. 6B). It consists of a packstone, rich in bioclasts and iron ooids. Bioclasts

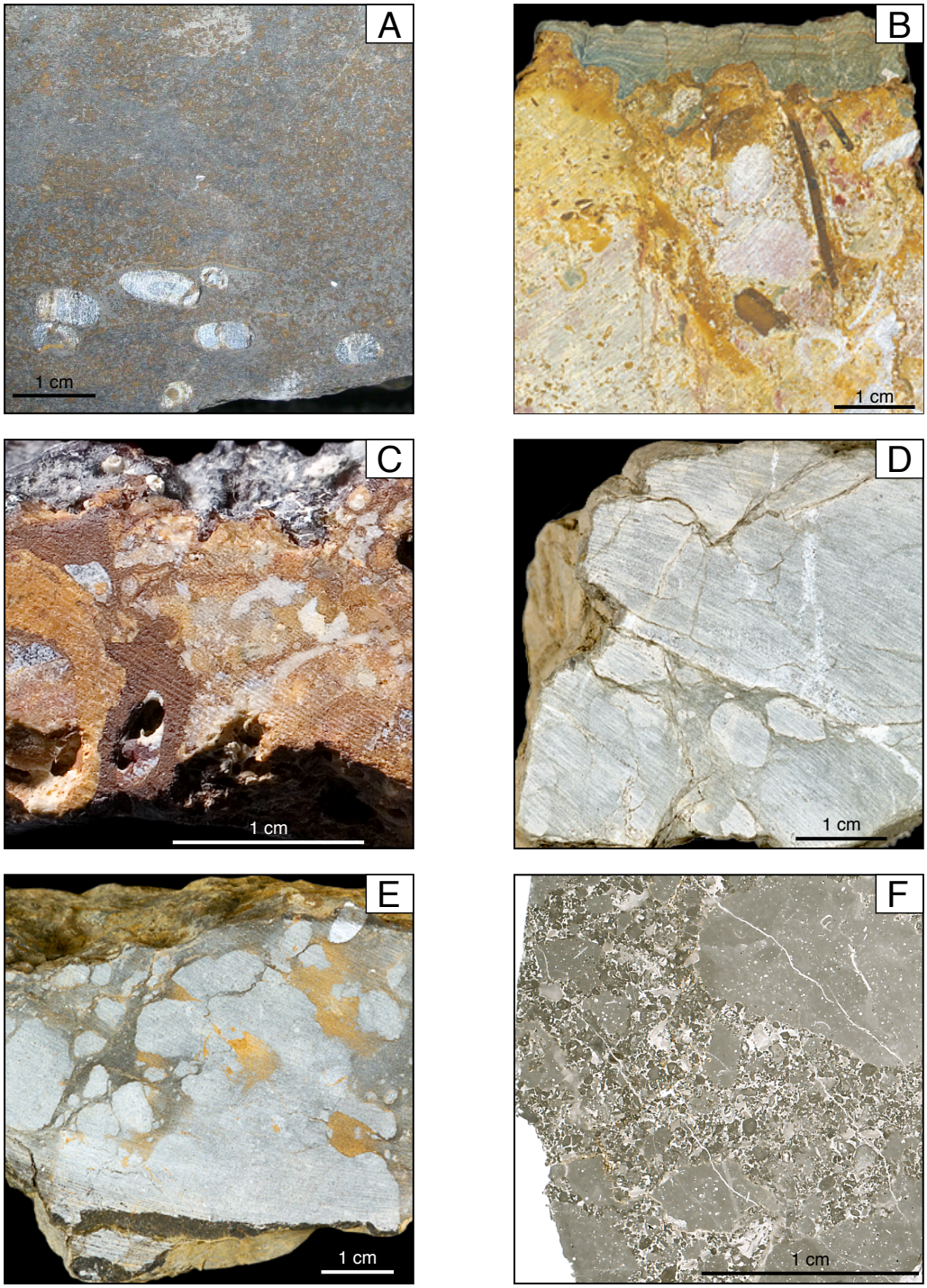

Figure 6:
Pictures of condensed beds and nodular limestones. A: Anceps-Athleta Bed from Weiach with iron ooids (brown dots). Seven belemnites are regrouped at the base of this sample. B: The Schellenbrücke Bed from Auenstein. The top of the bed is covered by a green microbial mat. C: Modern hardground formed by scouring of oceanic currents. Marion Plateau, Australia. D: Nodular limestone from Gantrisch. Stylolites are commonly found around nodules. E: Nodular Schilt limestone from Nissibach. F: Thin-section of the Gantrisch nodular limestone. In this sample, the matrix between the micritic nodules consists of a sparitic, shallow-water limestone.

are dominant and iron ooids are less abundant compared to Weiach. The structure of this bed is very irregular with intraclasts up to several centimetres in size. Cavities of up to several centimetres in diameter, filled with sparry calcite, are distributed throughout the bed. Iron mineralization crusts up to 2 mm thick have also been observed. The majority of the macrofauna is pelagic and consists of up to 80% ammonites and belemnites (Gygi and Persoz, 1986). Echinoderms, bivalves, bryozoans, sponge fragments and algae were also observed. The bioclasts and the lithoclasts are frequently covered by a limonitic crust and perforated by benthic organisms. Several kinds of encrusters like serpulids and encrusting foraminifera have also been identified. In Auenstein, stromatolitic crusts usually cover the top of the bed (Fig. 6B), and are also found around the lithoclasts and as erosive horizons traversing the bed. They consist of a thin-laminated green layer, which is up to 1 cm-thick. A small amount (<1%) of detrital quartz has also been observed.
The "Blegi-Oolith" of Nissibach is a 100 cm thick bed also containing iron ooids. The Blegi-Oolith consists of a biomicritic limestone with an irregular distribution of the components in the matrix (mudstone to packstone), due to the presence of bioturbation and intraclasts. The red, yellow or green coloration of the sediment attests of the presence of iron, which is also concentrated in glauconitic pebbles, mineralized crusts, and iron ooids. The distribution of iron ooids is irregular. In some areas, they represent 90% of the components, whereas they are scarce in other places. The bioclasts are less abundant than in Auenstein. Also here, cephalopods dominate the macrofauna. The remaining fossils include globigerinoids, echinoderm fragments, sponge spicules, calcispheres. Stromatolites form thin layers of 1 mm thickness. They encrust cemented sediment and bioclasts. The detrital content is low, quartz grains represent <1% of the components. Cavities partly or totally filled with coarse, sparry calcite crystals were observed either within the sediment or in shells. Their size varies from a few millimetres to two centimetres.

Nodular limestones

Above the hardgrounds, a nodular limestone facies of variable thickness is observed in Auenstein (5 m), Nissibach (6 m) and Gantrisch (12 m) (Fig. 6D,E,F). It consists of decimetre- to metre-thick bedded limestones. Nodules are similar in the three locations, and consist of a mudstone with pelagic fossils and a few echinoderm and sponge clasts. The pelagic fauna consists mainly of planktonic foraminifera (globigerinoids), belemnites and ammonites. Between the nodules, the matrix is composed of micritic to microsparitic iron-rich calcite with few unidentified bioclasts. The carbonate content is higher in nodules (91% on average) than in the surrounding sediment (68% on average). The nodule size, shape and

distribution can be heterogeneous vertically and horizontally. Their diameters vary from a few millimetres to several centimetres. They are usually sub-rounded and the boundary with the surrounding matrix is mostly sharp and often marked by the presence of stylolites. An ammonite shell is occasionally delimiting the border of nodules. Sometimes nodules are covered by encrusting organisms, indicating a subaquatic exposure at the sediment surface. One sample in Gantrisch shows typical hemipelagic nodules, surrounded by a sparitic matrix with shallow-water clasts composed of pellets, miliolids and aggregate grains.

Isotopic measurements on hardgrounds and nodular limestones

Oxygen and carbon isotopes were measured on 44 different components of the hardgrounds from Auenstein and Weiach, and another 34 samples were analyzed on nodular limestones. An example from the Anceps-Athleta Bed from Weiach and a compilation of the data on the Gantrisch nodular limestones are shown in Fig. 7.

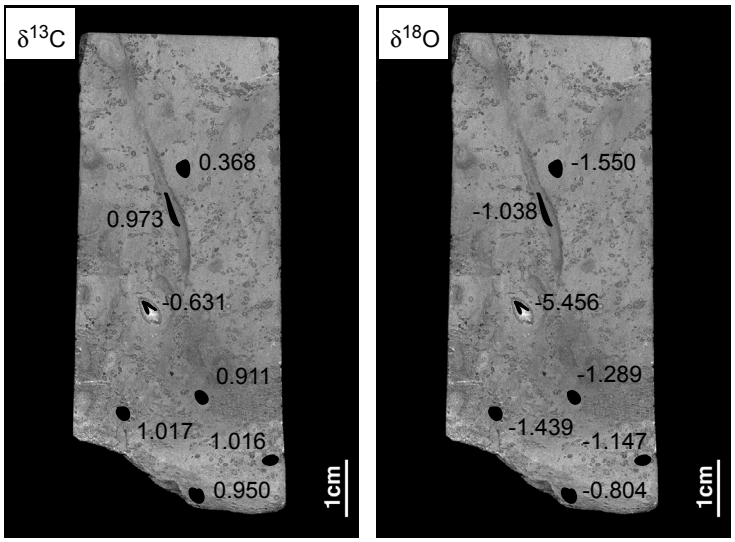

Sample position	$\delta^{13}C$	$\delta^{18}O$
Grey matrix	0.368	-1.550
Bioturbation	0.973	-1.038
Cavity infill	-0.631	-5.456
Grey matrix	0.911	-1.289
Grey matrix	1.017	-1.439
Light grey matrix	1.016	-1.147
Light grey matrix	0.950	-0.804

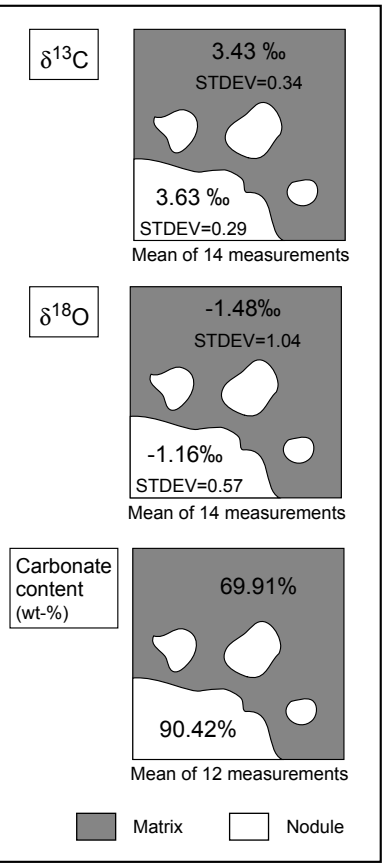

Figure 7:
Left part: carbon and oxygen isotope measurements on condensed lithologies. Example of the Anceps-Athleta Bed from Weiach. Right part: Average values of carbon and oxygen isotopes, and carbonate content from the Gantrisch nodular limestone.

The analyses of carbonate from the hardgrounds reveal that, within one sample, the $\delta^{13}C$ and $\delta^{18}O$ measured in the micritic matrix are homogeneous, whereas cavity infills show $\delta^{18}O$ values ranging between - 5.4‰ and - 7.9‰. Carbon isotope compositions of the micritic matrix range between 0.3‰ and 1.6‰, depending on the sample and its position in the hardground. The oxygen isotope composition of bulk rock shows in average less negative values in the hardgrounds than in the upper part of the section. In Weiach $\delta^{18}O$ values range from - 0.6‰ to - 3.6‰ in the Anceps-Athleta Bed, and from - 2.5‰ to - 4.1‰ in the Birmensdorf and Effinger Members (Fig. 2).
The nodular limestones have similar $\delta^{13}C$ and $\delta^{18}O$ in the nodules and in the encasing lithologies (Fig. 3,4,5). Only a small difference of $\delta^{13}C$ and $\delta^{18}O$ between nodules and the surrounding matrix is observed (Fig. 7). The nodules have a carbon-isotope composition in average 0.2‰ higher than the matrix. For oxygen isotopes, nodules are up to 1.17‰ less negative (0.32‰ in average).

5. Carbon and oxygen isotope stratigraphy

Carbon and oxygen data from the studied sections

Carbon and oxygen isotope results are presented in Fig. 2–5 and carbon isotopes are graphically summarized in Fig. 8. In Weiach, Auenstein and Nissibach, the measured carbon isotope record starts with a sharp positive shift of more than 1.5‰ (Fig. 2,3,4). The most positive values recorded in the sediments situated just above the hardgrounds fall within a range of 2.8‰ to 3.3‰. The upper part of the carbon isotope curve shows values between 1‰ and 3‰. The shift to lower values in the Auenstein and Nissibach sections are discussed by Padden et al. (2001) and Louis-Schmid (2006). In Gantrisch, the values increase progressively from 2.3‰ in the Formation Calcaréo-argileuse to a maximum of 3.7‰ within the Knollenkalk. The oxygen isotope values fluctuate between - 3‰ and - 0.5‰ in the sediments from the sections Weiach, Auenstein and Gantrisch (Fig. 2,3,5). The section Nissibach shows more depleted $\delta^{18}O$ values, ranging from - 6‰ to - 4‰ (Fig. 4).

Reference section for carbon-isotope stratigraphy

We compare the established carbon isotope records with a high-resolution carbon-isotope curve from southeastern France (Fig. 8), where an accurate ammonite stratigraphy was established (Gaillard et al., 1996; Pellenard, 2003; Gaillard et al., 2004). Here we only summarize the most important characteristics of this section, a detailed description can be found in Louis-

Schmid et al. (in press). The isotopic record was established on a composite section from the eastern part of the Subalpine Basin. The Callovian-Oxfordian deposits correspond to the uppermost part of the "Terres Noires", a succession of marlstones punctuated by rust-colored limestone beds (Pellenard et al., 1999). The rapidly subsiding Subalpine Basin corresponds to a sedimentary sink with high sedimentation rates. High sedimentation rates, carbonate contents of more than 40% (Louis Schmid et al., in press) and a rich ammonite fauna make it a good reference section for carbon-isotope stratigraphy.

Most remarkable in the carbon-isotope record from the composite Subalpine Basin section is a positive $\delta^{13}C$ excursion culminating at 3.1‰ in the Transversarium ammonite Zone (Louis-Schmid et al., in press). A short excursion towards values near 1‰ marks the end of the positive carbon isotope anomaly. The upper part of the carbon isotope curve shows a decreasing trend of the values from 2.5‰ to 2‰.

6. Discussion

The Callovian-Oxfordian sedimentation

The Callovian and the early part of the Oxfordian was a time of intermittent sedimentation and erosion, which resulted in the formation of hardgrounds. These hardgrounds, which consist of a few tenths centimetres of sediments in the studied sections, are the only archives of a period estimated at about six million years (Gradstein et al., 2004). Sedimentological, geochemical and palaeontological evidences indicate that these hardgrounds are of a submarine origin and were formed in an outer-shelf to upper slope environment. The presence of encrusting organisms, iron impregnations and mineralization of iron crusts confirm that they were exposed for a long period at the sea floor surface.

The processes which might trigger the formation of hardgrounds include: a) extreme dissolution of carbonates at the sea floor (Garrison and Fischer, 1969; Schlager, 1974), b) low sediment input from platforms and emerged lands (Schlager, 1989; Dromart, 1992), c) scouring of the sea floor by bottom currents (Fuersich, 1979). A strong dissolution can be excluded for the following reasons: First, the fossils observed are well preserved, even thin-shelled fossils and they do not present evidence for strong dissolution. Moreover, the bathymetry was too shallow to fall below the aragonite or calcite compensation depth. Auenstein sediments were accumulated at an estimated depth of 100 m below sea level (Gygi and Persoz, 1986).

Rapid sea-level variations can result in a decrease of sediment input to the deposition area, by emergence or drowning of the sediment source region, or by local changes in sediment

distribution patterns. However, the duration of the Callovian-Oxfordian condensation event, lasting for about six million years (Gradstein et al., 2004), is too long to be explained only by sea-level variations. Furthermore, the presence of bioclasts and quartz grains in the hardgrounds indicates that there was at least intermittent sediment supply to the seafloor.

The last hypothesis to be tested is that strong oceanic currents were sweeping the seafloor of the northern Tethyan margin and were removing the particles from the exposed area. This model is more realistic considering the time involved in the condensation event, as oceanic currents can be active for several millions of years. Moreover, the general distribution pattern of sediments is also concordant: the particles were winnowed from the area exposed to currents, i.e. the upper slope and the shelf, whereas deeper basins collected the particles. This explains the high accumulation rates of the Subalpine Basin. Three sedimentological features suggest an important current activity: a) reworked hardground fragments redeposited as intraclasts, b) the presence of rounded iron ooids (Burkhalter, 1995) and c) fossils, which were transported and accumulated at the same place.

In order to confirm this hypothesis, we compared the Oxfordian hardgrounds with modern hardgrounds forming under comparable conditions. The Marion Plateau offshore NE Australia (ODP leg 194), and the Great Australian Bight "shaved shelf" (James et al., 2001) are two examples of recent hardgrounds forming under strong oceanic currents in a rather shallow carbonatic environment. In the southern Marion Plateau, the elevated topography combined with strong bottom currents (up to 2.5 m/s) prevents sedimentation of particles. Hardgrounds were formed since the Late Miocene/Early Pliocene (Isern et al., 2001). Pieces of the submarine hardground, situated at 117 m and 300 m water depth, were recovered by dredging (Fig. 6C). The hardground dredged from the Marion Plateau is a 3 cm-thick crust, which shows features similar to the Jurassic hardgrounds. First, iron imparts the same yellowish and reddish colors to the sediment. The bed consists of biomicritic carbonate clasts covered by a laminated crust, very similar to the stromatolites of Auenstein and Nissibach. The crust is extensively colonized by serpulids, bryozoans and solitary corals. The carbonate clasts contain abundant planktonic foraminifera and bioclasts from bryozoans, mollusks and corals (Heck et al., in prep). The hardground contains many cavities very similar to the ones of the Jurassic hardgrounds, except that they have no diagenetic infill. The time involved is also comparable, with lacking of sedimentation during 5 My.

James et al. (2001) investigated sedimentation patterns along the Great Australian Bight. They identified widespread palimpsest deposits and reduced carbonate sedimentation due to the strong and complex influence of oceanic currents along the shelf-edge. The resulting palimpsest sediments are also similar to the Jurassic hardgrounds, with calcareous relict intraclasts and biofragments. The intraclasts are enriched in iron (goethite and chamosite).

The hard substrates are colonized by encrusting fauna, mollusks, sponges, and bryozoans, but the sediment generated there is swept away by strong currents. The sediment repartition pattern is distinctive on different sectors of the shelf, with areas protected from currents where sediment accumulates, and exposed areas where the particles are winnowed. The Great Australian Bight can be taken as a modern analogue of the northern Tethyan margin during the Oxfordian. The sections of Weiach, Auenstein and Nissibach correspond to the exposed areas and therefore recorded a hardground and Gantrisch would correspond to a local basinal area protected from the current effect, where sediment could settle.

Nodular limestones

Several models have been developed to explain the formation of the nodular fabrics (see Fluegel, 2004 for a recent review). The only common condition thought to lead to nodular fabric is a low sedimentation rate. Based on an investigation of modern intraclasts formation on the Bahamas, Mullins et al. (1980) suggest that the nodular limestones are formed under fluctuating oceanic current activity. The current, in a first stage, supplies the necessary ions for the early cementation of the carbonate ooze by creating a flux of water moving through the sediment. After that, intraclasts are formed and reworked by a combination of bioturbation and current action, which creates the nodular fabric. This model is in agreement with our own observations: the numerous ammonites indicate a slightly condensed episode, nodules were obviously reworked and are sometimes covered by encrusting organisms, which shows that they were exposed at the seafloor. However, another process has to be added to this model to explain the angular shape of some intraclasts and the sample from Gantrisch, which is composed of pelagic nodules surrounded by a shallow water matrix (Fig. 6D,E,F). We propose that, in addition to the early cementation of carbonate ooze by the action of currents and bioturbation, there was a remobilization of the intraclasts and a regular sediment transport from a carbonate platform to deeper settings. This model explains the variable shape of the intraclasts, depending on their degree of cementation before the remobilization, but also the coarser grained matrix surrounding the nodules. Similar resedimentation processes have been observed on the Little Bahama Bank (Lantzsch et al., 2005). The structure of the redeposited sediment is comparable to the nodular limestones with cemented fine-mud pebbles surrounded by a coarser matrix.

Carbon isotope stratigraphy

Previous biostratigraphic work on the studied sections indicated a Middle Oxfordian age for the first sediments overlying the hardgrounds. According to Gygi (2000) in Auenstein and Kugler (1987) in Nissibach, the nodular limestones are part of the Transversarium ammonite Zone. Likewise the nodular limestones of the Gantrisch section are dated as middle Oxfordian by Furrer (1979). To improve the accuracy of the correlation between the different sections, we used carbon isotope stratigraphy in addition to biostratigraphy.

Before discussing the use of the carbon isotopes for stratigraphy, we have to exclude an influence of diagenesis on the measured samples. In Weiach, Auenstein and Gantrisch, $\delta^{18}O$ values (Fig. 2,3,5) indicate a moderate diagenetic overprint. Therefore, oxygen isotopes cannot be used as a palaeotemperature proxy. The section Nissibach shows more negative $\delta^{18}O$ values (Fig. 4) due to the tectonic position of the section, which suffered a strong burial diagenesis during the formation of the Alps. The carbon-isotope composition, which is less sensible to high burial temperature than oxygen-isotopes, did not suffer a strong diagenetic overprint and preserved the original trend, even in Nissibach (Padden et al., 2002). Moreover, we consider that a strong diagenetic influence on the studied sections can be excluded for the following reasons: a) microfossils are well preserved and show no evidence for recrystallization. b) a covariance between the carbon and the oxygen isotope records is lacking (Fig. 2,3,4,5). c) the carbon isotope records show an excellent correlation across depositional environments and lithologies (Fig. 2,3,4,5). The robustness of the $\delta^{13}C$ signal is supported by the overlapping curves of the five different sections. The Gantrisch carbon-isotope record proves that the isotopic signal is clearly not linked to lithological changes. There, the positive excursion starts one metre below a lithological boundary and the curve does not mirror the transition from marls to nodular limestones.

Seafloor cementation and early diagenesis can influence oxygen and carbon isotope signals (see Mutti and Bernoulli, 2003 for a recent review). Oxygen isotopes measured on the studied hardgrounds could reflect the effect of a seafloor cementation, which produce isotopically heavier cement due to cooler bottom water temperatures (Mutti and Bernoulli, 2003). The $\delta^{13}C$ is generally less affected by seafloor cementation than $\delta^{18}O$ (Marshall and Ashton, 1980; Aghib et al., 1991). Isotopic measurements performed on cavity infills indicate a late-diagenetic alteration (Fig. 7) (Mettraux et al., 1989). Therefore, only the measurements on the micritic matrix reflect an original marine carbon isotope signal (Cecca et al., 2001). In conclusion, the isotopic values measured on the hardgrounds should be taken with some caution, and therefore, in this study, the age of the hardgrounds is based on ammonite stratigraphy. The specific analyses performed on nodular limestones reveal that carbon and

oxygen isotope results were not influenced by seafloor cementation. The very small difference of $\delta^{13}C$ and $\delta^{18}O$ between the nodules and the surrounding matrix (Fig. 7) is probably due to the difference in carbonate content between the nodules and the matrix (Fig. 7). The lower carbonate content of the matrix makes it more sensible to diagenetic overprinting. Therefore, we always used nodule samples for the construction of the carbon isotope curve.

The mid-Oxfordian positive $\delta^{13}C$ excursion, already documented by Jenkyns (1996) and Weissert and Mohr (1996), could be reproduced in all the studied sections. The large amplitude shift of the carbon-isotope curve enables a good correlation with the composite Subalpine Basin section (Fig. 8). The high frequency variations of the $\delta^{13}C$ record and their reproducibility allowed us to identify an interval marked by lower values within the positive excursion and to use this interval for correlation (dark-grey zone, Fig. 8). Based on the correlation with the biostratigraphically dated C-isotope curve of the Subalpine Basin we can demonstrate that post-hardground sedimentation started towards the end of the Plicatilis ammonite zone and that the change in sedimentation is synchronous in the four studied sections.

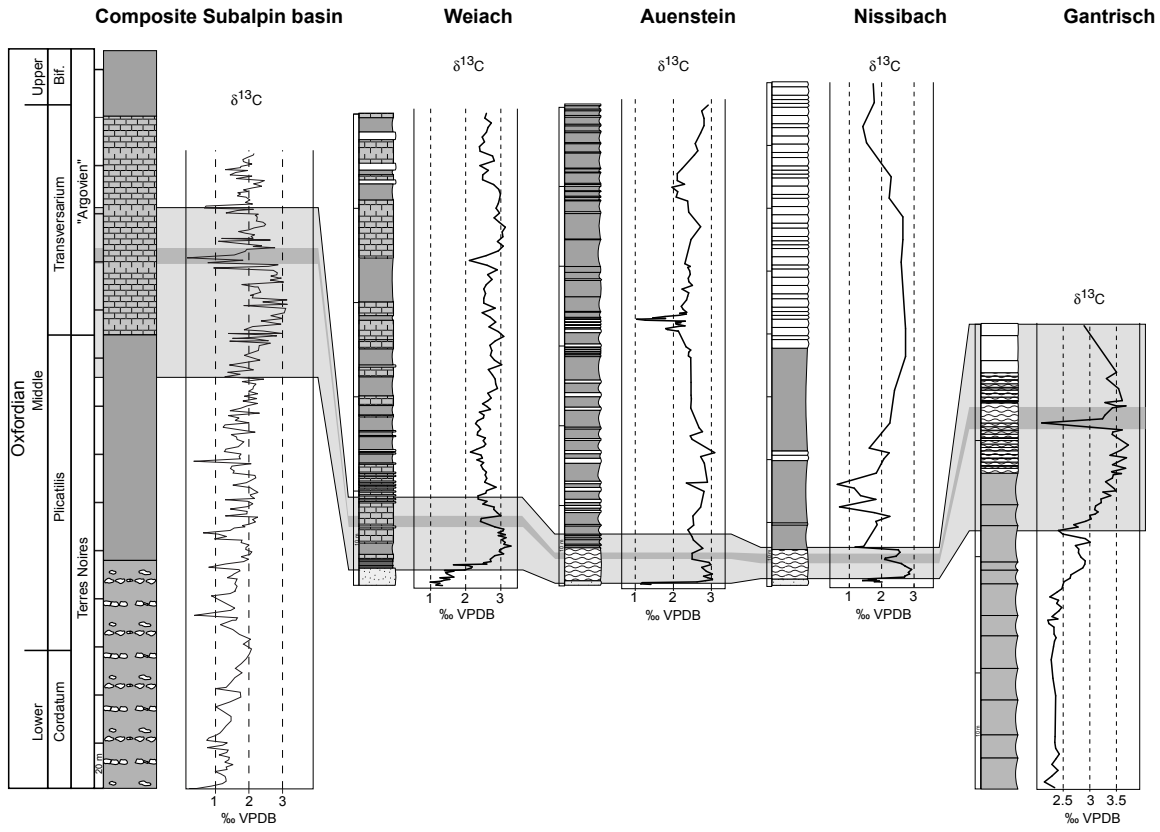

Figure 8:
Correlation of the studied sections and the reference section from the Subalpine basin (Louis-Schmid et al., submitted). The light-grey zone corresponds to the Plicatilis-Transversarium positive excursion, the dark-grey zone represent the interval marked by lower values within the positive excursion.

Sedimentation and current history of the northern Tethyan margin

The sedimentary sequence described above shows that strong shelf currents were active along the northern Tethyan margin creating hardgrounds similar to the ones forming today on the Marion Plateau or along the Great Australian Bight "shaved shelf". Hardgrounds were formed on the exposed seafloor, whereas deeper basins or protected areas collected sediment particles winnowed by currents. We interpret the nodular limestones immediately following the hardgrounds as an expression of a last pulse of oceanic current activity marked by decreasing intensity. This phase is followed by the deposition of marls and carbonate ooze, which mark the onset of the Late Jurassic "carbonate oceans".

By combining bio- and chemostratigraphy, we were able to reconstruct an accurate time frame of the depositional events (Fig. 8,9). Three different depositional histories can be identified from the sections: a) a continuous sedimentation in deep protected areas in the Subalpine Basin, b) a strong sediment-starved phase on the sections exposed to currents (Weiach, Auenstein, Nissibach) and c) for Gantrisch an intermediate evolution.

The Subalpine Basin was protected from currents by its morphology and its depth. The deposition was continuous from Late Callovian to Middle Oxfordian, there is no sedimentary

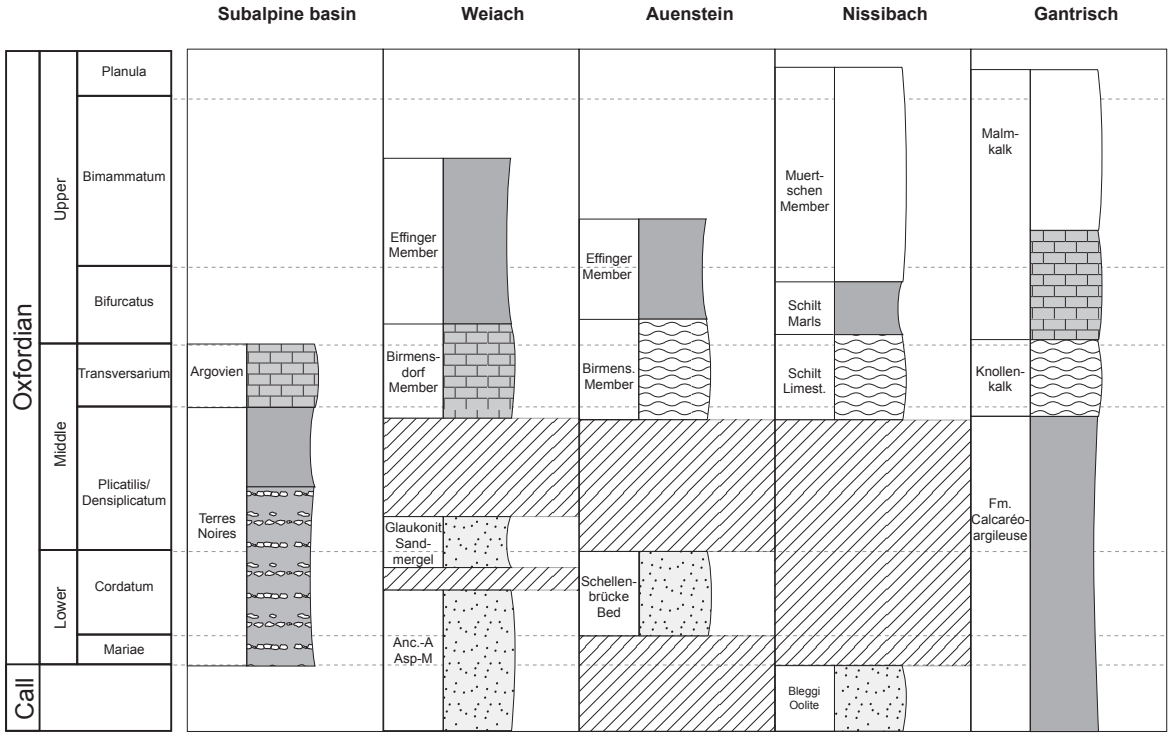

Figure 9:
Lithostratigraphical correlation. This figure is not to scale.

or chemostratigraphic evidence for hiatuses or current activity. On the contrary, the high accumulation rates for this period (Louis-Schmid et al., in press) indicate that the Subalpine Basin acted as a sedimentary sink.

In the three sections of Weiach, Auenstein and Nissibach, hardgrounds were formed during the Callovian and Early Oxfordian. The onset of the current activity is provided by the age of the underlying lithologies, dated as Middle Bathonian to Lower Callovian (Gygi and Persoz, 1986; Kugler, 1987; Matter et al., 1988). Shelf current intensity started to weaken at the end of the Plicatilis Zone and stopped within the Transversarium Zone. Our detailed carbon isotope stratigraphy allows to determine that this transition is synchronous in the three sections, although they are situated at different depositional sites. In Auenstein and Nissibach, the deposition of nodular limestones can be considered as a signature of decreasing current activity. In Weiach, the deposition of fine marls and limestones directly above the hardgrounds indicates that after the Plicatilis Zone, currents were also less effective at a greater palaeodepths.

C-isotope data indicate that the sediments of the studied Gantrisch section were accumulated in a local basinal setting on the northwestern Tethyan Briançonnais high, where deposition was apparently continuous until the Plicatilis Zone. The fine-grained marls from the Formation Calcaréo-argileuse were deposited in a low energy zone. However, this section is not necessarily representative for the whole Briançonnais High. Furrer (1979) reported other locations from the same area recording a hiatus and/or hardgrounds during that time. Therefore, Gantrisch was probably an area protected from the currents by a submarine topographic high. Nevertheless, this section records the nodular limestone unit, which indicates that a moderate current activity was forming nodules which later were redeposited an accumulated in the Gantrisch basin (Winkler, 1977). The onset of the nodular limestone deposition was synchronous with Auenstein and Nissibach.

Global evolution of oceanography and climate during the Callovian and the Oxfordian.

The weakening of shelf current intensity along the northern Tethyan margin is only one of the changes, which occurred during the Middle Oxfordian. A variety of other climate and oceanography proxies indicate that the Oxfordian marks a turning point in Mesozoic palaeoceanography. Evidence for strong currents during the Callovian-Middle Oxfordian is not restricted to the alpine region. Similar sediments have been reported from several other geographical provinces all over the world: Tunisia (Cordey et al., 2005), Pakistan (Fatmi, 1972), India (Fuersich et al., 1992), Madagascar (Besairie and Collignon, 1971), Argentina (Legarreta, 1991).

Middle and Upper Jurassic radiolarites formed in pelagic settings of the western Tethys are interpreted as indicators of intense equatorial upwelling (Cottereau and Lautenschlager, 1994; Bombardiere and Gorin, 2000). Palaeontological evidence suggests that the transition from radiolarites to radiolarian limestones occurred during the Middle Oxfordian (Baumgartner, 1987), which suggests that weakening of equatorial upwelling coincided with waning of shelf currents.

Sea-level variations during this period are still debated. Some authors deduce a global transgression (Legarreta, 1991; Norris and Hallam, 1995), where others see an extreme regression (Dromart et al., 2003b; Cecca et al., 2005). The Haq curve shows gentle second order variations within a first order transgressive trend (Fig. 10).

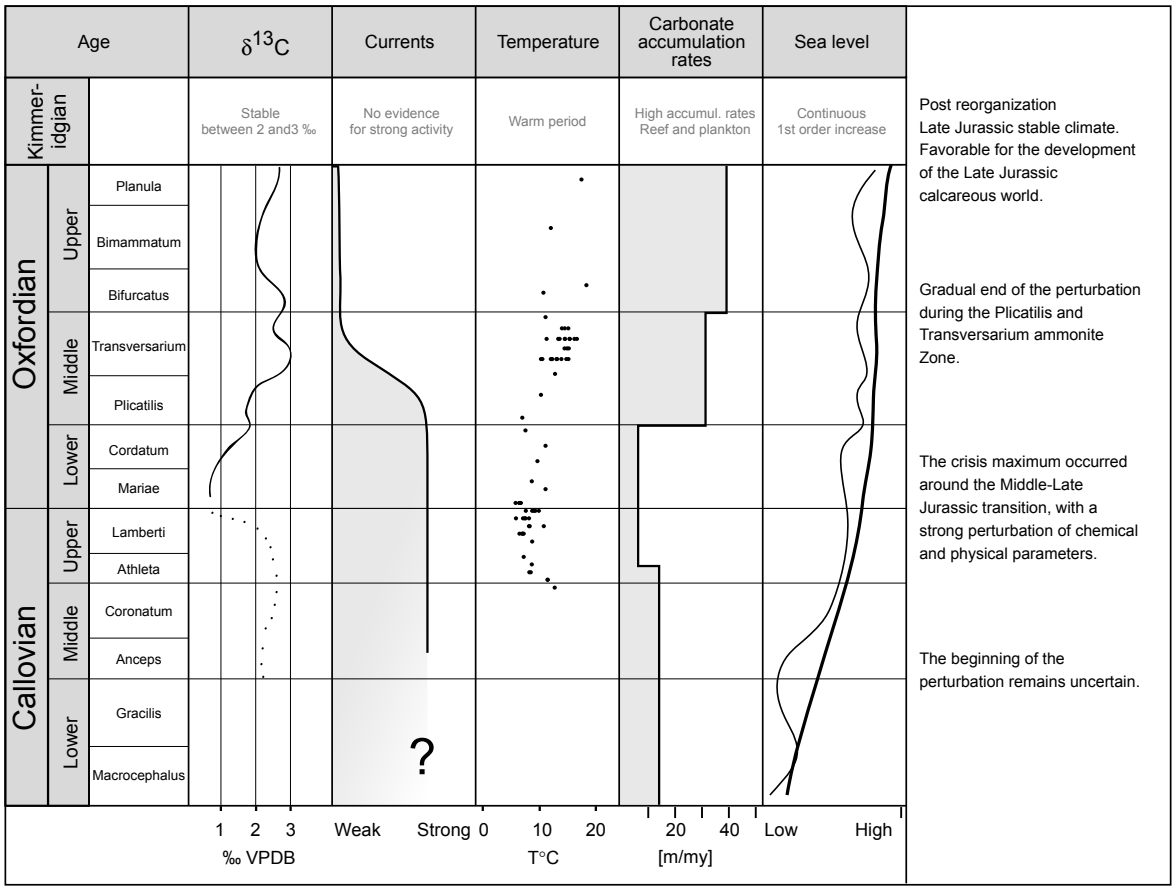

Figure 10:
Comparison of the measured C-isotopes and the currents activity with temperature, sea level variations and carbonate accumulation rates. ∂13C (dotted line) and carbonate accumulation rates after Dromart et al. (2003a). Temperatures compiled by Dromart et al. (2003a) from data by Riboulleau et al. (1998) and Veizer et al. (1999). Sea level curve after Haq (1988).

The time of widespread hardground formation coincided with cold global temperatures (Riboulleau et al., 1998; Abbink et al., 2001; Lécuyer et al., 2003). A stepwise warming starting in the Middle Oxfordian is documented by oxygen isotopes on belemnites from the Russian Platform (Fig. 10) and on fish teeth from the northern Tethys (Riboulleau et al., 1998; Wierzbowski, 2002; Lécuyer et al., 2003; Wierzbowski, 2004). Temperature change is also suggested by the migration of boreal ammonites to higher latitudes (Enay, 1980) and by palynological investigation in the southern North Sea (Abbink et al., 2001). The temperature increase was accompanied by an extension of the arid climate belt in the northern hemisphere, documented by evaporites and coal distribution (Hallam, 1985; Parrish, 1993), and by studies on palynology and clay mineralogy (Rioult et al., 1991; Abbink et al., 2001; Hautevelle, 2005).
The Middle Oxfordian climate warming associated with a general sea-level rise was favorable for the development of carbonate producing organisms (Leinfelder et al., 2002). First, on platforms, with the explosion of the number of reef sites and the diversity of reef builders (Fluegel, 2004) but also in pelagic environments with the expansion of calcareous nannofossils (Bartolini et al., 1996).

A change in tectonics and oceanography

According to sedimentary and chemical records, the Oxfordian stage represents a time of major change for the Mesozoic oceanography. We propose that the breakup of the Pangaean continent (Ziegler, 1988; Scotese, 2001; Stampfli and Borel, 2002) may have caused these changes (Dercourt et al., 1994). The seafloor spreading activity was exceptionally high during Late Callovian and Oxfordian (Corbin et al., 2000; Cogne and Humler, 2004). The strontium-isotope curve ($^{87}Sr/^{86}Sr$), which reaches its lowest values of the Mesozoic in the Oxfordian (McArthur et al., 2001), may reflect the intense mid-ocean ridge hydrothermal activity (Jones et al., 1994) and highlights this period as a turning point in ocean chemistry.
The modification of small oceanic seaways might have influenced the oceanic circulation pattern during the Oxfordian, for example in the North Sea region (Riboulleau et al., 1998; Pellenard et al., 1999; Abbink et al., 2001), the closure of the Meliata Ocean (Stampfli and Borel, 2002; Csontos and Voros, 2004), or the migration of the Bihor-Getic microplate (Csontos and Voros, 2004). However, the most important change in the ocean morphology is the deepening of the Hispanic Corridor separating Laurasia and Gondwana. The first shallow-water connection between Tethys/Atlantic and Pacific is dated as Pliensbachian-Toarcian by bivalve migration (Aberhan, 2001). Through continuous deepening of the Hispanic Corridor associated with a first order sea-level rise, a seaway that allowed significant water mass

exchange between the two basins was established during the Late Jurassic (Riccardi, 1991; Winterer, 1991; Stille et al., 1996; Hallam, 2001; Hotinski and Toggweiler, 2003). Studies on reef development (Leinfelder et al., 2002) or brachiopods (Ager and Walley, 1977; Voros, 1993) confirm the establishment of a first true seaway around the Callovian-Oxfordian boundary.

Climate models reveal that the opening of a low latitude passage triggered a reorganization of ocean current pattern with a new existing east-west current system and the improvement of latitudinal heat exchange (Winterer, 1991; Hotinski and Toggweiler, 2003), which caused the warming of high-latitude surface water (Riboulleau et al., 1998; Abbink et al., 2001). The change in oceanography resulted in the reduction of moisture transport to these latitudes, and to the Late Jurassic shift to drier conditions (Abbink et al., 2001). In other words, the Middle-Late Jurassic change in oceanography corresponds to at least a partial breakdown of the previous megamonsoonal climate system (Parrish, 1993) and the onset of a circumequatorial ocean circulation, which persisted until the Cenozoic (Winterer, 1991; Moore et al., 1992; Hotinski and Toggweiler, 2003). The rifting of Laurasia from Gondwana removed the principal forcing factor of the Early Mesozoic megamonsoon, the Pangaean geography. The homogenization of the surface temperature, the establishment of a dry low latitude climate belt combined with the expansion of new epicontinental seas offered ideal conditions for the widespread carbonate deposition in Late Jurassic neritic and deep water environments.

Acknowledgements:

This project was supported by the Swiss Science Foundation, grant No. 2–77549–04. We thank the Swiss National Cooperative for the Storage of Radioactive Waste (NAGRA) for providing us the samples of the Weiach section. Thanks to Flavio Anselmetti for providing information and samples from the Marion Plateau. Finally, we would like to thank the two anonymous reviewers for their constructive comments on the original manuscript.

References:

Abbink, O., Targarona, J., Brinkhuis, H. and Visscher, H., 2001. Late Jurassic to earliest Cretaceous palaeoclimatic evolution of the southern North Sea. Global and Planet. Change 30(3-4), 231-256.

Aberhan, M., 2001. Bivalve palaeobiogeography and the Hispanic Corridor; time of opening and effectiveness of a proto-Atlantic seaway. Palaeogeogr., Palaeoclimatol., Palaeoecol. 165(3-4), 375-394.

Ager, D.V. and Walley, C.D., 1977. Mesozoic brachiopod migrations and the opening of the North Atlantic. Palaeogeogr., Palaeoclimatol., Palaeoecol. 21(2), 85-99.

Aghib, F.S., Bernoulli, D. and Weissert, H., 1991. Hardground formation in the Bannock Basin, eastern Mediterranean. In: Cita Maria, B., de Lange Gert, J. and Olausson, E. (Eds.), Anoxic basins and sapropel deposition in the eastern Mediterranean; past and present. Elsevier, Amsterdam, Netherlands, pp. 103-113.

Allenbach, R.P., 2001. Synsedimentary tectonics in an epicontinental sea: A new interpretation of the Oxfordian basins of northern Switzerland. Eclogae Geol. Helv. 94, 265-287.

Bartolini, A., Baumgartner, P.O. and Hunziker, J.C., 1996. Middle and Late Jurassic carbon stable-isotope stratigraphy and radiolarite sedimentation of the Umbria-marche Basin (Central Italy). Eclogae Geol. Helv. 89, 831-879.

Baumgartner, P.O., 1987. Age and genesis of Tethyan Jurassic radiolarites. Eclogae Geol. Helv. 80(3), 831-879.

Besairie, H. and Collignon, M., 1971. Géologie de Madagascar. I. Les Terrains sédimentaires. Annales Géol. Madagascar 35.

Bombardiere, L. and Gorin, G.E., 2000. Stratigraphical and lateral distribution of sedimentary organic matter in Upper Jurassic carbonates of SE France. Sediment. Geol. 132(3-4), 177-203.

Burkhalter, R.M., 1995. Ooidal ironstones and ferruginous microbialites; origin and relation to sequence stratigraphy (Aalenian and Bajocian, Swiss Jura Mountains). Sedimentology 42(1), 57-74.

Cecca, F., Savary, B., Bartolini, A., Remane, J. and Cordey, F., 2001. The Middle Jurassic-Lower Cretaceous Rosso Ammonitico succession of Monte Inici (Trapanese Domain, western Sicily); sedimentology, biostratigraphy and isotope stratigraphy. Bull. Soc. Geol. Fr. 172(5), 647-659.

Cecca, F., Martin Garin, B., Marchand, D., Lathuiliere, B. and Bartolini, A., 2005. Paleoclimatic control of biogeographic and sedimentary events in Tethyan and peri-Tethyan areas during the Oxfordian (Late Jurassic). Palaeogeogr., Palaeoclimatol., Palaeoecol. 222(1-2), 10-32.

Cogne, J.-P. and Humler, E., 2004. Temporal variation of oceanic spreading and crustal production rates during the last 180 My. Earth Planet. Sci. Lett. 227, 427-439.

Collin, P.Y., Loreau, J.P. and Courville, P., 2005. Depositional environments and iron ooid formation in condensed sections (Callovian-Oxfordian, south-eastern Paris basin, France). Sedimentology 52(5), 969-987.

Corbin, J.C., Person, A., Iatzoura, A., Ferre, B. and Renard, M., 2000. Manganese in pelagic carbonates; indication of major tectonic events during the geodynamic evolution of a passive continental margin (the Jurassic European margin of the Tethys-Ligurian Sea). Palaeogeogr., Palaeoclimatol., Palaeoecol. 156(1-2), 123-138.

Cordey, F., Boughdiri, M. and Sallouhi, H., 2005. First direct age determination from the Jurassic radiolarian-bearing siliceous series (Jédidi Formation) of northwestern Tunisia. C.R. Geosciences 337(8), 777-785.

Cottereau, N. and Lautenschlager, M., 1994. Tethyan oceanic circulations during the Latest Jurassic; a GCM simulation. C.R. Acad. Sci., Ser II 318(3), 389-396.

Csontos, L. and Voros, A., 2004. Mesozoic plate tectonic reconstruction of the Carpathian region. Palaeogeogr., Palaeoclimatol., Palaeoecol. 210(1), 1-56.

Dercourt, J., Fourcade, E., Cecca, F., Azema, J., Enay, R., Bassoullet, J.P. and Cottereau, N., 1994. Palaeoenvironment of the Jurassic system in the Western and Central Tethys (Toarcian, Callovian, Kimmeridgian, Tithonian); an overview. In: Geobios (Ed.), 3eme Symposium international de stratigraphie du Jurassique. Memoire Special 17, pp. 625-644.

Dollfus, S., 1961. Über das Alter des Blegi-Ooliths in der Glärnisch-Gruppe. Mitteil. Geol. Inst. ETHZ und Univ. Zürich 302.

Dromart, G., 1992. Jurassic deep-water microbial biostromes as flooding markers in carbonate sequence stratigraphy. In: Cotillon, P. (Ed.), Mesozoic eustacy record on western Tethyan margins. Elsevier, Amsterdam, Netherlands, pp. 219-228.

Dromart, G., Garcia, J.P., Gaumet, F., Picard, S., Rousseau, M., Atrops, F., Lecuyer, C. and Sheppard, S.M.F., 2003a. Perturbation of the carbon cycle at the Middle/ Late Jurassic transition; geological and geochemical evidence. Am. J. Sci. 303(8), 667-707.

Dromart, G., Garcia, J.P., Picard, S., Atrops, F., Lécuyer, C. and Sheppard, S.M.F., 2003b. Ice age at the Middle-Late Jurassic transition? Earth Planet. Sci. Lett. 213, 205-220.

Enay, R., 1980. Paleobiogeographie et Ammonites jurassiques; "rythmes fauniques" et variations du niveau marin; voies d'echanges, migrations et domaines biogeographiques, Livre jubilaire du cent cinquantenaire 1830-1980., pp. 261-281.

Fatmi, A.N., 1972. Stratigraphy of the Jurassic and lower Cretaceous rocks and Jurassic ammonites from northern areas of West Pakistan. Bull. Brit. Mus., Nat. Hist., Geol. Series 20(7), 301-380.

Fluegel, E., 2004. Microfacies of carbonate rocks; analysis, interpretation and application. Springer, Berlin.

Fuersich, F.T., 1979. Genesis, environments, and ecology of Jurassic hardgrounds. Neues Jahrb. Geol. Palaeont. 158(1), 1-63.

Fuersich, F.T., Oschmann, W., Singh, I.B. and Jaitly, A.K., 1992. Hardgrounds, reworked concretion levels and condensed horizons in the Jurassic of western India; their significance for basin analysis. J. Geol. Soc. London 149(3), 313-331.

Furrer, U., 1979. Stratigraphie des Doggers der oestlichen Prealpes medianes (Stockhorn-Gebiet zwischen Blumenstein und Boltigen, Kt. Bern). Eclogae Geol. Helv. 72(3), 623-672.

Gaillard, C., Atrops, F., Marchand, D., Hanzo, M., Lathuiliere, B., Bodeur, Y., Ruget, C., Nicoullin, J.P. and Werner, W., 1996. Description stratigraphique préliminaire des faisceaux alternants de l'Oxfordien moyen dans le bassin dauphinois (Sud-Est de la France). Géologie de la France 1, 17-24.

Gaillard, C., Emmanuel, L., Hanzo, M., Lathuiliere, B., Atrops, F., Bodeur, Y., Bouhamdi, A., Marchand, D., Enay, R., Ruget, C. and Werner, W., 2004. Une séquence disséquée du bassin à la plateforme: l'épisode carbonaté de l'Oxfordien moyen dans le Sud-Est de la France. Bull. Soc. Geol. Fr. 175, 107-119.

Garrison, R.E. and Fischer, A.G., 1969. Deep-water limestones and radiolarites of the Alpine Jurassic. In: Friedman, G.M. (Ed.), Depositional environments in carbonate rocks; a symposium. Soc. Econ. Paleonto. Mineralo., pp. 20-56.

Gehring, A.U., 1986. Untersuchungen zur Bildung von Eisenoolithen. Ph. D. thesis, ETH Zurich.

Gradstein, F.M., Ogg, J.G., Smith, A.G., Agterberg, F.P., Bleeker, W., Cooper, R.A., Davydov, V., Gibbard, P., Hinnov, L., House, M.R., Lourens, L., Luterbacher, H.P., McArthur, J., Melchin, M.J., Robb, L.J., Shergold, J., Villeneuve, M., Wardlaw, B.R., Ali, J., Brinkhuis, H., Hilgen, F.J., Hooker, J., Howarth, R.J., Knoll, A.H., Laskar, J.,

Monechi, S., Plumb, K.A., Powell, J., Raffi, I., Roehl, U., Sanfilippo, A., Schmitz, B., Shackleton, N.J., Shields, G.A., Strauss, H., van, D.J., van, K.T., Veizer, J. and Wilson, D., 2004. A geological time scale 2004. Geological Survey of Canada, Ottawa, Canada.

Gygi, R.A., 1981. Oolitic iron formations; marine or not marine? Eclogae Geol. Helv. 74(1), 233-254.

Gygi, R.A. and Marchand, D., 1982. Les faunes de Cardioceratinae (Ammonoidea) du Callovien terminal et de l'Oxfordien inferieur et moyen (Jurassique) de la Suisse septentrionale; stratigraphie, paleoecologie, taxonomie preliminaire. Geobios 15(4), 517-571.

Gygi, R.A. and Persoz, F., 1986. Mineralostratigraphy, litho- and biostratigraphy combined in correlation of the Oxfordian (Late Jurassic) formations of the Swiss Jura Range. Eclogae Geol. Helv. 79(2), 385-454.

Gygi, R.A., 2000. Integrated stratigraphy of the Oxfordian and Kimmeridgian (Late Jurassic) in northern Switzerland and adjacent southern Germany. Birkhauser Verlag, Basel, Switzerland.

Hallam, A., 1985. A review of Mesozoic climate. J. Geol. Soc. London 142(3), 433-445.

Hallam, A., 2001. A review of the broad pattern of Jurassic sea-level changes and their possible causes in the light of current knowledge. Palaeogeogr., Palaeoclimatol., Palaeoecol. 167(1-2), 23-37.

Haq, B.U., Hardenbol, J. and Vail, P.R., 1988. Mesozoic and Cenozoic chronostratigraphy and cycles of sea-level change. In: Wilgus Cheryl, K., Hastings Bruce, S., Ross Charles, A., Posamentier Henry, W., Van Wagoner, J. and Kendall Christopher, G.S.C. (Eds.), Sea-level changes; an integrated approach. SEPM (Society for Sedimentary Geology), Tulsa, OK, United States, pp. 72-108.

Hautevelle, Y., 2005. Géochimie organique des série argilo-carbonatées du Callovo-Oxfordien de l'Est du bassin de Paris et d'Angleterre. Variabilités et implications paléoenvironnementales. Ph. D. Thesis, Université Henri Poincaré.

Heck, P.R., Frank, M., Anselmetti Flavio, S. and Kubik, P.W., in prep. Origin and age of submarine ferromanganese hardgrounds from the Marion Plateau, offshore NE Australia.

Homewood, P. and Winkler, W., 1977. Les calcaires détritiques et noduleux du Malm des Médianes Platiques dans les Préalpes fribourgeoises. Bull. Soc. Frib. Sc. Nat. 66(2), 116-140.

Hotinski, R.M. and Toggweiler, J.R., 2003. Impact of a Tethyan circumglobal passage on ocean heat transport and "equable" climates. Paleoceanography 18(1), 7.

Isern, A.R., Anselmetti, F.S., Blum, P., Andresen, N., Birke, T.K., Bracco, G.G.L., Burns, S.J., Conesa, G.A.R., Delius, H., Dugan, B., Eberli, G.P., Ehrenberg, S., Fuller, M.D., Muller, P.H., Hine, A.C., Howell, M.W., John, C.M., Karner, G.D., Kindler, P.F., Olson, B.E., Sasaki, K., Stewart, D., Wei, W., White, T.S., Wood, J.L. and Yamada, T., 2001. Sites 1196 and 1199. Correlation of deep sea sediments and forereef carbonates in the Red Sea; an important clue for basin analysis. The Marion plateau carbonates (NE Australia); a platform-slope-shelf edifice shaped by sea level change and ocean currents. In: Isern Alexandra, R., Anselmetti Flavio, S., Blum, P., Andresen, N., Birke Tesfaye, K., Bracco Gartner Guido, L., Burns Stephen, J., Conesa Gilles, A.R., Delius, H., Dugan, B., Eberli Gregor, P., Ehrenberg, S., Fuller Michael, D., Muller Pamela, H., Hine Albert, C., Howell Michael, W., John Cedric, M., Karner Garry, D., Kindler Pascal, F., Olson Brooke, E., Sasaki, K., Stewart, D., Wei, W., White Timothy, S., Wood Jason, L., Yamada, T., May Krista, L., Nevill Heather, M., Cagle Lori, J. and Anonymous (Eds.), Proceedings of the Ocean Drilling Program; initial reports; constraining Miocene sea level change from carbonate platform evolution, Marion Plateau, Northeast Australia; covering Leg 194 of the cruises of the drilling vessel JOIDES Resolution, Townsville, Australia, to Apra Harbor, Guam, sites 1192-1199, 3 January-2 March 2001., pp. 255-267.

James, N.P., Bone, Y., Collins, L.B. and Kyser, T.K., 2001. Surficial sediments of the Great Australian Bight; facies dynamics and oceanography on a vast cool-water carbonate shelf. J. Sediment. Res. 71(4), 549-567.

Jenkyns, H.C., 1996. Relative sea-level change and carbon isotopes; data from the Upper Jurassic (Oxfordian) of central and southern Europe. Terra Nova 8(1), 75-85.

Jones, C.E., Jenkyns, H.C., Coe, A.L. and Hesselbo, S.P., 1994. Strontium isotopic variations in Jurassic and Cretaceous seawater. Geochim. Cosmochim. Acta 58(14), 3061-3074.

Kugler, C., 1987. Die Wildegg Formation im Ostjura und die Schilt-Formation um oestlichen Helvetikum; ein Vergleich. Ph. D. thesis, ETH Zurich.

Lantzsch, H., Roth, S., Reijmer, J.J.G. and Egenhoff, S., 2005. Sea-level related resedimentation processes on the northern slope of the Little Bahama Bank. In: 2005, E.G.U. (Ed.), Geophysical Research Abstracts.

Legarreta, L., 1991. Evolution of a Callovian-Oxfordian carbonate margin in the Neuquen Basin of west-central Argentina; facies, architecture, depositional sequences and global sea-level changes. In: Biddle, K.T. and Schlager, W. (Eds.), The record of sea-level fluctuations. Elsevier, Amsterdam, Netherlands, pp. 209-240.

Leinfelder, R.R., Schmid, D.U., Nose, M. and Werner, W., 2002. Jurassic reef patterns; the expression of a changing globe. In: Kiessling, W., Fluegel, E. and Golonka, J. (Eds.), Phanerozoic reef patterns. Soc. Sediment. Geol. (SEPM). Tulsa, US.

Louis-Schmid, B., 2006. Feedback mechanisms between carbon cycling, climate and oceanography: a combined geochemical, sedimentological and modeling approach. Ph. D. thesis, ETH Zurich.

Louis-Schmid, B., Rais, P., Bernasconi, S.M., Pellenard, P., Collin, P.Y. and Weissert, H., in press. Detailed record of the mid-Oxfordian (Late Jurassic) positive carbon-isotope excursion in two hemipelagic sections (France and Switzerland): a plate tectonic trigger? Palaeogeogr., Palaeoclimatol., Palaeoecol.

Lécuyer, C., Picard, S., Garcia, J.P., Sheppard, S.M.F., Grandjean, P. and Dromart, G., 2003. Thermal evolution of Tethyan surface waters during the Middle-Late Jurassic: Evidence from ∂18O values of marine fish teeth. Paleoceanography 18(3), 1076.

Marshall, J.D. and Ashton, M., 1980. Isotopic and trace element evidence for submarine lithification of hardgrounds in the Jurassic of eastern England. Sedimentology 27(3), 271-289.

Matter, A., Peters, T., Blasi, H.R., Meyer, J., Ischi, H. and Meyer, C., 1988. Sondierbohrung Weiach; Geologie. Landeshydrologie und -geologie; Bundesamt fuer Umweltschutz, Bern, Switzerland.

McArthur, J.M., Howarth, R.J. and Bailey, T.R., 2001. Strontium isotope stratigraphy; LOWESS Version 3; best fit to the marine Sr-isotope curve for 0-509 Ma and accompanying look-up table for deriving numerical age. J. Geol. 109(2), 155-170.

Mettraux, M., Weissert, H. and Homewood, P., 1989. An oxygen-minimum palaeoceanographic signal from early Toarcian cavity fills. J. Geol. Soc. London 146(2), 333-344.

Moore, G.T., Hayashida, D.N., Ross, C.A. and Jacobson, S.R., 1992. Paleoclimate of the Kimmeridgian/ Tithonian (Late Jurassic) world; I, Results using a general circulation model. Palaeogeogr., Palaeoclimatol., Palaeoecol. 93(1-2), 113-150.

Mullins, H.T., Neumann, A.C., Wilber, R.J. and Boardman, M.R., 1980. Nodular carbonate sediment on Bahamian slopes; possible precursors to nodular limestones. J. Sediment. Petro. 50(1), 117-131.

Mutti, M. and Bernoulli, D., 2003. Early marine lithification and hardground development on a Miocene ramp (Maiella, Italy); key surfaces to track changes in trophic resources in nontropical carbonate settings. J. Sediment. Res. 73(2), 296-308.

Norris, M.S. and Hallam, A., 1995. Facies variations across the Middle-Upper Jurassic boundary in Western Europe and the relationship to sea-level changes. Palaeogeogr., Palaeoclimatol., Palaeoecol. 116(3-4), 189-245.

Padden, M., Weissert, H. and de Rafelis, M., 2001. Evidence for Late Jurassic release of methane from gas hydrate. Geology 29(3), 223-226.

Padden, M., Weissert, H., Funk, H., Schneider, S. and Gansner, C., 2002. Late Jurassic lithological evolution and carbon-isotope stratigraphy of the western Tethys. Eclogae Geol. Helv. 95, 333-346.

Parrish, J.T., 1993. Climate of the supercontinent Pangea. J. Geol. 101(2), 215-233.

Pellenard, P., Deconinck, J.F., Marchand, D., Thierry, J., Fortwengler, D. and Vigneron, G., 1999. Controle geodynamique de la sedimentation argileuse du Callovien-Oxfordien moyen dans l'est du bassin de Paris; influence eustatique et volcanique. C.R. Acad. Sci., Ser II 328(12), 807-813.

Pellenard, P., 2003. Message terrigène et influences volcaniques au Callovien-Oxfordien dans les bassins de Paris et du sud-est de la France. Mém. Soc. Géol. Nord.

Riboulleau, A., Baudin, F., Daux, V., Hantzpergue, P., Renard, M. and Zakharov, V., 1998. Evolution de la paleotemperature des eaux de la plate-forme russe au cours du Jurassique superieur. C.R. Acad. Sci., Ser II 326(4), 239-246.

Riccardi, A.C., 1991. Jurassic and Cretaceous marine connections between the Southeast Pacific and Tethys. In: Channell James, E.T., Winterer Edward, L. and Jansa Lubomir, F. (Eds.), Palaeogeography and paleoceanography of Tethys., pp. 155-189.

Rioult, M., Dugue, O., Jan, D.C.R., Ponsot, C., Fily, G., Moron, J.M. and Vail, P.R., 1991. Outcrop sequence stratigraphy of the Anglo-Paris Basin, Middle to Upper Jurassic (Normandy, Maine, Dorset). Bull. Cent. Rech. Explor. Prod. Elf-Aquitaine 15(1), 101-194.

Sandy, M.R., 1991. Aspects of Middle-Late Jurassic-Cretaceous Tethyan brachiopod biogeography in relation to tectonic and paleoceanographic developments. In: Channell James, E.T., Winterer Edward, L. and Jansa Lubomir, F. (Eds.), Palaeogeography and paleoceanography of Tethys., pp. 137-154.

Schlager, W., 1974. Preservation of cephalopod skeletons and carbonate dissolution on ancient Tethyan sea floors. In: Hsu, K.J. and Jenkyns, H.C. (Eds.), Pelagic sediments: on land and under sea. IAS Spec. Publ.

Schlager, W., 1989. Drowning unconformities on carbonate platforms. In: Crevello Paul, D., Wilson James, J., Sarg, J.F. and Read, J.F. (Eds.), Controls on carbonate platform and basin development., pp. 15-25.

Scotese, C.R., 2001. Atlas of Earth History. PALEOMAP Project, Arlington, Texas.

Smith, A.G., Smith, D.G. and Funnell, B.M., 1994. Atlas of Mesozoic and Cenozoic Coastlines. Cambrige University Press.

Stampfli, G.M. and Borel, G.D., 2002. A plate tectonic model for the Paleozoic and Mesozoic constrained by dynamic plate boundaries and restored synthetic oceanic isochrons. Earth Planet. Sci. Lett. 196(1-2), 17-33.

Stille, P., Steinmann, M. and Riggs, S.R., 1996. Nd isotope evidence for the evolution of the paleocurrents in the Atlantic and Tethys oceans during the past 180 Ma. Earth Planet. Sci. Lett. 144(1-2), 9-19.

Thierry, J., Abbate, E., Alekseev, A.S., Ait, O.R., Ait, S.H., Bouaziz, S., Canerot, J., Georgiev, G., Guiraud, R., Hirsch, F., Ivanik, M., Le, M.J., Le, N.Y.M., Medina, F., Mouty, M., Nazarevich, B., Nikishin, A.M., Page, K., Panov, D.L., Pique, A., Poisson, A., Sandulescu, M., Sapunov, I.G., Seghedi, A., Soussi, M., Tchoumatchenko, P.V., Vaslet, D., Vishnevskaya, V., Volozh, Y.A., Voznezenski, A., Walley, C.D., Wong, T.E., Ziegler, M., Barrier, E., Bergerat, F., Bracene, R., Brunet, M.F., Cadet, J.P., Guezou, J.C., Jabaloy, A., Lepvrier, C., Rimmele, G., de, W.P., Baudin, F., Belaid, A., Bonneau, M., Coutelle, A., Fekirine, B., Guillocheau, F., Hantzpergue, M., Julien, M., Kokel, F., Lamarche, J., Mami, L., Mansy, J.L., Mascle, G., Pascal, C., Robin, C., Stephenson, R., Sihamdi, N., Vera, J.A. and Vuks, V.J., 2000a. Early Kimmeridgian (146-144 Ma). In: Dercourt, J., Gaetani, M., Vrielynck, B., Barrier, E., Biju Duval, B., Brunet, M.F., Cadet, J.P., Crasquin, S. and Sandulescu, M. (Eds.), Peri-Tethys atlas; palaeogeographical maps; explanatory notes.

Thierry, J., Barrier, E., Abbate, E., Ait, O.R., Ait, S.H., Bouaziz, S., Canerot, J., Elmi, S., Georgiev, G., Guiraud, R., Hirsch, F., Ivanik, M., Le, M.J., Le, N.Y.M., Medina, F., Mouty, M., Nazarevitch, V., Nikishin, A.M., Page, K., Panov, D.L., Pique, A., Poisson, A., Sandulescu, M., Sapunov, I.G., Seghedi, A., Soussi, M., Tarkowski, R.A., Tchoumatchenko, P.V., Vaslet, D., Vishnevskaya, V., Volozh, Y.A., Voznezenski, A., Walley, C.D., Wong, T.E., Ziegler, M., Ait, B.L., Bergerat, F., Bracene, R., Brunet, M.F., Cadet, J.P., Guezou, J.C., Jabaloy, A., Lepvrier, C., Rimmele, G., de, W.P., Belaid, A., Bonneau, M., Coutelle, A., Fekirine, B., Guillocheau, F., Julien, M., Kokel, F., Lamarche, J., Mami, L., Mansy, J.L., Mascle, G., Meister, C., Pascal, C., Robin, C., Sihamdi, N., Stephenson, R., Vera, J.A. and Vuks, V.J., 2000b. Middle Callovian (157-155 Ma). In: Dercourt, J., Gaetani, M., Vrielynck, B., Barrier, E., Biju Duval, B., Brunet, M.F., Cadet, J.P., Crasquin, S. and Sandulescu, M. (Eds.), Peri-Tethys atlas; palaeogeographical maps; explanatory notes.

Tribovillard, N.P., 1988. Geochimie organique et minerale dans les Terres Noires calloviennes et oxfordiennes du bassin dauphinois (France SE); Mise en evidence de cycles climatiques. Bull. Soc. Geol. Fr., Huitieme Serie 4(1), 141-150.

Veizer, J., Ala, D., Azmy, K., Bruckschen, P., Buhl, D., Bruhn, F., Carden, G.A.F., Diener, A., Ebneth, S., Godderis, Y., Jasper, T., Korte, C., Pawellek, F., Podlaha, O.G. and Strauss, H., 1999. 87Sr/86Sr,∂13C and ∂18O evolution of Phanerozoic seawater. In: Veizer, J. (Ed.), Earth system evolution; geochemical perspective. Elsevier, Amsterdam, Netherlands, pp. 59-88.

Voros, A., 1993. Jurassic microplate movements and brachiopod migrations in the western part of the Tethys. In: Mancenido, M.O. (Ed.), Brachiopod and molluscan biogeography, palaeoecology and stratigraphy; a tribute to Derek Ager. Elsevier, Amsterdam, Netherlands, pp. 125-145.

Weissert, H. and Mohr, H., 1996. Late Jurassic climate and its impact on carbon cycling. Palaeogeogr., Palaeoclimatol., Palaeoecol. 122(1-4), 27-43.

Wierzbowski, H., 2002. Detailed oxygen and carbon isotope stratigraphy of the Oxfordian in central Poland. Int. J. Earth Sci. 91(2), 304-314.

Wierzbowski, H., 2004. Carbon and oxygen isotope composition of Oxfordian-early Kimmeridgian belemnite rostra; palaeoenvironmental implications for Late Jurassic seas. Palaeogeogr., Palaeoclimatol., Palaeoecol. 203(1-2), 153-168.

Winkler, W., 1977. Zur Geologie zwischen Gantisch und Muscherenschlund (Préalpes médianes plastiques, Préalpes externes). Diploma thesis, Univ. Freiburg.

Winterer, E.L., 1991. The Tethyan Pacific during Late Jurassic and Cretaceous times. In: Channell James, E.T., Winterer Edward, L. and Jansa Lubomir, F. (Eds.), Palaeogeography and paleoceanography of Tethys. Elsevier, Amsterdam, Netherlands, pp. 253-265.

Ziegler, P.A., 1988. Evolution of the Arctic-North-Atlantic and the western Tethys. American Association of Petroleum Geologists, Tulsa, OK, United States.

CHAPTER 3

Links between the Late Jurassic radiolarite to limestone transition in the southern Alpine Tethys and the sedimentary evolution on its northern margin.

Abstract

In this study, the sedimentation history of the southern Alpine Tethys during the Late Jurassic is revisited and compared to northern Tethyan sedimentation patterns. Carbon isotope stratigraphy was used in combination with biostratigraphy to correlate the sedimentary evolution across different paleoenvironments of the southern margin: the Lombardian Basin, the Trento Plateau, and the Belluno Trough. The facies changes were compared to the sediment succession of two paleoenvironments of the northern margin: the northern Tethyan Shelf and the Subalpine Basin. Based on these correlations, the Late Jurassic sedimentation is divided in four stages: 1) At the beginning of the Oxfordian, siliceous sedimentation dominated the southern margin, while the organic-rich "Terres noires" were deposited in the Subalpine Basin. Carbonate accumulation rates were low, and sedimentation was condensed or lacking on submarine highs of both margins. 2) An increase of carbonate accumulation rates occurred during the Middle Oxfordian, with the deposition of bedded or nodular limestones. Sedimentation remains siliceous in the Lombardian Basin. 3) The first limestones in the Lombardian Basin were deposited during the Early Kimmeridgian. A gradual increase of carbonate deposition is observed in all environments. 4) The Late Tithonian and the Berriasian pelagic sedimentation was dominated by carbonates. We propose that the Late Jurassic changes in sedimentation patterns resulted from a reorganization of ocean currents, creating favorable conditions for calcareous organisms at the end of the Jurassic.

Keywords:

Late Jurassic; Alpine Tethys; Southern Alps; Stratigraphy; Paleoceanography

1. Introduction

The sedimentation history of the southern Alpine Tethys during the Late Jurassic reflects important changes in oceanography (Hsu, 1976; Muttoni et al., 2005; Ogg, 1981). The sediment succession, preserved in the Southern Alps, records a transition from radiolarian cherts in the earliest Late Jurassic to almost pure nannofossil limestones at the end of the Late Jurassic. These sedimentation changes are interpreted as evidence for variations in Calcite Compensation Depth (CCD), oceanic currents, surface water fertility, and/or plankton ecology (Hsu, 1976; Muttoni et al., 2005; Winterer and Bosellini, 1981). Comparable changes in sedimentation pattern and carbonate accumulation rates are observed along the northern margin of the Tethys, suggesting that the oceanic reorganization was not restricted to the southern Alpine Tethys. In order to determine the extent and the nature of the Late Jurassic changes, we compared the sediment evolution of the Southern Alps with the sedimentation pattern evolution along the northern Tethyan margin.

In the first part of this study, we revisit the sediment succession of the southern Alpine Tethys, where we focus on the transition from radiolarites to limestones and on sediment accumulation rates. Three paleoenvironments were investigated: the Lombardian Basin, the Trento Plateau and the Belluno Trough (Fig. 1). A carbon isotope stratigraphy was established for the studied sections and was used as a correlation tool in addition to previous works on biostratigraphy. In the second part, we compare our findings to Late Jurassic sedimentation evolution of the northern Tethys. The sediment successions of two different paleoenvironments are described: the northern Tethyan Shelf and the Subalpine Basin. Finally, we discuss how changes in oceanography caused a coupled change in ocean circulation and in sediment production.

2. Methods

Six sections from northeastern Italy were investigated to illustrate the Late Jurassic lithological evolution of the southern Alpine Tethys. Sediments were characterized by microscopic analyses of thin sections and field observations. Closely spaced samples (5–20 cm) were collected for stable isotope analyses. Bulk carbon and oxygen isotope composition were measured on a VG-Prism mass spectrometer fitted with an automated Isocarb common-acid bath preparation system, and on a Thermo Delta V Plus mass spectrometer equipped with a Kiel IV carbonate preparation module. Samples were reacted in 100% phosphoric acid at 90°C on the VG-Prism and 70°C on the Thermo Delta V Plus to obtain CO_2. The isotopic compositions are reported in the conventional delta-notation with respect to VPDB. Analytical reproducibility is better than 0.1‰ for both carbon and oxygen isotopes. The Late

Jurassic $\delta^{13}C$-curve was compiled by using the program AnalySeries 2.0.3 (Paillard et al. 1996). Time scale is based on Gradstein et al. (2004) and Jaquin et al. (1998).

3. Southern margin: Paleoenvironment and lithological succession

The studied sections consist of radiolarites, radiolaritic limestones, and nannofossil limestones, which were deposited in the southern Alpine Tethys, along the passive continental margin of Adria (Bernoulli and Jenkyns, 1974) (Fig. 1). These Jurassic sediments are exposed in the Southern Alps of northern Italy (Fig. 1). Facies analyses (Ogg, 1981; Winterer and Bosellini, 1981) indicate that this part of the margin was characterized by a number of basins and sedimentary highs. The region is usually separated into four paleogeographic domains: the Lombardian Basin, the Trento Plateau, the Belluno Trough and the Friuli Platform (Ogg, 1981). The sediment succession of the three pelagic domains is presented in this work.

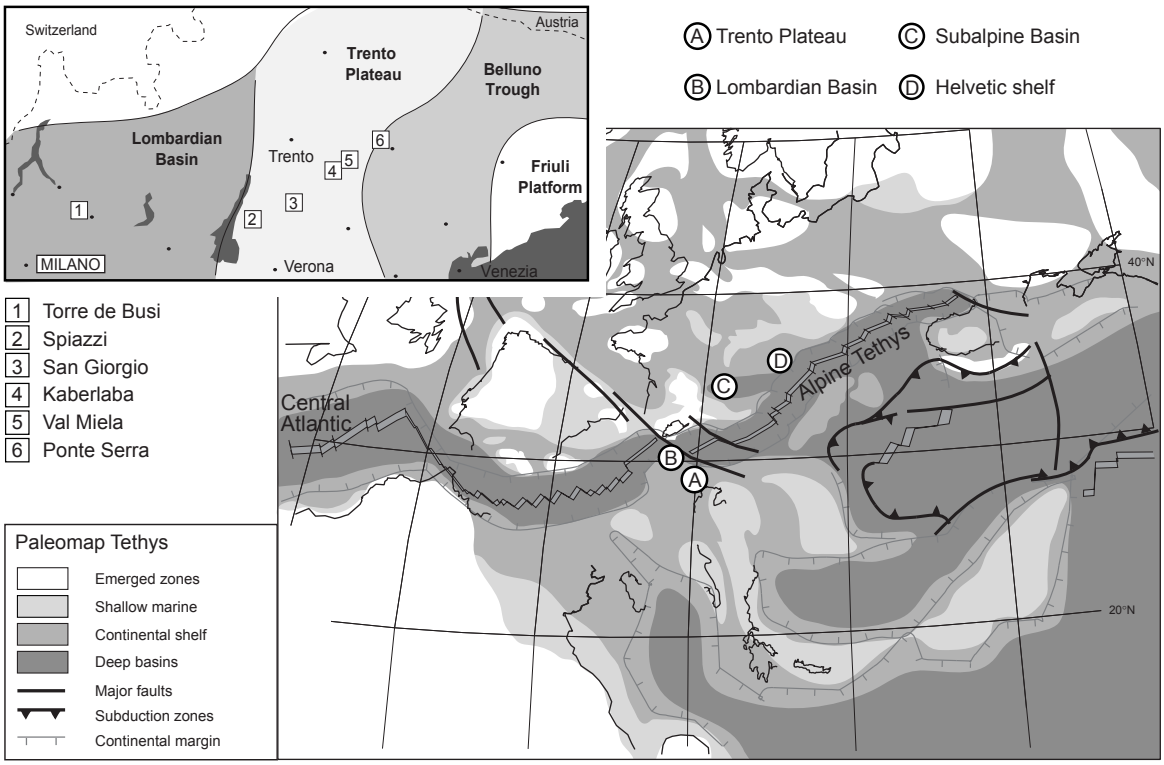

Figure 1:
Top: Structural units of the southern Alps during the Late Jurassic, and position of the studied sections (after Ogg, 1981). Bottom: Paleogeographic map of the western Tethys (Oxfordian), compiled and modified after Stampfli and Borel (2002) (for continent position and tectonic symbols), Ziegler (1988) and Thierry et al. (2000a; 2000b) (for depositional environments).

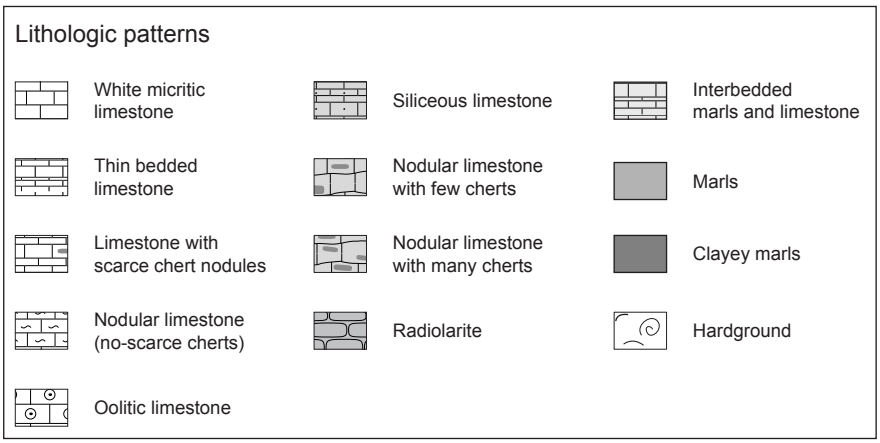

Figure 2:
Keys to lithological patterns used in the stratigraphic sections (Fig. 3 to 11).

Lombardian Basin

The section Torre de Busi (Fig. 3), situated along the Torre de Busi-Sogno road (Weissert, 1979), was part of the deep pelagic Lombardian Basin. The section starts with almost carbonate-free radiolarites. The basal part of the radiolarites consists of ribbon-bedded mostly green cherts followed by a succession of dark-red knobby radiolarite beds. Winterer (1981) estimated the age of the radiolarite episode as Late Callovian to Early Kimmeridgian, whereas Baumgartner (1987) proposed a Bathonian to Lower-Middle Oxfordian age, based on radiolarian stratigraphy. The radiolarites are overlain by the dm-beds of red cherty limestones of the Rosso ad Aptici. The Rosso ad Aptici contains locally abundant aptychi and belemnites, whereas ammonite shells are absent. The red color and the siliceous fraction decrease gradually upsection. The overlying Maiolica Formation consists of a lithified nannofossil-ooze outcropping in 20–50cm thick beds, and is Late Tithonian to Aptian in age (Weissert and Channell, 1989).

Trento Plateau

Four sections, Spiazzi, San Giorgio, Kaberlaba, and Val Miela are located on the Trento Plateau. Situated between the Lombardian Basin and the Belluno Trough, the Trento Plateau was an exclusively pelagic domain influenced by the scouring of oceanic currents. The sedimentary sequence of the Middle and Late Jurassic, known as the “Rosso Ammonitico Veronese”, consists of red nodular limestones, formed by reworking of semi-lithified pebbles under oceanic currents influence (Martire, 1992). The sediment accumulation was extremely

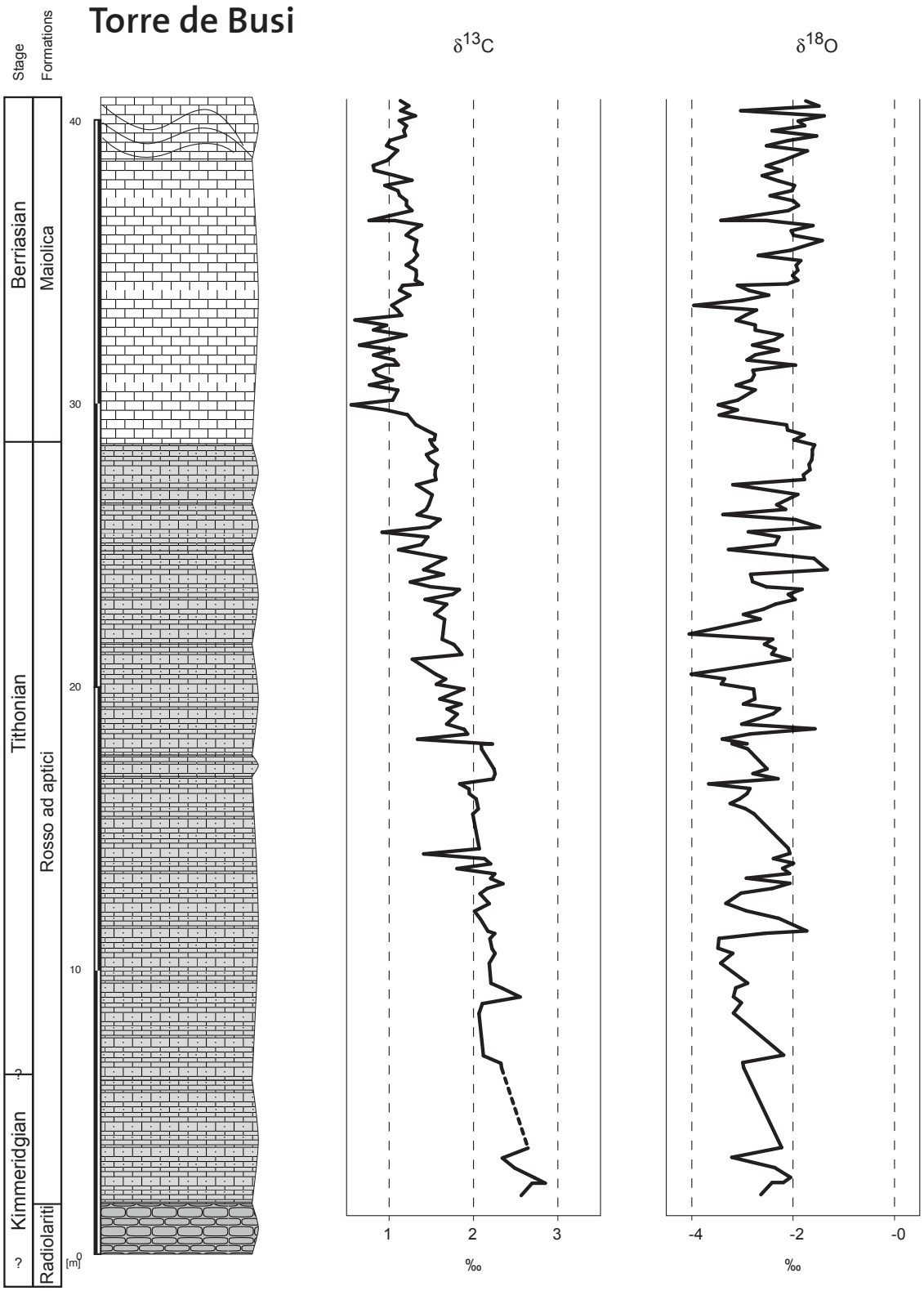

Figure 3:
Lithology, stratigraphy, and stable isotopes of the Torre de Busi section.

reduced, the formation spans from Bajocian to Tithonian and its thickness rarely exceeds 30 m (Martire, 1992). The presence of clear-cut surfaces often mineralized with iron and manganese oxides is evidence for interruption of sedimentation during long periods. On the Trento Plateau, the Rosso Ammonitico Veronese is generally divided into a lower, a middle and an upper unit.

The lower unit, called Rosso Ammonitico Inferiore (RAI) consists of thick and massive beds of pinkish nodular limestone. The nodules consist of a wackestone to packstone containing mainly thin-shelled bivalves, recrystallized radiolarians and scarce echinoderm fragments. The matrix surrounding the nodules is a packstone with locally abundant closely packed thin-

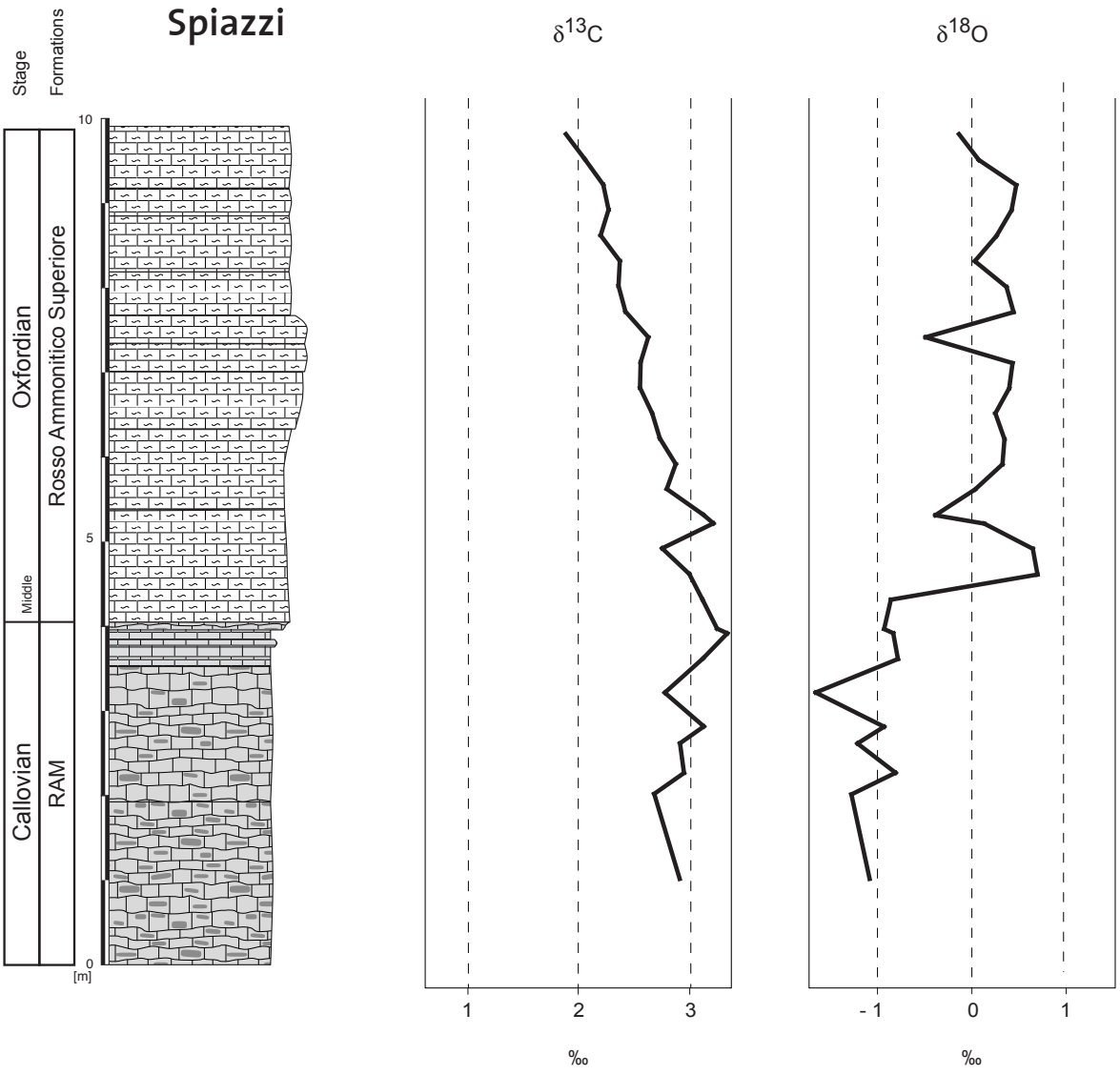

Figure 4:
Lithology, stratigraphy, and stable isotopes of the Spiazzi section. Additional biostratigraphic information from Beccaro (2002).

shelled bivalves. Matrix differs from nodules by its darker-red color, but does not weather differentially. The Middle unit (RAM) is cherty and well bedded and can be easily identified by its dark red color and by the weak competence of the beds. In the studied sections, the RAM is 4 to 5 m-thick, but in other areas of the Trento Plateau it is completely missing (Martire, 1996). The cherts have a dark-red color and are present in nodules, lenses or layers of variable abundance. They are usually associated with limestones containing radiolarians,

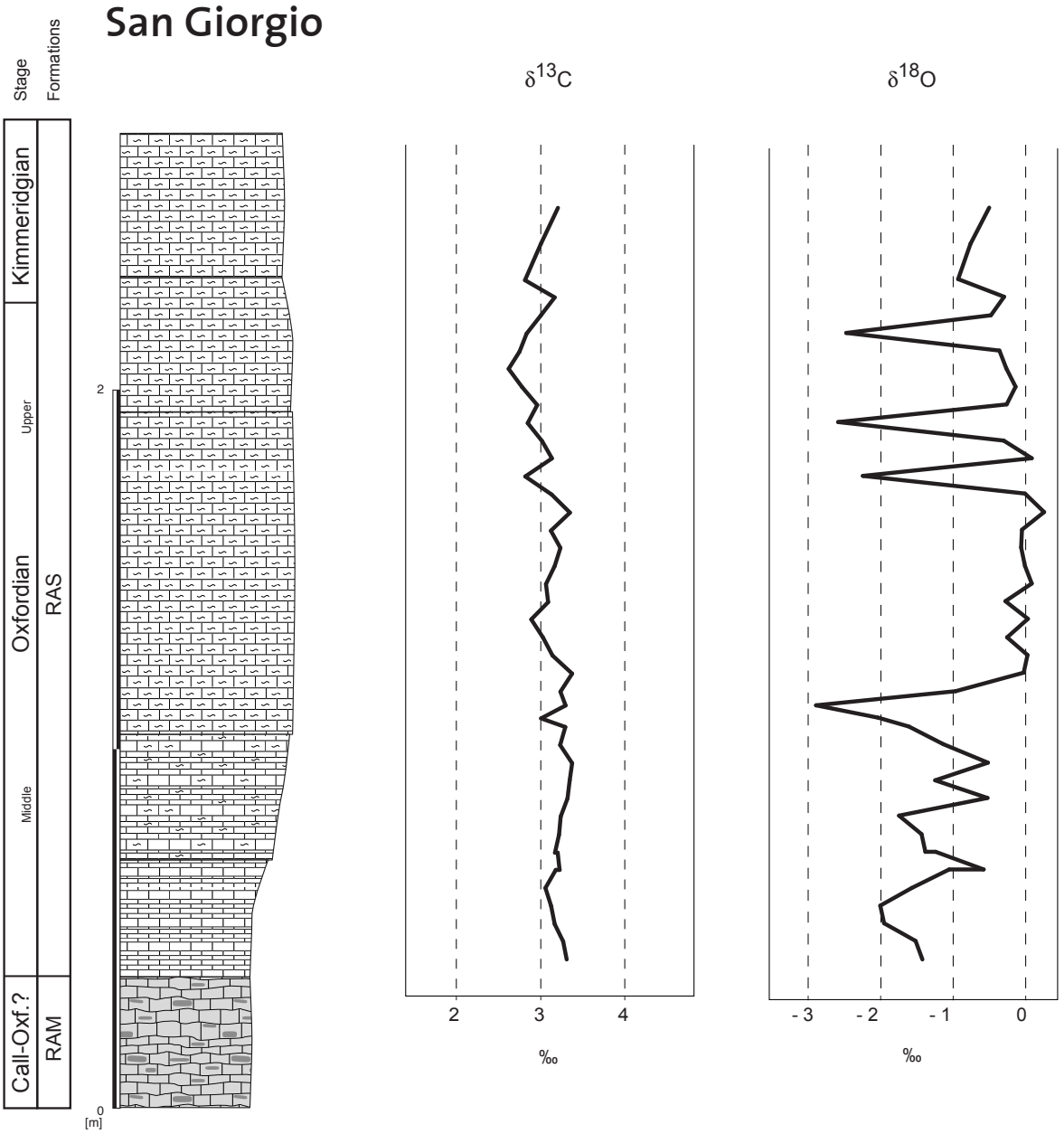

Figure 5:
Lithology, stratigraphy, and stable isotopes of the San Giorgio section. Additional biostratigraphic information from Pavia (1987).

peloids, sponge spicules and echinoderms in a micritic or microsparitic matrix. The upper unit, the Rosso Ammonitico Superiore (RAS) shows again a thicker bedding similar to the RAI, but has a higher clay content (Martire, 1996), which causes a differential weathering between the pink nodules and the dark red matrix. In addition to the pelagic fauna present in the previous units, the RAS contains abundant relics of the pelagic crinoids "*saccocoma*". The Rosso Ammonitico Formation is overlain by the white pelagic limestones of the Maiolica Formation.

The section Spiazzi (Fig. 4), situated near the Garda Lake, is outcropping along the road leading to the Sanctuary of Madonna della Corona, close to the village of Spiazzi (Weissert, 1979). The RAI is hardly accessible in this section, but the RAM, RAS and the Maiolica are well exposed. In a quarry close to Spiazzi (Cava Vianini), ammonites of the Transversarium ammonite Zone (Middle Oxfordian) have been found at the base of the RAS (Beccaro, 2002).

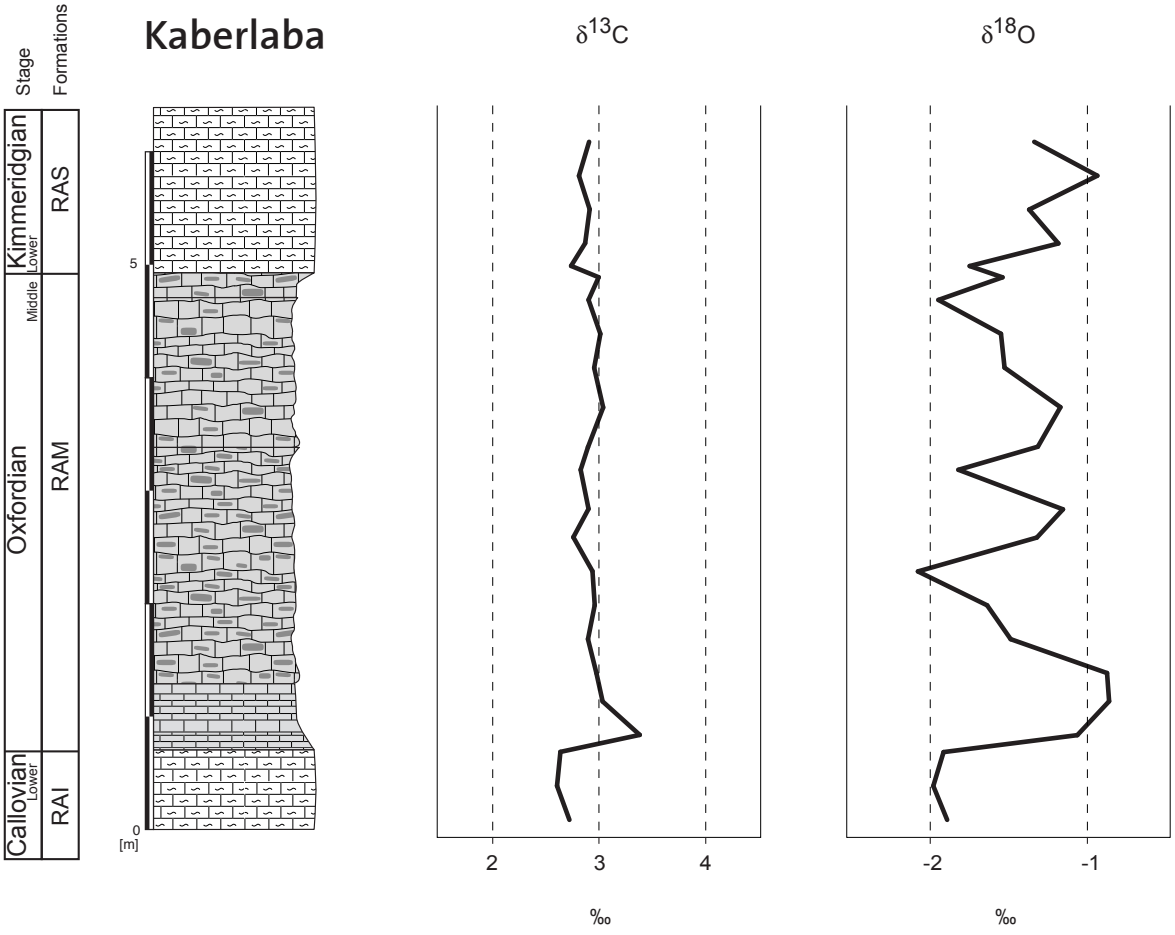

Figure 6:
Lithology, stratigraphy, and stable isotopes of the Kaberlaba section. Additional biostratigraphic information from Martire (1992).

The village of San Giorgio is located in the Lessini Mountains. The samples were collected from a section composed of the RAM and the RAS (Fig. 5), situated along the road to Branchetto, 50 m southwest of the village. Pavia et al. (1987) have shown that, in the Lessini mountains, the first two meters of the RAS are extremely condensed and contain ammonites spanning from Middle Oxfordian to Early Kimmeridgian (Divisum Zone).

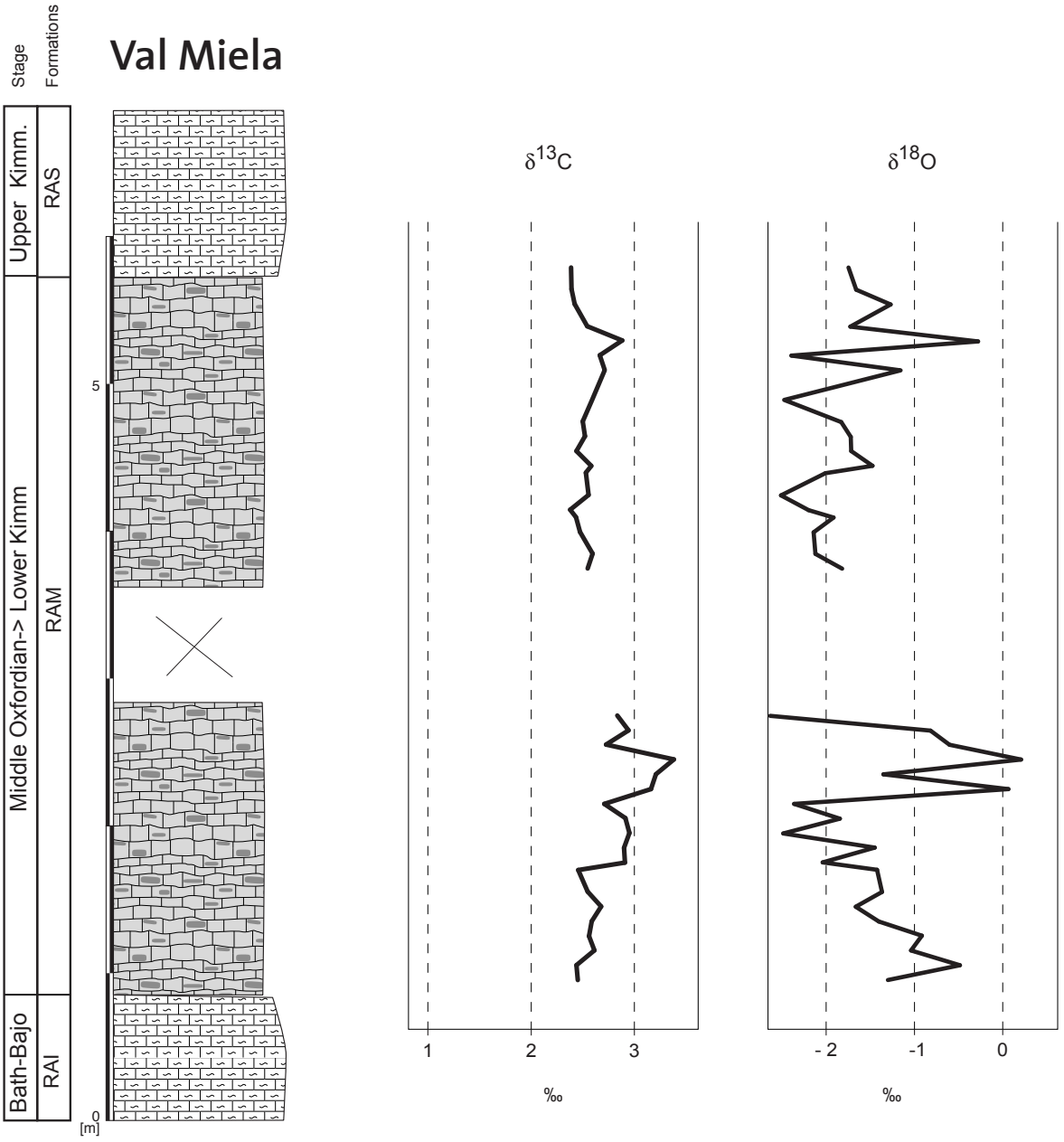

Figure 7:
Lithology, stratigraphy, and stable isotopes of the Val Miela section. Additional biostratigraphic information from Benigni (1982). A part of the section is not outcropping (X).

The section Kaberlaba (Fig. 6) is located in an active quarry 4 km southeast of Asiago (Martire, 1989). The three units of the Rosso Ammonitico Veronese are present and well exposed. Ammonite stratigraphy indicates a Middle Oxfordian age (Transversarium Zone) for the top of the RAM and an Early Kimmeridgian age (Divisum Zone) for the base of the

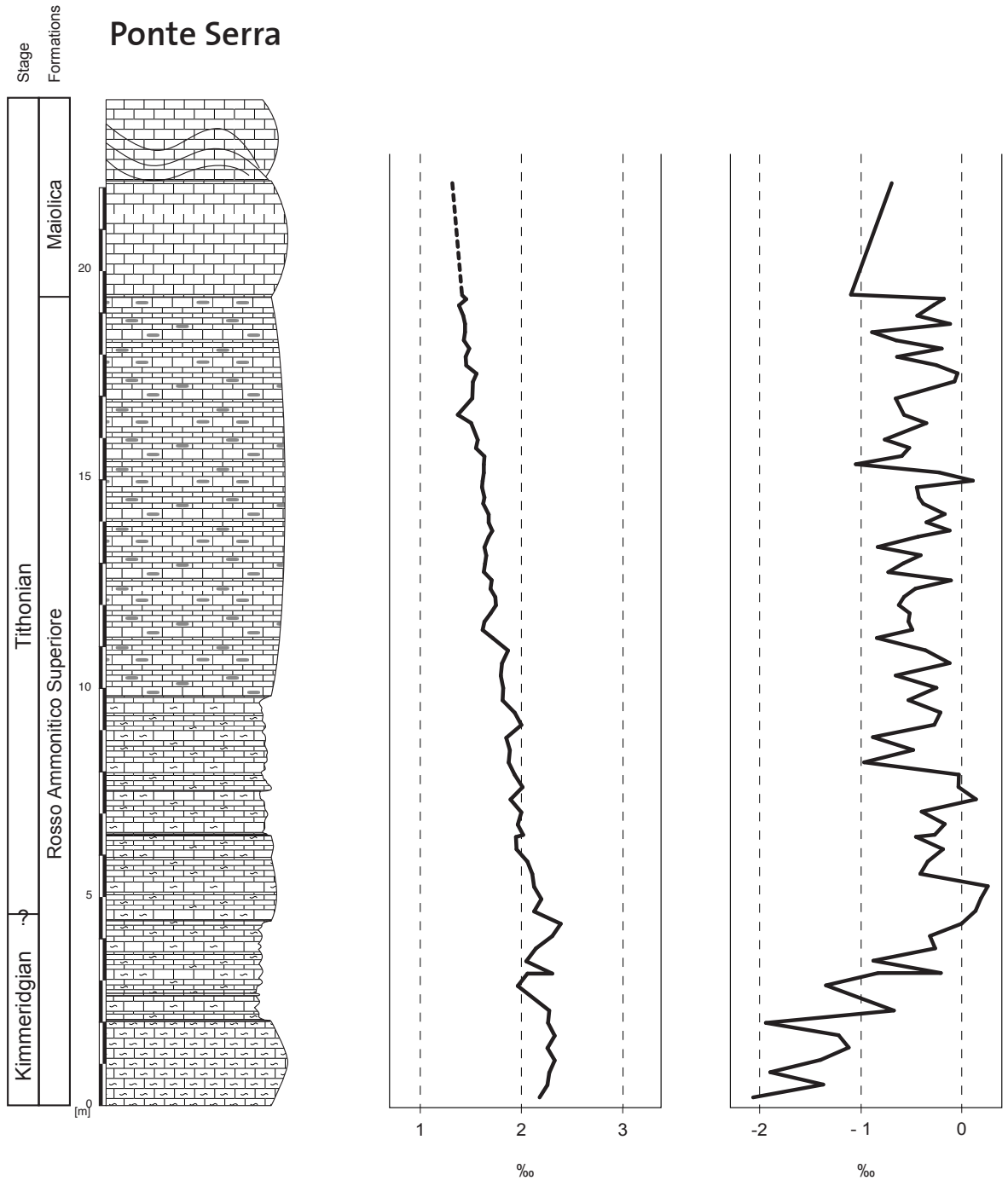

Figure 8:
Lithology, stratigraphy, and stable isotopes of the Ponte Serra section. Additional biostratigraphic information from Cobianchi (2002).

RAS, thus suggesting a gap between these two units spanning from the Upper Oxfordian to the Lower Kimmeridgian (Martire, 1992).
The last section of the Trento Plateau, Val Miela (Fig. 7), is located along the road Foza-Asiago, about 2 km west of Foza. Benigni et al. (1982) estimated a Bajocian-Bathonian age for the RAI, a Late Oxfordian to Early Kimmeridgian for RAM, and a Late Kimmeridgian age for the onset of the RAS, with a lot of uncertainties on these boundaries due to the lack of indicative biomarkers.

Belluno Trough

The Belluno Trough was a narrow depression situated between the Friuli Platform and the Trento Plateau. Its sedimentation history is strongly influenced by the sediment production on the Friuli Platform, illustrated by thick series of turbidites (Bosellini et al., 1981). The Ponte Serra section (Fig. 8), situated on the western side of the Belluno Basin, only recorded the distal expression of these turbidites (Fig. 1). The section is accessible along a little road near the Serra Bridge, above the village of Fonzaso, North of Feltre. The Late Jurassic sediment succession starts with the Fonzaso Formation, a cherty limestone rich in radiolarians. The RAS of the Ponte Serra section is slightly different from the Trento Plateau, and consists of a succession of greenish or reddish beds of nodular limestones. The color intensity and the nodular texture decrease towards the top of the section. The clay content is variable, and is concentrated in thin beds, or as a matrix between calcareous nodules. Dark red cherts are scattered throughout the RAS, and have a nodular or angular shape. The fauna consists of *saccocoma*, thin-shelled bivalves, and radiolarians. The RAS is overlain by the white pelagic mudstones of the Maiolica. The base of the RAS in Ponte Serra is dated by nannofossil stratigraphy as Kimmeridgian, and the transition to the Maiolica as Tithonian (Cobianchi, 2002).

4. Southern margin: Carbon isotope stratigraphy

Carbon and oxygen isotope data are graphically displayed in figures three to eight, and compiled in figure 9. The lithological transitions are difficult to correlate due to the strong condensation of the sediments and the lack of well-preserved ammonites. Therefore, a carbon isotope stratigraphy was established for the studied sections and was used in addition to previous biostratigraphic studies (Beccaro, 2002; Martire, 1996; Pavia et al., 1987) to improve the accuracy of the correlation between the different paleoenvironments.

Preservation of the isotopic signal

Before using carbon isotope stratigraphy as a correlation tool, we have to exclude a resetting of the values during diagenesis of the sediments. In the studied sections, the lack of covariance between oxygen and carbon isotopes excludes a strong influence of diagenesis on the isotopic signal. Oxygen isotopes values in Torre de Busi range between -4‰ and -2‰ (Fig. 3), indicating a moderate diagenetic influence. The sections from the Trento Plateau and the Belluno Trough are characterized by relatively high $\delta^{18}O$ values (Fig. 4,5,6,7,8) ranging from -2.8‰ to 0.8‰. Using a $\delta^{18}O$ value of -1‰ for SMOW, these values would correspond to surface temperatures of 24°C to 9°C. Considering the condensed nature of the sediments, the $\delta^{18}O$ more likely reflects the effect of seafloor cementation producing isotopically heavier cement due to cooler seawater temperature in depth (Mutti and Bernoulli, 2003). The $\delta^{13}C$ is less affected by seafloor cementation than $\delta^{18}O$ (Aghib et al., 1991; Marshall and Ashton, 1980).

Section correlation and Late Jurassic $\delta^{13}C$ curve

Two main carbon-isotope trends were identified in the studied sections (Fig. 9). In Torre de Busi and in Ponte Serra, the $\delta^{13}C$ shows a gradual decrease from around 2.5‰ to 1‰. In the sections from the Trento Plateau (Spiazzi, San Giorgio, Kaberlaba, and Val Miela) the $\delta^{13}C$ shows more positive values, ranging from 1.9‰ to 3.4‰. In order to improve the correlation, the isotopic curves of the studied sections were compared to a composite carbon-isotope curve based on four Late Jurassic sections, well constrained by ammonite- or magnetostratigraphy (Table 1): a composite Subalpine Basin section (Louis-Schmid, 2006), Weiach (Rais et al., submitted), Montsalvens (Padden et al., 2002), and Valle del Mis (Weissert and Channell, 1989). The Late Jurassic composite curve can be divided into three parts (Fig 9): 1) The basal part of the curve is marked by an increasing carbon-isotope curve,

Time range	Section Name	Tectonic realm	Reference
Early and Middle Oxfordian	Composite Subalpine Basin	Subalpine Basin	Louis-Schmid, 2006
Early to Late Oxfordian	Weiach, Switzerland	Jura	Rais et al., submitted
Late Oxfordian to Early Tithonian	Montsalvens, Switzerland	Ultrahelvetic	Padden et al., 2002
Late Kimmeridgian to Berriasian	Valle del Mis, N-Italy	Southern Alps	Weissert & Channell, 1989

Table 1:
Information on the sections used for the creation of the Late Jurassic C-isotope curve.

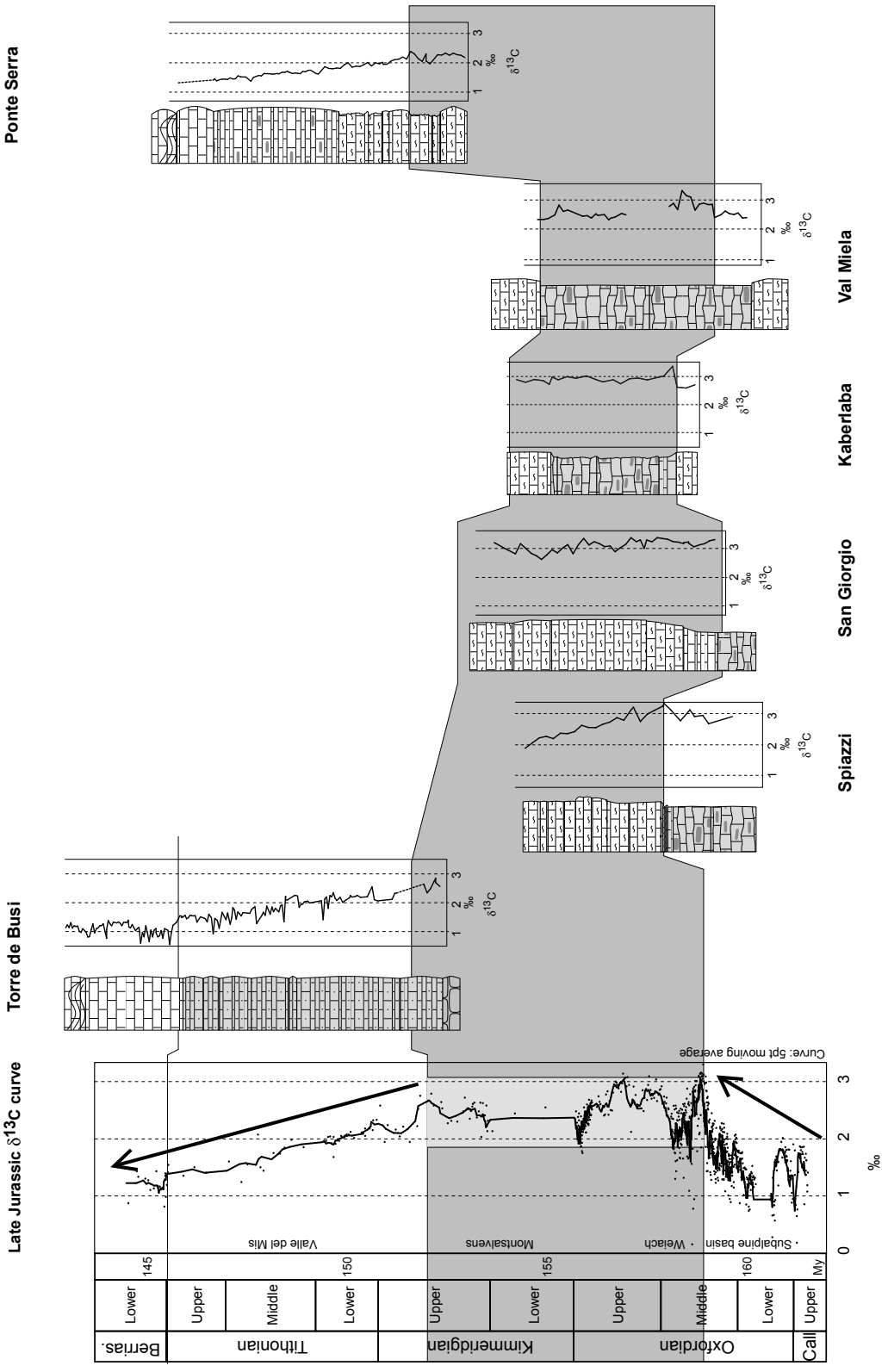

Figure 9:
Correlation of the studied sections and reconstructed Late Jurassic C-isotope curve (references and complementary information in Table 1). The grey zone corresponds to the time of high C-isotope values, spanning from the Middle Oxfordian to the Late Kimmeridgian.

starting with values of 0.8 to 1.8‰ in the Lower Oxfordian and reaching maximum values of 3.2‰ during the Middle Oxfordian (Transversarium Zone). 2) The period spanning from the Middle Oxfordian to the Upper Kimmeridgian is characterized by relatively high values between 2 and 3.2‰. 3) The upper part of the curve is marked by a slow decrease of the $\delta^{13}C$ from 2.5‰ in the Upper Kimmeridgian to 1‰ in the Berriasian.

The carbon isotope records from Torre de Busi and Ponte Serra clearly correspond to the Late Kimmeridgian to Berriasian decreasing trend in the reference curve (Fig. 9). The base of the Torre de Busi section, despite a low resolution, shows $\delta^{13}C$ values around 2.7‰ prior to the latest Jurassic continuous decreasing trend, corresponding to Kimmeridgian ages. At the transition from the Rosso ad Aptici to the Maiolica, the $\delta^{13}C$ curve shows a small shift to lower values, which was correlated with the C-isotope shift at the very end of the Upper Tithonian. In Ponte Serra, the $\delta^{13}C$ starts to decrease five meters above the base of the section, suggesting an Early Kimmeridgian age for the beginning of the RAS. The carbon-isotope record at the beginning of the Maiolica corresponds to the Upper Tithonian values in the reference section.

The heavy $\delta^{13}C$ signal from the Trento Plateau corresponds to the period of high C-isotope values in the reference section, spanning from the Middle Oxfordian to the Late Kimmeridgian. In Spiazzi and Val Miela the values above 3‰ probably correspond to the Middle Oxfordian Transversarium positive excursion (Jenkyns et al., 2002; Louis-Schmid et al., submitted). The ammonite found at the base of the RAS in Spiazzi points to the same age (Beccaro, 2002). In San Giorgio and Kaberlaba, the correlation is complicated by the lack of clear variations of the carbon-isotope signal, probably due to the numerous sedimentation gaps. However, previous works on these sections (Martire, 1996; Pavia et al., 1987) provide a good time-control, based on ammonite stratigraphy (see above).

5. Late Jurassic sedimentation history of the southern margin

The Late Jurassic sediment succession of the southern Alpine Tethys is presented in figure 10. The studied sections show a general evolution from a siliceous to a calcareous sedimentation. The main sediment changes are not synchronous in the Lombardian Basin and in the Trento Plateau. In Torre de Busi, the carbon isotope stratigraphy gives an Early Kimmeridgian age for the onset of the calcareous sedimentation, as proposed by Winterer & Bosellini (1981), but in contradiction with the datation of Baumgartner (1987). From the Lower Kimmeridgian, the silica content decrease gradually towards the Upper Tithonian. The almost pure calcareous ooze of the Maiolica Formation started to be deposited in the Late Tithonian. On the Trento Plateau, the sedimentation was dominated by biogenic silica

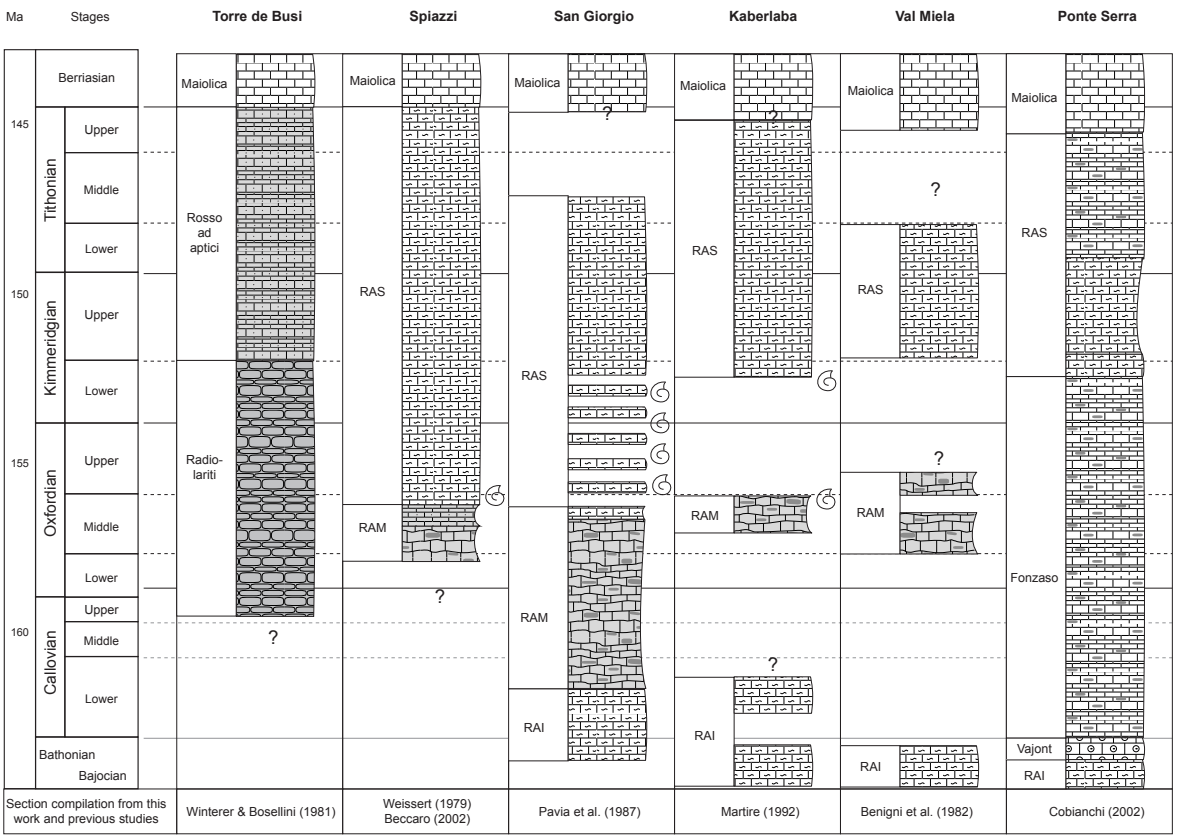

Figure 10:
Lithostratigraphical correlation of the studied sections. Ammonite symbols indicate a datation based on ammonite biostratigraphy. This figure is not to scale.

from the Early Callovian to the Middle Oxfordian (Martire, 1992). Sediment accumulation rates were extremely low and biostratigraphy indicates long sedimentary gaps. In Spiazzi, the transition from cherty limestones to nodular limestones is dated by ammonite stratigraphy as Transversarium ammonite Zone (Middle Oxfordian). In San Giorgio, the transition also occurred in the Middle Oxfordian, but the sediment accumulation was extremely reduced until the Early Kimmeridgian (Pavia et al., 1987). The situation is similar in Kaberlaba, where a long gap spans from the last radiolarite bed, dated as Middle Oxfordian, to the onset of the nodular limestones in the Early Kimmeridgian (Martire, 1992). In Val Miela, the age of the top RAM bed is not clear, but the onset of the RAS is dated as Late Kimmeridgian (Benigni et al., 1982). The situation is completely different at Ponte Serra, where the sediment succession does not record a “radiolaritic event”. This is due to the paleogeographic position of the Belluno Trough, where a large input of calcareous turbidites from the Friuli Platform diluted radiolarian sedimentation (Bosellini et al., 1981). Carbon isotope stratigraphy indicates an Early Kimmeridgian age for the base of the RAS, which is consistent with

nannofossils stratigraphy (Cobianchi, 2002). The transition to the Maiolica occurs during the Late Tithonian.

In summary, the evolution of the sedimentation can be divided in four phases: 1) A phase of silica-dominated sedimentation until the Middle Oxfordian, except in the Belluno Trough. Sedimentation on the Trento Plateau was extremely condensed or lacking. 2) The period spanning from the Middle Oxfordian to the Early Kimmeridgian corresponds to the first pulses of carbonate deposition on the Trento Plateau. Sediment accumulation rates remained low in most of the sections. Siliceous sedimentation remained dominant in the Lombardian Basin. 3) At the end of the Early Kimmeridgian, nodular limestones were formed on the Trento Plateau and in the Belluno Trough. This period also corresponds to the onset of the carbonate ooze deposition in the Lombardian Basin and the gradual decrease of biogenic silica in the sediments investigated. 4) In the Late Tithonian, the deposition of almost pure carbonate ooze was deposited in the three pelagic domains.

6. Sediment succession of the northern Tethyan margin

On the northern Alpine Tethys, the Late Jurassic sedimentation was dominated by marls and limestones (Fig. 11). The sediment succession of a shallow and a deep paleoenvironment is presented here: the northern Tethyan Shelf and the Subalpine Basin (Fig. 1). Sediments formed on the northern Shelf are exposed today in the Helvetic Nappes of the Swiss Alps and in the Jura Mountains. Detailed descriptions of Late Jurassic sections of the northern Tethyan Shelf are documented by Rais et al. (submitted), Padden et al. (2002), Gygi and Persoz (1986), and Weissert and Mohr (1996). Callovian and Early Oxfordian sediments consist of colorful biomicritic limestones rich in fossils characterized by the presence of rounded iron ooids and reworked rock fragments, and are defined as hardgrounds (Gygi and Persoz, 1986; Kugler, 1987; Rais et al., submitted). The fauna is largely dominated by ammonites and belemnites. The hardgrounds are overlain by nodular limestones and marls with 50 to 70 wt-% carbonate of Middle and Late Oxfordian age (Padden et al., 2002). These beds are overlain by thin-bedded limestones and marl-limestone alternations dated as Kimmeridgian. The end of the Jurassic is dominated by limestones. These sediments indicate that the area of deposition was characteristic of an open-marine environment influenced by terrigenous input.

The sediment succession of the Subalpine Basin is exposed in south-eastern France, and was compiled from Louis et al. (submitted) and Seguret et al. (2001). During the Late Jurassic, the region was a deep epeiric basin collecting pelagic and detrital particles (Louis-Schmid et al., submitted). The Early and early Middle Oxfordian deposits correspond to the “Terres

noires", a clayey marlstone with 30 to 40 wt-% carbonate and up to 1.5% organic carbon (Tribovillard, 1988). From the Middle Oxfordian to the Kimmeridgian, sediments consist of bedded limestones and interbedded marls and limestones. The overlying lithology is composed of massive micritic limestone beds of Tithonian and Berriasian age.

7. Comparison of the sedimentation history in northern and southern Alpine Tethys

Comparable changes in sedimentation pattern are observed in the northern and southern margins of the Alpine Tethys (Fig. 11). Condensed sediments were deposited on the Trento Plateau and on the northern Tethyan Shelf at the beginning of the Late Jurassic. The onset

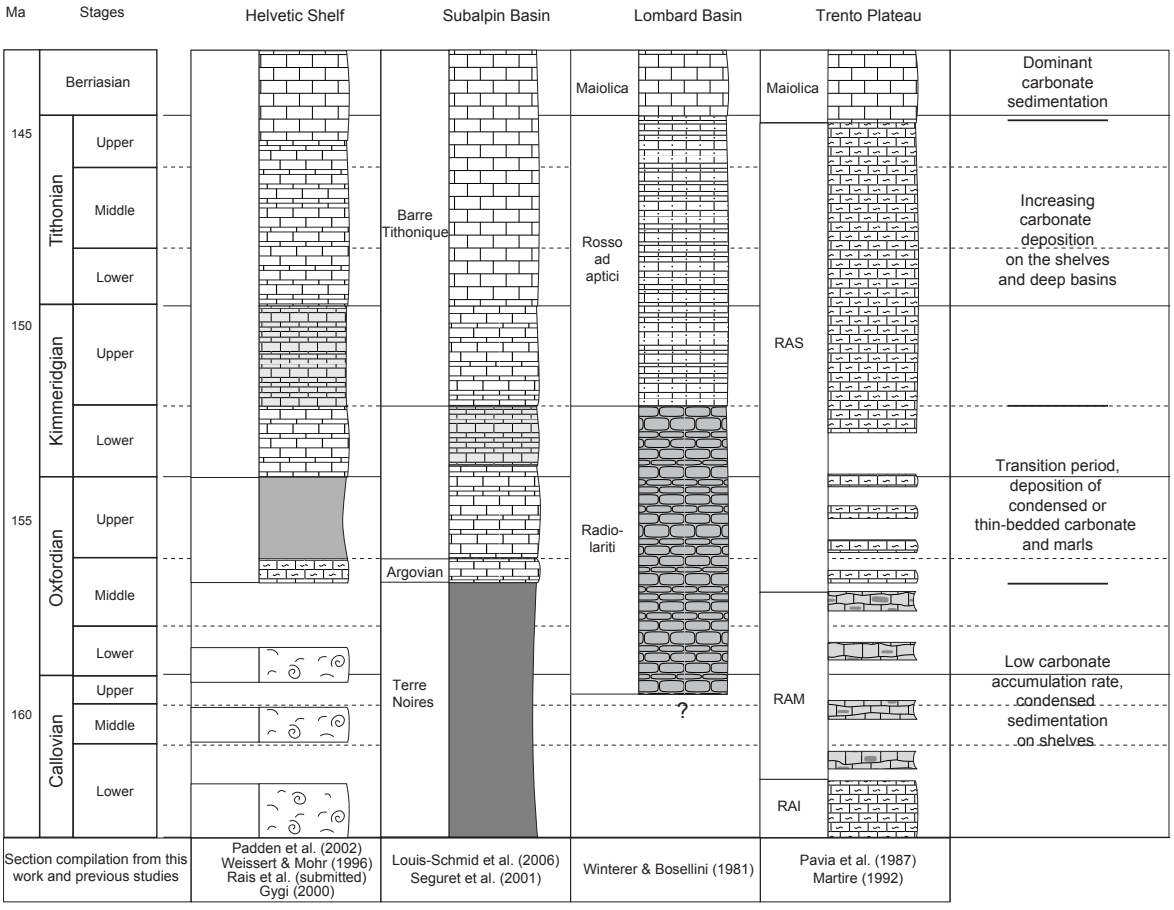

Figure 11:
Lithostratigraphical correlation of the sections from the northern and southern Alpine Tethys. This figure is not to scale.

of condensed sedimentation cannot be precisely determined due to the lack of information on the amount of sediment eroded. The end of the sediment condensation is clearly dated as Middle Oxfordian on the northern Tethyan Shelf (Rais et al., submitted). On the Trento Plateau, sediment accumulation rates also increased during the Middle Oxfordian. However, the sedimentation remained very reduced in most of the sections until the Kimmeridgian.
The second correspondence between the northern and southern sedimentation history is the evolution from low carbonate accumulation rates at the beginning of the Late Jurassic to a sedimentation dominated by carbonate in latest Jurassic times. The Early Oxfordian and the first part of the Middle Oxfordian are characterized by low carbonate accumulation rates: clayey marls were deposited in the Subalpine Basin, radiolarian ooze in the Lombardian Basin, and sedimentation was condensed on sedimentary highs. Carbonate accumulation rates suddenly increased during the Middle Oxfordian on the northern Tethyan Shelf, in the Subalpine Basin and on the Trento Plateau, when nodular limestones and bedded-limestones were deposited. In the Lombardian Basin, the first limestones are dated by carbon isotope stratigraphy as Early Kimmeridgian. From the Early Kimmeridgian to the Tithonian, carbonate sedimentation increased in all paleoenvironments. Tithonian and Lower Berriasian sedimentation is largely dominated by limestones.

8. Late Jurassic paleoceanographic changes

The similar evolution of the sedimentation on the northern and southern margins of the Alpine Tethys suggests that the whole region was affected by oceanographic changes. The presence of hardgrounds and long sedimentary gaps on the northern margin testify of a strong shelf current activity at the beginning of the Late Jurassic (Rais et al., submitted). Sedimentological features of the hardgrounds such as rounded iron ooids and reworked rock fragments, and the similarity to modern hardgrounds forming under strong oceanic currents along Australian shelves (Isern et al., 2001; James et al., 2001) confirm the presence of intense currents (Rais et al., submitted). Strong oceanic currents were active during a large part of the Callovian and the Early Oxfordian. The increase of sediment accumulation rates at the end of the Plicatilis ammonite Zone (Middle Oxfordian) indicates a decrease of current strength on the northern Tethyan Shelf (Rais et al., submitted). On the southern margin, oceanic currents were continuously sweeping the Trento Plateau from the Bajocian to the Tithonian (Martire, 1992; Ogg, 1981). However, the extreme condensation of the RAM (Martire, 1996) also suggests an intensification of current activity during the same time interval as on the northern margin, from the Callovian to the Middle Oxfordian.

Carbon-isotope stratigraphy indicates that in the Lombardian Basin the first limestones overlying the radiolarites are of Early Kimmeridgian age. Two reasons can explain the younger age of the increase in carbonate accumulation rates in the Lombardian Basin compared to the northern margin and the Trento Plateau: 1) The Lombardian basin was less sensitive to changes in carbonate production than shallower environments due to its deeper depositional environment, situated near the calcite compensation depth (Steinmann, 1905; Winterer and Bosellini, 1981). 2) The Middle Oxfordian age from Baumgartner (1987) based on radiolarian stratigraphy is more accurate. Carbon-isotope stratigraphy could not document the period spanning from Middle Oxfordian to Early Kimmeridgian due to presence of a gap between this two formations.

The important deposits of radiolarians cherts in the Lombardian Basin and on the Trento Plateau indicate the presence of upwelling currents creating areas of nutrient-rich surface waters, where siliceous organisms preferentially develop (De Wever and Baudin, 1996; Hsu, 1975; Muttoni et al., 2005). A recent study by Muttoni et al. (2005), concluded that the decline of upwelling currents, triggering the weakening of radiolarians and the development calcareous nannofossils, was caused by the migration of the Adria Plate out of the near-equatorial upwelling zone. Even if this hypothesis cannot be excluded, our data suggest that the decline of upwelling currents was part of a more global reorganization of ocean circulation. The onset of the carbonate-dominated sedimentation on both margins and the synchronous changes in ocean currents indicate a large-scale alteration of oceanic conditions. Moreover, several studies from different regions have reported similar changes in sedimentation and in oceanic current patterns, but also in climate during the same period (Abbink et al., 2001; Aberhan, 2001; Dromart et al., 2003; Hotinski and Toggweiler, 2003; Leinfelder et al., 2002). Therefore, we propose that the changes in sedimentation pattern observed on the southern margin of the Alpine Tethys during the Late Jurassic are an expression of a global reorganization of oceanic currents and climate, creating favorable conditions for the development of calcareous nannofossils at the end of the Jurassic.

References:

Abbink, O., Targarona, J., Brinkhuis, H. and Visscher, H., 2001. Late Jurassic to earliest Cretaceous palaeoclimatic evolution of the southern North Sea. Global and Planet. Change, 30(3-4): 231-256.

Aberhan, M., 2001. Bivalve palaeobiogeography and the Hispanic Corridor; time of opening and effectiveness of a proto-Atlantic seaway. Palaeogeogr., Palaeoclimatol., Palaeoecol., 165(3-4): 375-394.

Aghib, F.S., Bernoulli, D. and Weissert, H., 1991. Hardground formation in the Bannock Basin, eastern Mediterranean. In: B. Cita Maria, J. de Lange Gert and E. Olausson (Editors), Anoxic basins and sapropel deposition in the eastern Mediterranean; past and present. Mar. Geol., pp. 103-113.

Baumgartner, P.O., 1987. Age and genesis of Tethyan Jurassic radiolarites. Eclogae Geol. Helv., 80(3): 831-879.

Beccaro, P., 2002. Radiolarian biostratigraphy of Middle-Upper Jurassic pelagic siliceous successions of Western Sicily and Southern Alps (Italy), Università di Firenze, Firenze.

Benigni, C., Casati, P. and Radrizzani, C.P., 1982. Stratigrafia del giurassico dei dintorni di Foza (Altopiano di Asiago). Rivista Ita. Paleonto. Strati., 88(1): 45-74.

Bernoulli, D. and Jenkyns, H.C., 1974. Alpine, Mediterranean, and central Atlantic Mesozoic facies in relation to the early evolution of the Tethys, Modern and Ancient Geosynclinal Sedimentation; Deep-sea pelagic sediments and ophiolite assemblages. Soc. Econ. Paleonto. and Mineralo., Special Publication, pp. 129-160.

Bosellini, A., Masetti, D. and Sarti, M., 1981. A Jurassic "Tongue of the Ocean" infilled with oolitic sands; the Belluno Trough, Venetian Alps, Italy. In: B. Cita Maria and B.F. Ryan William (Editors), Carbonate platforms of the passive-type continental margins. Mar. Geol., pp. 59-95.

Cobianchi, M., 2002. I nannofossili calcarei del Giurassico medio e superiore del Bacino di Belluno (Alpi Calcaree Meridionali). Atti Ticine. Sci. Terra, 43: 3-24.

De Wever, P. and Baudin, F., 1996. Palaeogeography of radiolarite and organic-rich deposits in Mesozoic Tethys. Geol. Rundschau, 85(2): 310-326.

Dromart, G. et al., 2003. Perturbation of the carbon cycle at the Middle/ Late Jurassic transition; geological and geochemical evidence. Am. J. Sci., 303(8): 667-707.

Gradstein, F.M., Ogg, J.G., Smith, A.G., Bleeker, W. and Lourens, L.J., 2004. A new geologic time scale, with special reference to Precambrian and Neogene. Episodes, 27(2): 83-100.

Gygi, R.A. and Persoz, F., 1986. Mineralostratigraphy, litho- and biostratigraphy combined in correlation of the Oxfordian (Late Jurassic) formations of the Swiss Jura Range. Eclogae Geol. Helv., 79(2): 385-454.

Hotinski, R.M. and Toggweiler, J.R., 2003. Impact of a Tethyan circumglobal passage on ocean heat transport and "equable" climates. Paleoceanography, 18(1): 7.

Hsu, K.J., 1975. Paleoceanography of the Mesozoic Alpine Tethys. Geology (Boulder), 3(6): 347-348.

Hsu, K.J., 1976. Paleoceanography of the Mesozoic Alpine Tethys. GSA, Special Paper, 170.

Isern, A.R. et al., 2001. Sites 1196 and 1199. Correlation of deep sea sediments and forereef carbonates in the Red Sea; an important clue for basin analysis. The Marion plateau carbonates (NE Australia); a platform-slope-shelf edifice shaped by sea level change and ocean currents. In: R. Isern Alexandra et al. (Editors), Proceedings of the Ocean Drilling Program; initial reports; constraining Miocene sea level change from carbonate platform evolution, Marion Plateau, Northeast Australia; covering Leg 194 of the cruises of the drilling vessel JOIDES Resolution, Townsville, Australia, to Apra Harbor, Guam, sites 1192-1199, 3 January-2 March 2001. Mar. Geol., pp. 255-267.

Jacquin, T., Dardeau, G., Durlet, C., de, G.P.C. and Hantzpergue, P., 1998. The North Sea cycle; an overview of 2nd-order transgressive/ regressive facies cycles in Western Europe. In: C. de Graciansky Pierre, J. Hardenbol, T. Jacquin and R. Vail Peter (Editors), Mesozoic and Cenozoic sequence stratigraphy of European basins. Soc. Sed. Geol., Special Publication, pp. 445-466.

James, N.P., Bone, Y., Collins, L.B. and Kyser, T.K., 2001. Surficial sediments of the Great Australian Bight; facies dynamics and oceanography on a vast cool-water carbonate shelf. J. Sediment. Res., 71(4): 549-567.

Jenkyns, H.C., Jones, C.E., Groecke, D.R., Hesselbo, S.P. and Parkinson, D.N., 2002. Chemostratigraphy of the Jurassic system; applications, limitations and implications for palaeoceanography. J. Geol. Soc. London, 159 Part 4: 351-378.

Kugler, C., 1987. Die Wildegg Formation im Ostjura und die Schilt-Formation um oestlichen Helvetikum; ein Vergleich. Mitteilungen aus dem Geologischen Institut der Eidgenoessischen Technischen Hochschule und der Universitaet Zuerich, Neue Folge, 259. Geologischen Institut der Eidgenoessischen Technischen Hochschule: Universitaet Zuerich, Zurich, Switzerland, 209 pp.

Leinfelder, R.R., Schmid, D.U., Nose, M. and Werner, W., 2002. Jurassic reef patterns; the expression of a changing globe. In: W. Kiessling, E. Fluegel and J. Golonka (Editors), Phanerozoic reef patterns. Soc. Sediment. Geol. (SEPM). Tulsa, US.

Louis-Schmid, B., 2006. Feedback mechanisms between carbon cycling, climate and oceanography: a combined geochemical, sedimentological and modeling approach, ETHZ, Zurich.

Louis-Schmid, B. et al., submitted. The Oxfordian, a major turning point in Mesozoic oceanography: new evidence from high-resolution carbon-isotope records. Palaeogeogr., Palaeoclimatol., Palaeoecol.

Marshall, J.D. and Ashton, M., 1980. Isotopic and trace element evidence for submarine lithification of hardgrounds in the Jurassic of eastern England. Sedimentology, 27(3): 271-289.

Martire, L., 1989. Analisi biostratigrafica e sedimentologica del Rosso Ammonitico Veronese dell'Altopiano di Asiago, University of Torino, Torino, 166 pp.

Martire, L., 1992. Sequence stratigraphy and condensed pelagic sediments; an example from the Rosso Ammonitico Veronese, northeastern Italy. Palaeogeogr., Palaeoclimatol., Palaeoecol., 94(1-4): 169-191.

Martire, L., 1996. Stratigraphy, facies and synsedimentary tectonics in the Jurassic Rosso Ammonitico Veronese (Altopiano di Asiago, NE Italy). Facies, 35: 209-236.

Mutti, M. and Bernoulli, D., 2003. Early marine lithification and hardground development on a Miocene ramp (Maiella, Italy); key surfaces to track changes in trophic resources in nontropical carbonate settings. J. Sediment. Res., 73(2): 296-308.

Muttoni, G., Erba, E., Kent, D.V. and Bachtadse, V., 2005. Mesozoic Alpine facies deposition as a result of past latitudinal plate motion. Nature (London), 434(3378): 59-62.

Ogg, J.G., 1981. Middle and Upper Jurassic sedimentation history of the Trento Plateau (northern Italy). In: A. Farinacci and S. Elmi (Editors), Rosso Ammonitico symposium., pp. 479-503.

Padden, M., Weissert, H., Funk, H., Schneider, S. and Gansner, C., 2002. Late Jurassic lithological evolution and carbon-isotope stratigraphy of the western Tethys. Eclogae Geol. Helv., 95: 333-346.

Pavia, G., Benetti, A. and Minetti, C., 1987. Il Rosso Ammonitico dei Monti Lessini Veronesi (Italia NE), faune ad ammoniti e discontinuita stratigrafiche nel Kimmeridgiano inferiore. Boll. Soc. Paleonto. Italiana, 26(1-2): 63-92.

Rais, P., Louis-Schmid, B., Bernasconi, S.M. and Weissert, H., submitted. Paleoceanographic and paleoclimatic reorganization around the Middle-Late Jurassic transition. Palaeogeogr., Palaeoclimatol., Palaeoecol.

Seguret, M., Moussine, P.A., Gabaglia, G.R. and Bouchette, F., 2001. Storm deposits and storm-generated coarse carbonate breccias on a pelagic outer shelf (South-East Basin, France). Sedimentology, 48(2): 231-254.

Stampfli, G.M. and Borel, G.D., 2002. A plate tectonic model for the Paleozoic and Mesozoic constrained by dynamic plate boundaries and restored synthetic oceanic isochrons. Earth Planet. Sci. Lett., 196(1-2): 17-33.

Steinmann, G., 1905. Die geologische Bedeutung der Tiefseeabsätze und der ophiolthischen Massengesteine. Berichte Naturf. Gesell. Freiburg, 16: 44-65.

Thierry, J. et al., 2000a. Early Kimmeridgian (146-144 Ma). In: J. Dercourt et al. (Editors), Peri-Tethys atlas; palaeogeographical maps; explanatory notes.

Thierry, J. et al., 2000b. Middle Callovian (157-155 Ma). In: J. Dercourt et al. (Editors), Peri-Tethys atlas; palaeogeographical maps; explanatory notes.

Tribovillard, N.P., 1988. Geochimie organique et minerale dans les Terres Noires calloviennes et oxfordiennes du bassin dauphinois (France SE); Mise en evidence de cycles climatiques. Bull. Soc. Geol. France, Huitieme Serie, 4(1): 141-150.

Weissert, H., 1979. Die Paläoozeanographie der südwestlichen Tethys in der Unterkreide, ETH, Zurich, 174 pp.

Weissert, H. and Channell, J.E.T., 1989. Tethyan carbonate carbon isotope stratigraphy across the Jurassic-Cretaceous boundary; an indicator of decelerated global carbon cycling? Paleoceanography, 4(4): 483-494.

Weissert, H. and Mohr, H., 1996. Late Jurassic climate and its impact on carbon cycling. Palaeogeogr., Palaeoclimatol., Palaeoecol., 122(1-4): 27-43.

Winterer, E.L. and Bosellini, A., 1981. Subsidence and sedimentation on Jurassic passive continental margin, Southern Alps, Italy. AAPG Bulletin, 65(3): 394-421.

Ziegler, P.A., 1988. Evolution of the Arctic-North-Atlantic and the western Tethys. AAPG Memoir, 43. American Association of Petroleum Geologists, Tulsa, OK, United States, 198 pp.

CHAPTER 4

Late Jurassic changes in oceanography and climate as a result of plate tectonics.

Abstract

In this study, we use Tethyan sediments as archives of the evolution of Late Jurassic oceanography and climate. Based on different paleoenvironments from shallow northern Tethyan shelf to deep southern Alpine Tethys basin, we demonstrate that important changes in ocean circulation and marine productivity occurred during the Middle Oxfordian. The Lower Oxfordian was characterized by the deposition of radiolarian ooze and carbonate-poor ooze in deep basins, and by a strongly condensed sedimentation in shallower shelf environments. Carbonate accumulation rates increased during the Middle Oxfordian and developed progressively to a carbonate-dominated sedimentation at the end of the Jurassic in pelagic and shelf environments. A positive carbonate carbon-isotope excursion coincides with the mid-Oxfordian change in sedimentation pattern, which indicates that changes in oceanography were accompanied by a perturbation of the carbon cycle. We present new oxygen-isotope measurements on Oxfordian belemnites, which indicate almost stable sea-surface temperatures at low latitude. The observed changes in Late Jurassic sedimentation pattern and temperatures match the evolution of oceanography and climate predicted by model simulations of the opening of a low latitude seaway. The change in oceanography resulted in a dry low latitude climate and in warming restricted to high latitude environments. Based on these comparisons, we propose that the Late Jurassic changes are linked to the progressively opening Hispanic Corridor connecting western Tethys and Pacific, which triggered the onset of a circumglobal current and improved latitudinal heat exchange. The lowest Mesozoic $^{87}Sr/^{86}Sr$ values measured on mid-Oxfordian belemnites may be an expression of rapid fragmentation of Pangea.

Keywords:
Late Jurassic, Paleoceanography, Climate, Carbon isotopes, Strontium isotopes, Hispanic Corridor

1. Introduction

The breakup of the Pangea continent during Mesozoic times induced important changes in oceans and in continent configuration. The separation of Gondwana and Laurasia caused the opening of the Hispanic Corridor, connecting the western Tethys to the Pacific. The rapid decline in seawater strontium isotopes during the Jurassic, reaching the lowest values of the Mesozoic during the Oxfordian, attests of an accelerated hydrothermalism associated with a major pulse in tectonic activity (Jones et al., 1994; McArthur et al., 2001).

Several authors suggested that the oceanographic, climatic and sedimentologic changes occurring during the Late Jurassic were related to the reorganization of continental masses related to the fragmentation of Pangea (Moore et al., 1992a; Parrish, 1993; Hallam, 2001; Leinfelder et al., 2002; Hotinski and Toggweiler, 2003). Late Jurassic deposits are marked by a widespread switch from carbonate-poor to carbonate-rich sediments. Climate proxies record an increase of sea surface temperatures at high latitudes during the Middle Oxfordian (Riboulleau et al., 1998; Abbink et al., 2001; Dromart et al., 2003b; Lécuyer et al., 2003), and the development of arid conditions in the northern hemisphere (Hallam, 1985; Parrish, 1993; Abbink et al., 2001). Changes in climate are associated with a first order sea-level rise (Haq et al., 1988; Hallam, 2001) and altered oceanic circulation pattern. The carbon-isotope records also show strong perturbation of the carbon cycle during the Late Jurassic and an increase of pCO_2 was identified for this period (Louis-Schmid, 2006; Royer, in press 2006). These changes are comparable to the results of Hotinski & Toggweiler (2003), who simulated the impact of a Tethyan circumglobal passage on oceanography and climate. Their experiments using an ocean general circulation model reveal that the opening of a low latitude passage triggered a reorganization of ocean current pattern and the improvement of latitudinal heat exchange. They concluded that the Late Jurassic and Cretaceous temperatures were controlled by a circumequatorial ocean circulation coupled with high atmospheric CO_2 concentrations.

In this study, we investigate if changes in Late Jurassic sedimentation and climate can be related to the climate scenario presented by Hotinski & Toggweiler (2003). Sedimentological and geochemical methods were used to reconstruct in detail the evolution of Late Jurassic climate and ocean dynamics. The Alpine Tethys, a narrow seaway close to the opening Hispanic Corridor, was chosen for investigation. Well-dated sections along a transect from the northern to the southern margin of the Alpine Tethys were studied. We measured oxygen isotopes on belemnites to reconstruct Oxfordian temperature variations, and we tested if

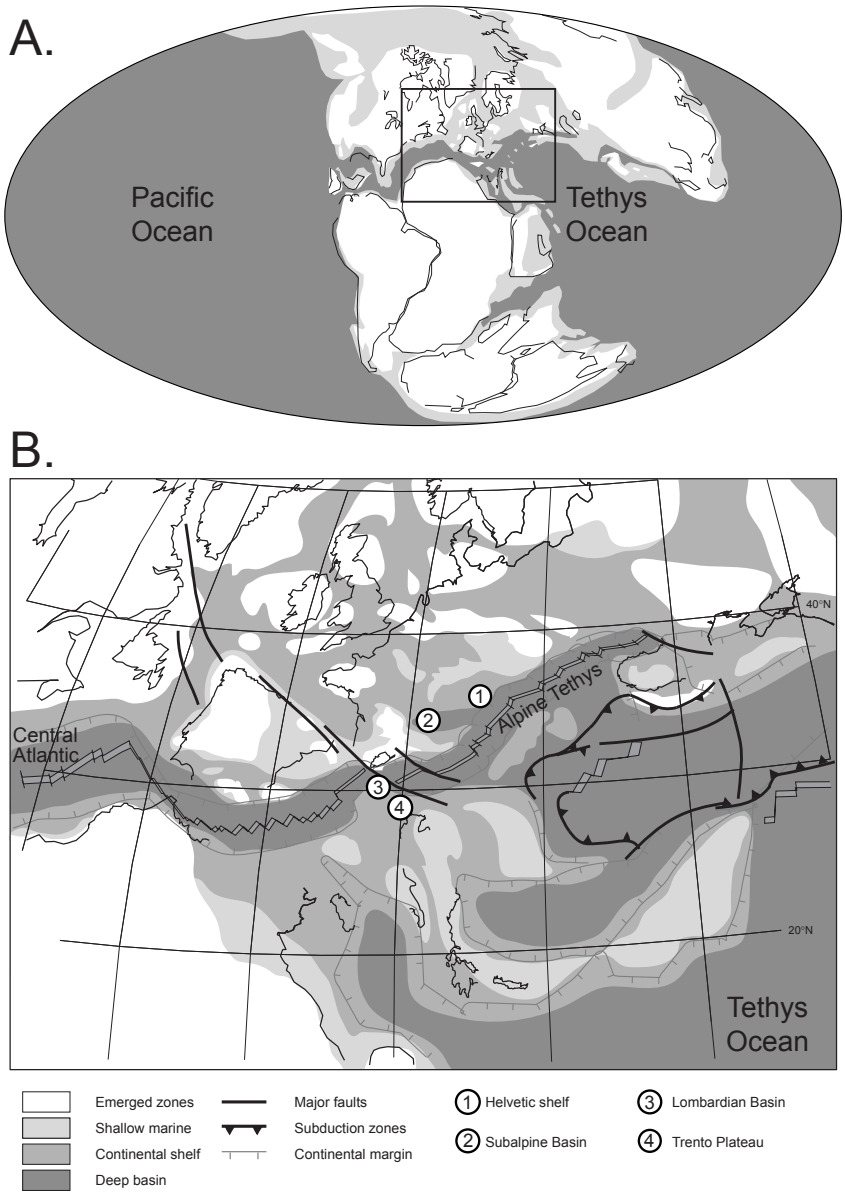

Figure 1:
A. Paleogeographic map of the Earth during the Kimmeridgian, after Vrielynck and Bouysse (2003) B. Paleogeographic map of the western Tethys during the Oxfordian, compiled and modified after Stampfli and Borel (2002) for continent position and tectonic symbols, Ziegler (1988) and Thierry et al. (2000) for depositional environments.

neodymium isotopes can be measured on the same material. Strontium isotope ratios of Oxfordian belemnites were determined using Laser Ablation ICPMS. We focused our research on the changes observed during the Oxfordian, and compared the findings with the global evolution of climatic and oceanographic conditions during Late Jurassic.

2. Geological setting

The sections chosen for this study are today located in Switzerland, France and northern Italy. The sediments were deposited along a northeast-southwest transect of the Alpine Tethys, which was connected in its western part to the Hispanic Corridor (Fig. 1). The Alpine Tethys was delimited in the north by a complex of deep epeiric basins, shallow seas and emerged lands of the Laurasian Plate (Ziegler, 1988), and in the south by the passive margin of the Adria, a promontory of the African Plate (Bernoulli and Jenkyns, 1974; Stampfli and Borel, 2002).

On the north side of the Alpine Tethys, the northern Tethyan Shelf and the Subalpine Basin were investigated. The northern Tethyan Shelf sections are preserved in the Jura Montains and in the Helvetic Domain of the Swiss Alps and consist of neritic sediments deposited on a shelf of about 100-200 m depth (Gygi and Persoz, 1986). The sediments from the Subalpine Basin are exposed in southeastern France. During the Late Jurassic, the region was a deep basin of up to 1000 m depth with high accumulation rates of hemi-pelagic sediments (Louis-Schmid et al., in press).

Two paleoenvironments from the southern margin of the Alpine Tethys, the Trento Plateau and the Lombardian Basin, were investigated. The sediments of the southern margin are preserved in the Southern Alps (north-western Italy). Situated at a water depth of about 1000m, the Trento Plateau was an exclusively pelagic domain swept by oceanic currents (Winterer and Bosellini, 1981). The Lombardian Basin, up to 2 km deep, was located west of the Trento Plateau in a more distal part of the southern continental margin. The depth of the basin floor and the variation of the Calcite Compensation Depth (CCD) during Jurassic have been intensively discussed (Hsu, 1975; Hsu, 1976; Winterer and Bosellini, 1981; Muttoni et al., 2005).

3. Methods

$\delta^{18}O$, $^{87}Sr/^{86}Sr$ and εNd analyses were performed on belemnites from the northern Tethyan Shelf. Some of these belemnites were collected during our field investigations, the others come from the collection of Reinhart Gygi in the Naturhistorisches Museum Basel (noted as RG). All belemnites were screened for diagenetic recrystallization using cold cathodoluminescence microscopy. Samples for analyses were extracted from the non-luminescent part of the belemnites. Oxygen isotope compositions of the belemnites were determined on a Thermo Delta V Plus mass spectrometer equipped with a Kiel IV

carbonate preparation module. Samples were reacted in 100% phosphoric acid at 70°C. The $\delta^{18}O$ is reported in the conventional delta-notation with respect to VPDB, as defined by the measurement of NBS 18 with $\delta^{13}C$= 1.95‰ and $\delta^{18}O$= -2.2‰. Analytical reproducibility of duplicate standard measurements (Carrara marble) is better than 0.1‰.

Strontium isotope compositions were measured using a Laser Ablation ICPMS at ETH Zurich. The diameter of laser shot points was set to 120 µm, and each sample was shot 15 times, with a shot duration of 50 seconds. For a detailed description of the method see Burla et al. (submitted).

Neodymium isotope measurements on belemnites were performed on a MC-ICPMS at CGS Strasbourg, using standard technique described in Steinmann & Stille (1997). Nd-isotope ratios were corrected using the La Jolla Standard (0.511843). Extraction and enrichment methods are described in Stille et al. (2006). Belemnites for analyses were cut in thin slices, polished, and examined under cathodoluminescence microscopy. The luminescent parts were removed using a microdrill, the center and the external part were systematically removed. The selected pieces were then soaked in an HCl 1% bath for 3 min. Neodymium isotopic analyses of shark teeth were performed on MC-ICPMS (Nu-instruments) at the University of Florida. Typical operating conditions are described in Chadwick et al. (2005). Results were corrected to the JNdi-1 value of 0.51210. External reproducibility was 0.00002, corresponding to 0.4 εNd units.

4. Results

Late Jurassic sedimentation pattern

Important changes in sedimentation occurred during the Late Jurassic in the Alpine Tethys (Fig. 2). In order to illustrate these changes, four composite sections, representative for the four studied paleoenvironments, were compiled from our own investigations (Louis-Schmid et al., in press; Rais et al., Submitted-a; Rais et al., submitted-b), and from previous stratigraphical studies (Winterer and Bosellini, 1981; Pavia et al., 1987; Martire, 1992; Weissert and Mohr, 1996; Seguret et al., 2001; Beccaro, 2002; Padden et al., 2002).

The sediments deposited along the Northern Tethyan Shelf from the Callovian to the Middle Oxfordian are extremely condensed and long sedimentary gaps have been identified by ammonite stratigraphy (Gygi and Persoz, 1986; Kugler, 1987). These condensed beds, defined as hardgrounds, consist of a bioturbated wackestone to packstone containing abundant fossils, iron ooids, and reworked hardground fragments redeposited as intraclasts (Rais et al., submitted-b). About six million years (Gradstein et al., 2004) are condensed

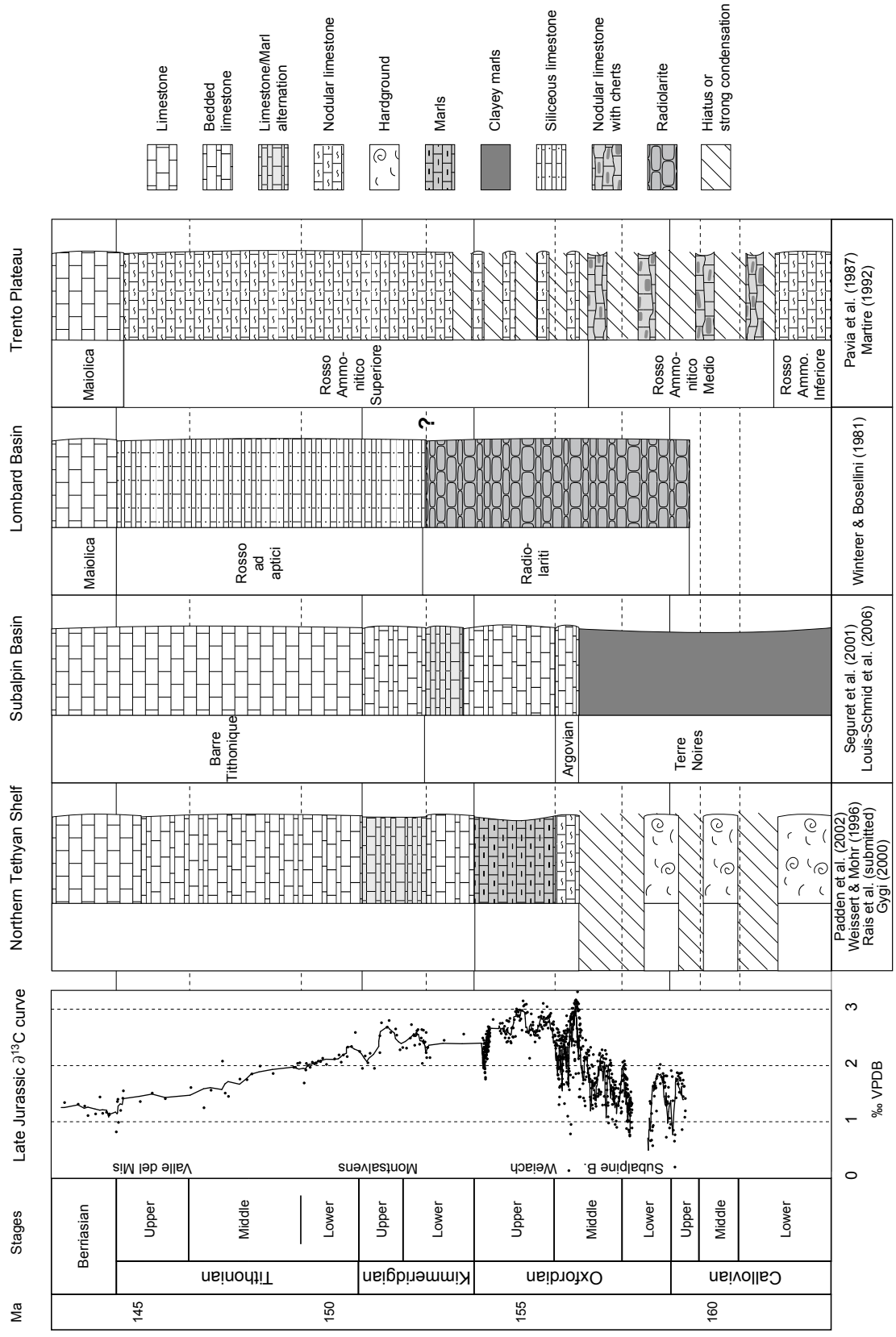
Limestone
Bedded limestone
Limestone/Marl alternation
Nodular limestone
Hardground
Marls
Clayey marls
Siliceous limestone
Nodular limestone with cherts
Radiolarite
Hiatus or strong condensation
Ma
Stages
Late Jurassic δ13C curve
Northern Tethyan Shelf
Subalpin Basin
Lombard Basin
Trento Plateau
Berriasian
Tithonian
Kimmeridgian
Oxfordian
Callovian
Upper
Middle
Lower
Valle del Mis
Montsalvens
Subalpine B.
Weiach
‰ VPDB
Barre Tithonique
Argovian
Terre Noires
Maiolica
Rosso ad aptici
Radio-lariti
Rosso Ammo-nitico Superiore
Rosso Ammo-nitico Medio
Rosso Ammo. Inferiore
?
Padden et al. (2002)
Weissert & Mohr (1996)
Rais et al. (submitted)
Gygi (2000)
Seguret et al. (2001)
Louis-Schmid et al. (2006)
Winterer & Bosellini (1981)
Pavia et al. (1987)
Martire (1992)

in a bed of a few decimeter thickness, indicating very low sediment accumulation rates. Hardgrounds are overlain by the nodular limestones and marls of the Schilt Formation at the end of the Plicatilis ammonite Zone (Middle Oxfordian) (Rais et al., submitted-b). The sediments deposited during the Kimmeridgian consist of bedded limestones and limestone and marl alternations (Gygi and Persoz, 1986; Mohr, 1992). Tithonian deposits are largely dominated by limestone (Mohr, 1992).

In the Subalpine Basin, the Callovian and Early Oxfordian deposits correspond to the "Terres noires", a clayey marlstone with 30 to 40 wt-% carbonate and up to 1.5% organic carbon (Tribovillard, 1988). A change in sedimentation also occurred during the Middle Oxfordian with the deposition of the thin-bedded limestones of the "Argovian" (Louis-Schmid et al., in press). Late Oxfordian and Kimmeridgian sediments consist of marlstones and limestones, and are overlain by massive limestones dated as Tithonian (Seguret et al., 2001 and reference therein).

The sediments deposited from the Callovian to the Early Kimmeridgian in the Lombardian Basin consist of almost carbonate-free radiolarites. The first siliceous limestone beds of the Rosso ad Aptici Formation are dated as late Early Kimmeridgian by carbon-isotope stratigraphy (Rais et al., Submitted-a), but as Middle Oxfordian by radiolarian stratigraphy (Baumgartner, 1987). The siliceous fraction decreases gradually upsection, and the transition to the almost pure limestones of the Maiolica Formation is dated as Late Tithonian (Winterer and Bosellini, 1981; Rais et al., Submitted-a).

On the Trento Plateau, the sedimentary sequence of the Middle and Late Jurassic, known as the Rosso Ammonitico Veronese Formation, consists of red nodular limestones. The sediment accumulation was extremely reduced, the formation spans from Bajocian to Tithonian and its thickness rarely exceeds 30 m (Martire, 1992). The presence of clear-cut surfaces often mineralized with iron and manganese oxides is evidence for interruption of sedimentation during long periods (Martire, 1992). Particularly low sediment accumulation rates are recorded in the middle part of the Rosso Ammonitico, spanning from Early Callovian to

←— **Figure 2:**
Late Jurassic composite $\delta^{13}C_{carb}$: Subalpine Basin (Louis-Schmid et al., submitted), Weiach (Rais et al., submitted-b), Montsalvens (Padden et al., 2002), and Valle del Mis (Weissert and Channell, 1989), and three point moving average curve. Late Jurassic lithostratigraphic correlation of the Northern Tethyan Shelf, the Subalpin Basin, the Lombardian Basin and the Trento Plateau. Blank below the Radiolariti Fm. indicates lack of age-significant fossils and possibly hiatuses. Lithologies of the northern Tethyan Shelf are not specified due to numerous different regional names.

Middle Oxfordian, which consists of nodular limestones and radiolarian chert layers (Rais et al., Submitted-a). The Rosso Ammonitico is overlain by the white limestones of the latest Tithonian Maiolica Formation.

Carbon-isotope stratigraphy

A composite $\delta^{13}C_{carb}$ curve was established for the Late Jurassic based on earlier published carbon-isotope data (Fig. 2). The Late Jurassic carbon-isotope record can be divided in three parts: 1) The first part, covering the Lower and the Middle Oxfordian, is characterized

Sample	Belemnite/ Shark teeth	Age	$\delta^{18}O$	Temp °C	87/86 Sr	Error	143/144 Nd 170Ma	εNd 170Ma	εNd Error
W 478.65 I	B	L.Call-E.Oxf	0.26	11.3	0.7068824	1.08E-05			
W 478.95	B	L.Call-E.Oxf	0.30	11.1	0.7068746	1.0327E-05			
W 479.5	B	L.Call-E.Oxf	0.35	10.9	0.7068973	8.2064E-06	0.51199	-8.40	1.6
W 478.39	B	L.Call-E.Oxf	0.15	11.7					
W 478.61-67 I	B	L.Call-E.Oxf	0.24	11.4					
W 478.86	B	L.Call-E.Oxf	0.34	11.0					
W 478.61-67 II	B	L.Call-E.Oxf	-0.04	12.5					
W 478.25	B	L.Call-E.Oxf	-0.69	15.2					
W 478.65 II	B	L.Call-E.Oxf	0.13	11.8					
RG 280/5a	B	Mariae	0.04	12.2					
RG 280/5b	B	Mariae	0.39	10.8					
RG 280/6b	B	Mariae	0.07	12.0	0.7068824	7.81E-06			
RG 280/7	B	Mariae	0.20	11.6	0.7068717	2.66E-05			
RG 280/7 15m	B	Mariae	-0.21	13.2					
RG 280/7 20m	B	Mariae	0.03	12.2					
RG 82/5	B	Cordatum	-0.05	12.5	0.7068445	5.05E-06			
RG 207/14a	B	Cordatum	-0.11	12.8	0.7068832	1.52E-05			
RG 207/14a	ST	Cordatum			0.7070205	1.60E-06	0.5122	-8.54	0.9
W 478.08	B	Cordatum	-0.23	13.3	0.7068318	8.07E-06	0.51197	-8.80	0.2
RG 280/7 49m	B	Cordatum	-0.33	13.7					
AU B2	B	Cordatum	0.03	12.2					
AU B3	B	Cordatum	-0.47	14.3					
AU B4	B	Cordatum	-0.12	12.8					
RG 212/7	ST	Plicatilis			0.7069960	1.10E-06	0.512204	-8.47	0.1
RG 81/14b	B	Plicatilis	0.05	12.1	0.7068756	9.8724E-06			
RG 207/16a	B	Plicatilis	-0.23	13.3	0.7068298	8.5367E-06			
RG 51/5	B	Plicatilis	-0.27	13.4	0.7068212	1.2102E-05			
RG 356/202	B	Plicatilis	-0.15	13.0	0.7068730	1.2258E-05			
RG 51/8	B	Plicat-Transv	0.02	12.3	0.7068311	9.76E-06			
W 474.23-28	B	Transversarium	0.09	12.0	0.7068626	8.08E-06			
RG 212/10	B	Transversarium	-0.10	12.8	0.7068758	1.3508E-05			
W 471.2	B	Transversarium	-0.63	14.9					
AU B6	B	Transversarium	-0.20	13.2					
MO B4	B	Transversarium	-0.48	14.3					
RG 276/502	B	Bifurcatus	-0.41	14.0	0.7068697	9.2456E-06			
RG 82/17	B	Bimamatum	-0.04	12.5	0.7068921	8.53E-06			

Table 1:
Oxygen, strontium, and neodymium isotope results from belemnites and shark teeth collected in northern Switzerland.

by a sharp increase from values around 1.5‰ to a maximum of 3.2‰ reached during the Transversarium ammonite Zone. 2) From the Middle Oxfordian to the Upper Kimmeridgian, $\delta^{13}C$ remained relatively high, ranging from 2‰ to 3‰. 3) The last period is characterized by a slow and regular decrease from 2.5‰ in the Upper Kimmeridgian to 1‰ at the end of the Upper Jurassic. The Late Jurassic curve is used for stratigraphical correlation between the northern and southern sections (Rais et al., Submitted-a; Rais et al., submitted-b).
This curve was compiled using the program AnalySeries 2.0.3 (Paillard et al., 1996) based on four Tethyan sections: a composite Subalpine Basin section (Louis-Schmid et al., in press), Weiach (Rais et al., submitted-b), Montsalvens (Padden et al., 2002), and Valle del Mis (Weissert and Channell, 1989). The time scale is based on Gradstein et al. (2004) and Jaquin et al. (1998).

Oxygen and carbon data from belemnites

Oxygen isotope values measured on Oxfordian belemnites range between -0.69‰ and 0.4‰ (Table 1, Fig. 3). The evolution of the average $\delta^{18}O$ per ammonite zone shows an increase of 0.52‰ from the Late Callovian to the Late Oxfordian. Isotopic results for belemnites of the same ammonite zone show a scatter of <1‰ for $\delta^{18}O$ and <2‰ for $\delta^{13}C$ (Table 1, Fig. 3). Comparable variations are frequently reported in the literature (Ditchfield et al., 1994; Price and Sellwood, 1997; Riboulleau et al., 1998), and can be explained by: 1) Variations of the

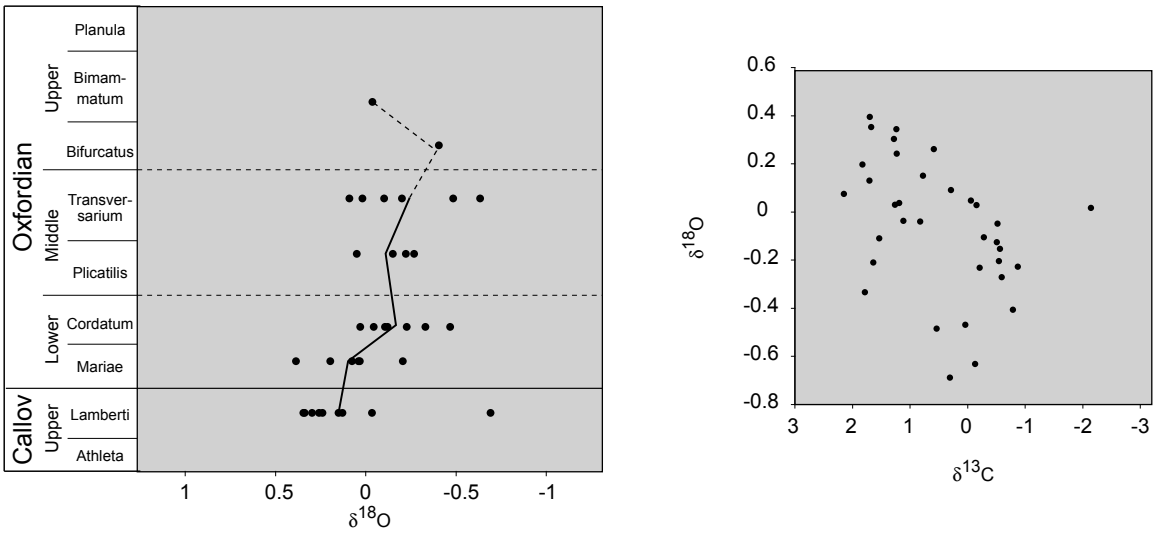

Figure 3:
Oxygen-isotope measurements on Oxfordian belemnites. $\delta^{18}O$ vs. age, the curve represents average $\delta^{18}O$ per ammonite zone. Crossplot of $\delta^{13}C$ vs. $\delta^{18}O$.

isotopic signal within the belemnite guard (Riboulleau et al., 1998), 2) Vital effect (Saelen et al., 1996) 3) Local temperature variations. We consider that the isotopic values measured on belemnites are not overprinted by diagenetic processes, as the samples were tested by cathodoluminescence microscopy, and $\delta^{18}O$ and $\delta^{13}C$ do not show any covariance (Fig. 3).

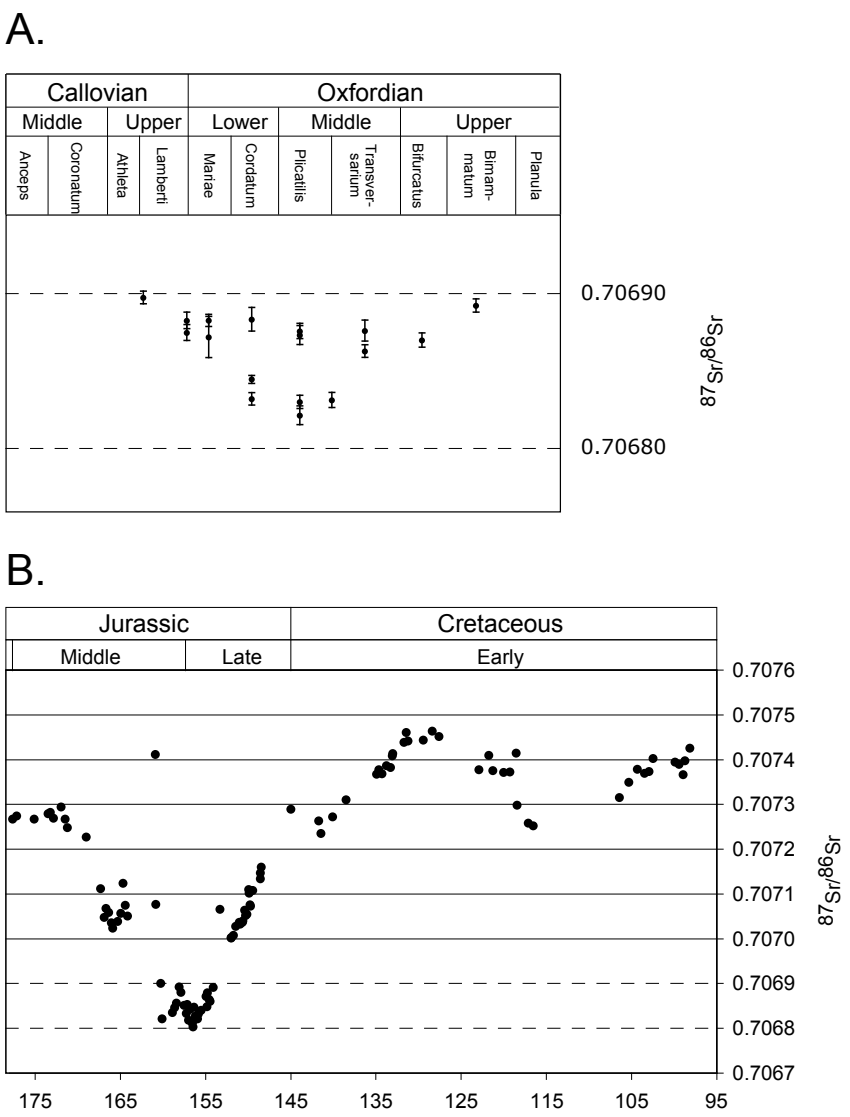

Figure 4:
A. Strontium isotope signal of the belemnites with error bars. B. Strontium isotope curve for Jurassic and Cretaceous after Jones et al. (1994).

Strontium isotopes

Strontium isotope analyses were performed on seventeen well-dated belemnites covering the Late Callovian and the Oxfordian (Table 1, Fig. 4A). The laser ablation method was used to extract only unaltered shell material. The $^{87}Sr/^{86}Sr$ results range between 0.706897 and 0.706821. The small data scatter during the Cordatum and Plicatilis ammonite Zones, is commonly observed in $^{87}Sr/^{86}Sr$ measurements and can be explained by a weak diagenetic alteration, which tends to increase the $^{87}Sr/^{86}Sr$ ratio (Burke et al., 1982; Jones et al., 1994). Therefore, the less radiogenic values are the best representative of original seawater values. Our results show a decrease from the Late Callovian to the Middle Oxfordian, followed by an increase from Middle to Late Oxfordian. The lowest values ($^{87}Sr/^{86}Sr$= 0.706821) are reached during the Plicatilis ammonite Zone.

Neodymium isotopes

Various studies have shown that water masses differ in their Nd-isotopic composition, owing the short residence time of the neodymium in the ocean (Piepgras et al., 1979; Stille et al., 1996). The main difficulty to obtain accurate Nd-isotope values is to find unaltered material carrying original seawater signal. It is established that fish teeth are a suitable material for Nd-isotope analyses (Vennemann et al., 1998; Martin and Haley, 2000; Martin and Scher, 2004), but they are very rare in the studied sediments. Therefore, Nd-isotope analyses were carried out on belemnites and were compared to shark tooth results of the same age and provenance (Table 1). The low concentration of neodymium in belemnites makes Nd-isotope analyses particularly difficult, and only two samples could be successfully measured. The results obtained for belemnites are εNd= -8.40 and εNd= -8.80. Strontium isotope values from these belemnites correspond to contemporaneous seawater values, indicating that the record has not been compromised by diagenetic alteration. The neodymium isotope results obtained from the shark teeth have values of εNd= -8.54 and εNd= -8.47 (Table 1). Strontium isotopes of shark teeth are more radiogenic than values of same age ($^{87}Sr/^{86}Sr$= 0.7070). It has been shown by Martin and Sher (2004) that $^{87}Sr/^{86}Sr$ values of the hydroxyapatite of fossil fish teeth can be altered through interactions with pore fluid Sr^{2+}. However, they concluded that a poor preservation of seawater strontium isotopes does not necessarily imply poor preservation of neodymium isotopes, due to their distinct geochemical behavior and to the low neodymium concentration in pore fluids. The difference between the shark tooth and the belemnite of the same age (Cordatum ammonite Zone, Early Oxfordian) is of 0.54 εNd units.

5. Discussion

Plate tectonics and timing of change

Sea-floor spreading and associated hydrothermal activity was accelerated during the Jurassic as mirrored by the continuous decrease of the seawater strontium isotope ratio starting in the Bajocian (Jones et al., 1994) (Fig. 4B). Based on $^{87}Sr/^{86}Sr$ measurements on belemnites, we documented that the lowest values of the Mesozoic were reached during the Plicatilis ammonite Zone, in the Middle Oxfordian (Fig. 4A), which represent a major pulse of hydrothermal activity. According to Jones (1994), the consecutive rise in strontium isotopes implies that the major phase of continental rifting had been completed, leaving normal fluctuations in mid-ocean ridge crustal generation rates. However, changing riverine strontium input associated to enhanced weathering cannot be ruled out (Weissert and Mohr, 1996).

Changes in plate tectonics during the Jurassic caused the opening of the Hispanic Corridor separating Eurasia and Gondwana (Fig. 1). Tectonics, associated with sea-level fluctuations determined the effectiveness of water transfer through the Hispanic Corridor. The first shallow water connection between the western Tethys and the Pacific Ocean is dated by bivalve and ammonite migration as Early Jurassic (Riccardi, 1991; Aberhan, 2001). The water circulation at that time was superficial, allowing only intermittent fauna exchange. A first order sea-level rise from the Bathonian to the Late Kimmeridgian (Haq et al., 1988) contributed significantly to the development of the seaway. Paleontologic evidence indicates that a wide seaway sufficiently deep for important water mass transfer was established during the Late Jurassic (Ager and Walley, 1977; Riccardi, 1991; Voros, 1993; Leinfelder et al., 2002). The seaway was further enlarged during the Cretaceous and reached its acme in the Late Cretaceous (Scotese, 2001; Hotinski and Toggweiler, 2003).

Late Jurassic sediments as an archive of paleoenvironmental change

Late Jurassic sediment successions reflect important changes in oceanography and marine productivity. The main changes in sedimentation occurred during the Middle Oxfordian, and were followed by a gradual increase of carbonate accumulation rates during the last part of the Late Jurassic (Rais et al., Submitted-a; Rais et al., submitted-b). An increase of sediment accumulation rates following a long period of condensation on the shallower environments coincided with a transition from a carbonate poor to a carbonate-dominated sedimentation. Along the northern Tethyan Shelf, in the Subalpine Basin and on the Trento Plateau,

sediments with low carbonate accumulation rates were replaced by nodular limestones, marls and thin-bedded limestones. Carbonate accumulation rates increased gradually from the Kimmeridgian in all paleoenvironments, and latest Jurassic sediments are largely dominated by limestones.

Carbon-isotope stratigraphy indicates a younger age for the increase of carbonate accumulation rates in the Lombardian Basin, the first siliceous limestone beds overlying the radiolarites are dated as late Early Kimmeridgian (Rais et al., Submitted-a). This difference can be attributed to the deep depositional environment of the basin, situated near the Late Jurassic CCD (Hsu, 1976; Winterer and Bosellini, 1981), thus less sensitive to changes in carbonate production compared to shallower environments, because of potential calcite dissolution. However, the Early Kimmeridgian age obtained from carbon-isotope stratigraphy is in contradiction with the radiolarian stratigraphy established by Baumgartner (1987), which indicates a Middle Oxfordian age for the transition from radiolarites to siliceous limestones. Therefore, we can not exclude that carbon isotopes did not record the period spanning from Middle Oxfordian to Early Kimmeridgian, due to a sedimentary gap.

The transition from a carbonate-poor to a carbonate-dominated sedimentation was not restricted to the Alpine Tethys, but appears to have been a widespread event (Dromart et al., 2003a). The Middle Oxfordian also corresponds to the worldwide rapid expansion of coral reefs (Leinfelder et al., 2002). Reefs are reported from high paleolatitudes (e.g. in Argentina and Japan). The carbonate sedimentation became dominant in pelagic environments during the Kimmeridgian-Tithonian, with the acceleration of nannofossil speciation (Roth, 1989).

The influence of a low latitude seaway on oceanography and climate: model results

Modifications of connections between oceanic basins have a strong influence on global climate and ocean circulation (e.g. Smith and Pickering, 2003), but also regionally on marine productivity and sediment production (e.g. Schneider and Schmittner, 2006). Based on experiments using an ocean general circulation model, Hotinski & Toggweiler (2003) showed that the presence of a low latitude passage has a significant impact on ocean circulation and global heat transport. In their model, the opening of the seaway triggers the replacement of equatorial gyres by a strong circumglobal westward flowing current. This ocean overturning promotes upwelling of large volume of cold water in the tropics, which provides a mechanism for strong export of heat from low latitudes to polar regions. This improvement of heat exchange triggers a warming at high latitudes, and consequently decreases latitudinal temperature gradients. By combining the opening of a low latitude gap with CO_2 concentrations six times higher than modern levels, they could reproduce Late

Jurassic and Cretaceous temperatures, and concluded in a warming of 7–11 °C of northern high latitudes, while tropical temperatures remained almost stable.
Moore et al. (1992a; 1992b) in their Kimmeridgian/Tithonian climate model also showed that the greatest warming occurred over the higher latitude oceans and the least over the equatorial and subtropical regions. They simulated two Late Jurassic paleoclimate models using 280 ppm CO_2 concentrations for one simulation and 1120 ppm for the other, and concluded that only the high pCO_2 model produces values corresponding to Late Jurassic paleotemperature records. In the following paragraphs, we compare climate simulations data with the results obtained from our investigation of Tethyan sediments.

Late Jurassic evidence for ocean current changes: Sediment data

Evidence for changes in ocean circulation during the Late Jurassic was found in the studied sediments. Sedimentological investigations on the Callovian-Oxfordian hardgrounds of the northern Tethyan Shelf reveal that they were formed under an intense oceanic current activity (Rais et al., submitted-b). Moreover, the sedimentological characteristics of the Jurassic condensed beds are similar to the modern hardgrounds of the Marion Plateau, offshore NE Australia (ODP leg 194), and on the Great Australian Bight "shaved shelf" (Isern et al., 2001; James et al., 2001; Rais et al., submitted-b), which are forming in a rather shallow carbonatic environment under strong oceanic currents. The observed increase in sediment accumulation rates during the Middle Oxfordian, is interpreted as an indicator of declining ocean current strength (Rais et al., submitted-b).
On the Trento Plateau the sedimentation rates are low throughout the Middle and Late Jurassic. As a submarine high, it was continuously swept by oceanic currents (Martire, 1992). The extremely reduced accumulation rates observed during the same time interval as on the northern margin (Callovian to Middle Oxfordian) also suggest an increased oceanic current activity (Ogg, 1981).
The deposition of radiolarian ooze in the Callovian-Oxfordian Lombardian Basin indicates the presence of nutrient-rich surface waters (De Wever and Baudin, 1996) associated with equatorial upwelling currents (Hsu, 1976; Muttoni et al., 2005). The transition from radiolarite to limestone reflects a regional decline of upwelling currents (Muttoni et al., 2005, Ogg, 1981; Rais et al., Submitted-a). The timing of this transition, Early Kimmeridgian according to carbon-isotope stratigraphy (Rais et al., Submitted-a) and Middle Oxfordian according to radiolarian stratigraphy (Baumgartner, 1987) is discussed above. If radiolarite stratigraphy is correct, change in CCD and in plankton ecology in basinal environments coincided with change in shallow current pattern. Previous works on fossil species distribution (Leinfelder et

al., 2002) and oxygen isotopes (Riboulleau et al., 1998) also indicate current pattern changes during the Middle Oxfordian, suggesting that this period experienced a global shift in ocean circulation (Rais et al., submitted-b; Rais et al., Submitted-a).
Neodymium isotopes were measured on belemnites and shark teeth to document these changes in oceanic circulation. However, due to the scarce appropriate material for analyses, the number of results obtained is insufficient for oceanic current pattern reconstruction, but the method is promising for further work. The εNd values of belemnites are similar to those of time-equivalent shark teeth (Table 1), suggesting that belemnites carry the original neodymium seawater signal. Oxfordian εNd values, ranging between -8.4 and -8.8, are close to continental crust values (Stille et al., 1996) and were possibly influenced by continental water masses mixed with riverine input.

Late Jurassic temperature variations: oxygen isotope data

In the models presented above, the onset of the circumglobal current has a strong impact on climate, and especially on high latitude temperatures. Oxfordian paleotemperatures for the northern Tethyan margin were calculated from $\delta^{18}O$ measurements on belemnites by applying the formula from Epstein et al. (1953) $T\ (°C)= 16.5–4.3(\delta_c–\delta_w)+0.14(\delta_c–\delta_w)^2$, where δ_c is the isotopic composition of the belemnites and $\delta_w = –1‰$ (SMOW) is chosen, which corresponds to the value for an ice-free world. Paleotemperatures range between 10.1°C and 15.2°C (Table 1). The evolution of the average temperatures per ammonite zone show a increase of 2°C from the Late Callovian to the Late Oxfordian (Fig.3). In order to estimate Oxfordian latitudinal temperature variations, our results are compared with temperature evolution at higher latitudes, determined from $\delta^{18}O$ measurements on belemnites from western Russia (Riboulleau et al., 1998; Veizer et al., 1999; Dromart et al., 2003a) and with a $\delta^{18}O$ record from the same latitude (30–35°N) measured on apatite enamel from fish teeth collected in eastern France and Switzerland (Dromart et al., 2003a; Lécuyer et al., 2003) (Fig. 5). All temperatures were calculated using $\delta_w = –1‰$. Both fish teeth and belemnites of subtropical latitudes show relatively stable temperatures throughout the Oxfordian. However, a difference of in average 6.4°C is observed between these two datasets. As diagenetic alteration of isotopic ratios has been excluded for both belemnites and fish teeth (Lécuyer et al., 2003), this difference can be attributed to distinct vital effects of the animals. It is commonly accepted that fish teeth record surface or near-surface water temperatures (Picard et al., 1998; Lécuyer et al., 2003), whereas for belemnites, the possible migration of the animals through the water column is largely unresolved (Spaeth et al., 1971; Jenkyns et al., 2002).

In contrast to the moderate temperature variations reported from subtropical latitudes, russian belemnites record an increase of 7 to 12°C during the Oxfordian, the maximum temperature increase occurring during Middle Oxfordian (Fig. 5). This temperature increase is confirmed by the migration of boreal ammonites to higher latitudes (Riboulleau et al., 1998 and references therein). Late Callovian to Middle Oxfordian temperatures from both regions were particularly low compared to recent sea-surface temperatures at the same latitudes (Lécuyer et al., 2003). This cold episode is extensively discussed by Dromart et al. (2003b). The temperature increase was accompanied by an extension of the arid climate

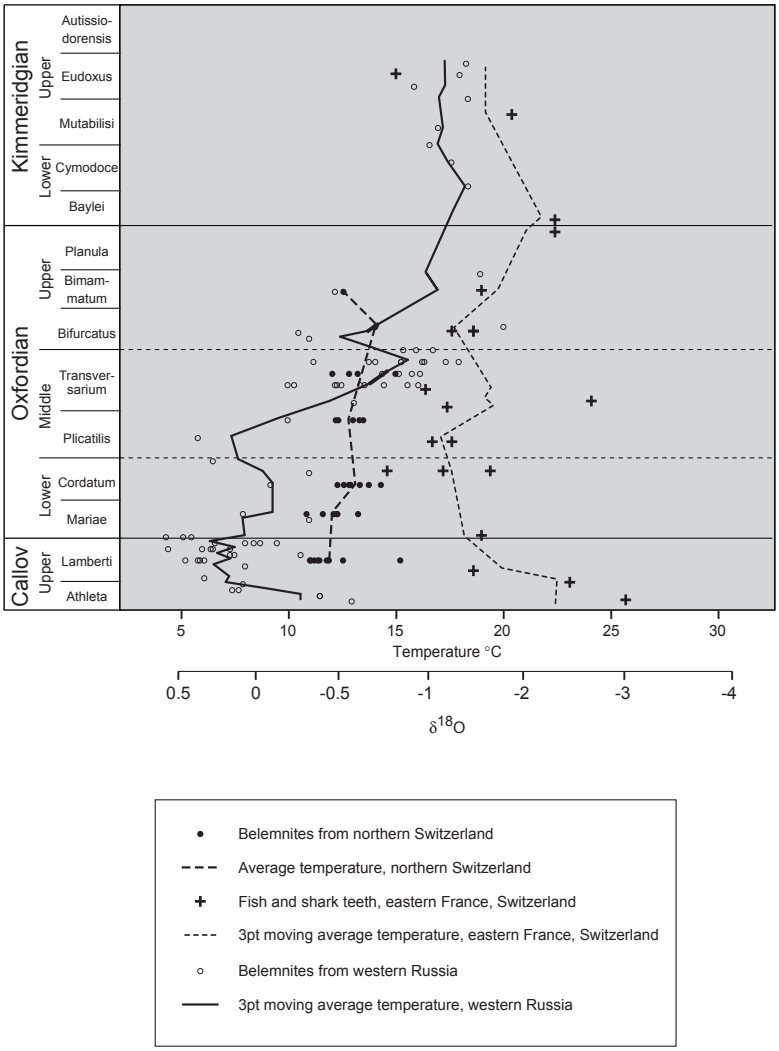

Figure 5:
Comparison of sea surface temperatures at ~30° latitude measured on belemnites, at the same latitude but measured on fish teeth, and at ~50° latitude measured on belemnites. Temperatures of fish teeth and russian belemnites are from Dromart et al. (2003a), compiled from Lécuyer (2003), Riboulleau et al. (1998) and Veizer et al. (1999).

belt in the northern hemisphere documented by evaporite and coal distribution (Hallam, 1985; Parrish, 1993). The change was gradual, and towards the end of the Late Jurassic arid conditions extended across the southern part of Eurasia. The more easterly parts of Laurasia and Gondwana, and high latitudes were persistently humid (Hallam, 1985; Moore et al., 1992a; Moore et al., 1992b). An increase in aridity during the Oxfordian is also documented in the North Sea and in France by studies on palynology and clay mineralogy (Rioult et al., 1991; Abbink et al., 2001; Hautevelle, 2005).
The warming of 7 to 12°C of high-latitude waters and the moderate temperature variations at lower latitude during the Middle Oxfordian match model simulations of the opening of a low latitude passage (Hotinski and Toggweiler, 2003). A 7 to 11 °C increase of high latitude waters was simulated in the model including high atmospheric CO_2 concentrations.

Late Jurassic pCO_2 reconstructions

Climate model simulations presented above suggest that Late Jurassic temperature increase was partly induced by high atmospheric pCO_2 (Moore et al., 1992a; Hotinski and Toggweiler, 2003). Louis-Schmid (2006) identified contrasting trends of $\delta^{13}C$ in carbonate and in organic matter (Fig. 6). Based on model simulations, he concluded that this divergence was due to an increase of atmospheric pCO_2 during the Middle Oxfordian from around 380 ppm to more than 600 ppm.
In addition to these results, we attempted to reconstruct pCO_2 levels for the Late Jurassic by comparing the composite Late Jurassic $\delta^{13}C_{carb}$ to marine organic-carbon isotope curve from the Kimmeridge Clay, England (Morgans et al., 2001; Jenkyns et al., 2002)(Fig. 6). Marine organic matter is largely dominant in the Kimmeridge Clay and variations in Total Organic Carbon (TOC) can be attributed to the addition of marine organic matter to a background of about 1% TOC of terrestrial inputs (Ramanampisoa and Disnar, 1994). The Early Kimmeridgian to Late Tithonian $\delta^{13}C_{org}$ record, shows values ranging from -27.8‰ and -23.6‰. The difference between $\delta^{13}C_{carb}$ and $\delta^{13}C_{org}$, noted as $\Delta\delta$ (Fig. 6), is an approximation of the ε_{TOC}, if the organic matter has a marine origin (Hayes et al., 1999). The ε_{TOC} is a function of the concentration of CO_2 in surface water, temperature, and various factors related to the physiology of primary producers (Hayes et al., 1999; Pagani, 2002). Louis-Schmid (2006) concluded that the $\Delta\delta$ increase observed in the Middle Oxfordian was essentially due to an increase in pCO_2. Assuming that pCO_2 is the main factor controlling the $\Delta\delta$ during that time, Late Jurassic pCO_2 trends can be divided in 1) a lower part from Early to Middle Oxfordian characterized by low values 2) a period of strong increase during the Middle Oxfordian, 3) relatively high pCO_2 from the Early Kimmeridgian to the Early Tithonian. These general

trends match the pCO_2 reconstructions of Royer et al. (Royer, in press 2006), which show an increase from 350 ppm to 859 ppm between the Callovian and the Kimmeridgian, followed by relatively high values during the Kimmeridgian and Tithonian (Fig. 6).

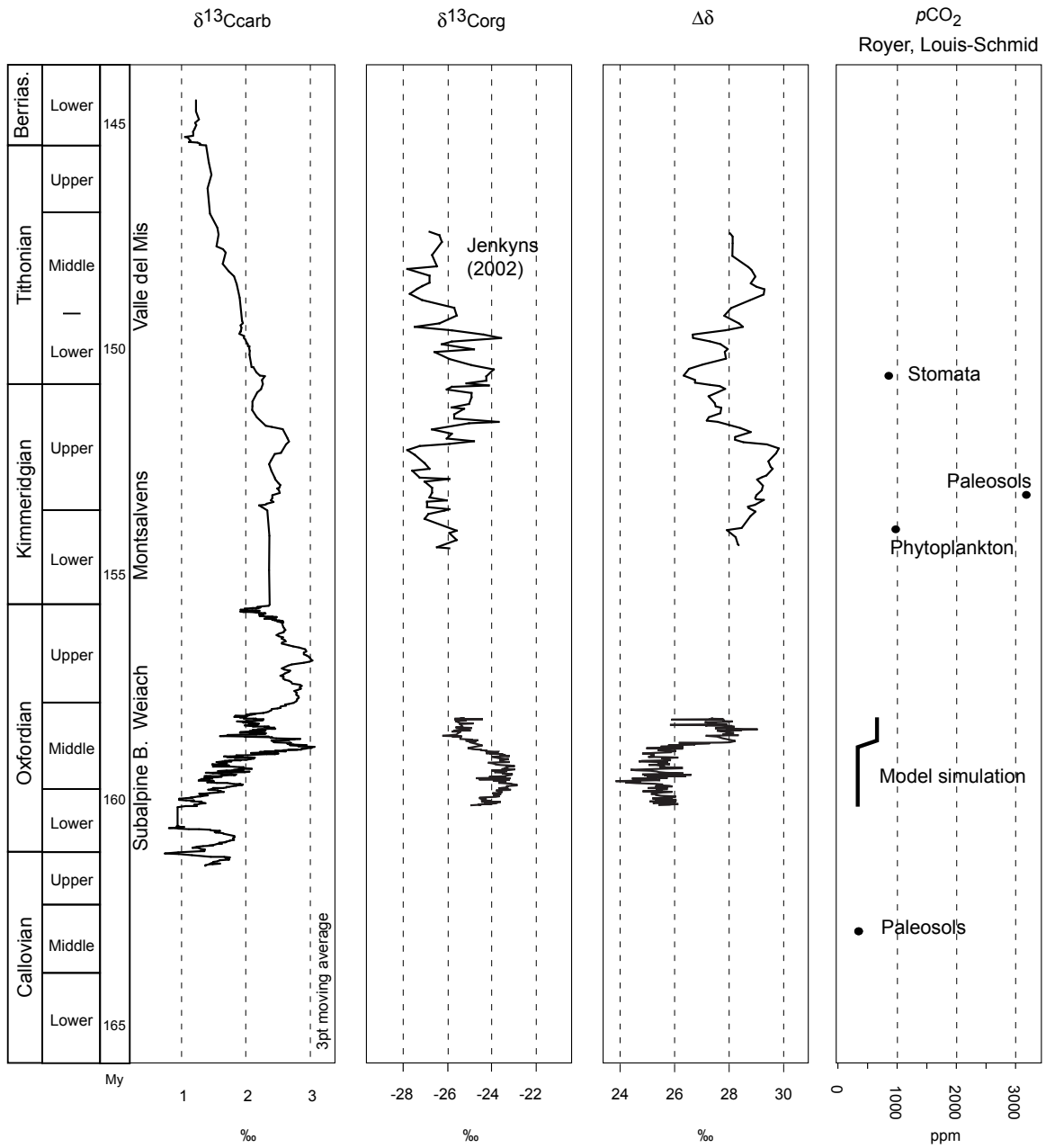

Figure 6:
$\delta^{13}C_{carb}$, $\delta^{13}C_{org}$, $\Delta\delta$ and pCO_2. Three point moving average from Late Jurassic composite $\delta^{13}C_{carb}$. $\delta^{13}C_{org}$ curves, lower part from the Subalpine Basin (Louis-Schmid, 2006), and upper part from England (Jenkyns et al., 2002). Calculated $\Delta\delta$ from $\delta^{13}C_{carb}$ and $\delta^{13}C_{org}$ curves. pCO_2 reconstructions: dots from Royer (in press 2006), and lines from Louis-Schmid (2006).

6. Conclusions

We propose that the Late Jurassic oceanic and climatic changes are related to the opening of the Hispanic Corridor, which was triggered by a major pulse of tectonic activity associated with a first order sea-level rise during the Jurassic. The Middle Oxfordian oceanographic and climatic changes are consistent with climate models simulating the opening of a low latitude passage. The shelf current pattern changes observed on both side of the Alpine Tethys, and the decline of upwelling current in the Lombardian basin may reflect the establishment of a circumglobal oceanic current. The moderate temperature variations at subtropical latitudes and the contrasting warming of 7 to 12°C of high-latitude waters during the Middle Oxfordian result of a combined effect of ocean current reorganization and increasing atmospheric CO_2 concentrations. The newly established climatic and paleoceanographic conditions favored the development of a calcareous organisms, which develop from the Middle Oxfordian and became dominant at the end of the Jurassic.

Acknowledgments

We thank Felix Oberli for assistance in the laboratory, Hellen Martin for Nd-isotope analyses at University of Florida, and the Naturhistorisches Museum Basel for providing us belemnites from the R. Gygi collection. Financial support from the Swiss Science Foundation is gratefully acknowledged.

References:

Abbink, O., Targarona, J., Brinkhuis, H. and Visscher, H., 2001. Late Jurassic to earliest Cretaceous palaeoclimatic evolution of the southern North Sea. Global and Planet. Change, 30(3-4): 231-256.

Aberhan, M., 2001. Bivalve palaeobiogeography and the Hispanic Corridor; time of opening and effectiveness of a proto-Atlantic seaway. Palaeogeogr., Palaeoclimatol., Palaeoecol., 165(3-4): 375-394.

Ager, D.V. and Walley, C.D., 1977. Mesozoic brachiopod migrations and the opening of the North Atlantic. Palaeogeogr., Palaeoclimatol., Palaeoecol., 21(2): 85-99.

Baumgartner, P.O., 1987. Age and genesis of Tethyan Jurassic radiolarites. Eclogae Geol. Helv., 80(3): 831-879.

Beccaro, P., 2002. Radiolarian biostratigraphy of Middle-Upper Jurassic pelagic siliceous successions of Western Sicily and Southern Alps (Italy), Università di Firenze, Firenze.

Bernoulli, D. and Jenkyns, H.C., 1974. Alpine, Mediterranean, and central Atlantic Mesozoic facies in relation to the early evolution of the Tethys, Modern and Ancient Geosynclinal Sedimentation; Deep-sea pelagic sediments and ophiolite assemblages. Special Publication - Soc. Econ. Paleont. Mineral., pp. 129-160.

Burke, W.H. et al., 1982. Variation of seawater (super 87) Sr/ (super 86) Sr throughout Phanerozoic time. Geology, 10(10): 516-519.

Burla, S., submitted. The timing of Early Cretaceous environmental changes in coastal settings of the North Atlantic: Implications from Sr-Isotope measurements using laser ablation.

Chadwick, J. et al., 2005. Magmatic effects of the Cobb hot spot on the Juan de Fuca Ridge.

De Wever, P. and Baudin, F., 1996. Palaeogeography of radiolarite and organic-rich deposits in Mesozoic Tethys. Geol. Rundschau, 85(2): 310-326.

Ditchfield, P.W., Marshall, J.D. and Pirrie, D., 1994. High latitude palaeotemperature variation; new data from the Tithonian to Eocene of James Ross Island, Antarctica. Palaeogeogr., Palaeoclimatol., Palaeoecol., 107(1-2): 79-102.

Dromart, G. et al., 2003a. Perturbation of the carbon cycle at the Middle/ Late Jurassic transition; geological and geochemical evidence. Am. J. Sci., 303(8): 667-707.

Dromart, G. et al., 2003b. Ice age at the Middle-Late Jurassic transition? Earth Planet. Sci. Lett., 213: 205-220.

Epstein, S., Buchsbaum, R., Lowenstam, H.A. and Urey, H.C., 1953. Revised carbonate-water isotopic temperature scale. Geol. Soc. Am. Bull., 64: 1315-1326.

Gradstein, F.M. et al., 2004. A geological time scale 2004. Miscellaneous Report - Geological Survey of Canada. 2004. Geological Survey of Canada, Ottawa, Canada.

Gygi, R.A. and Persoz, F., 1986. Mineralostratigraphy, litho- and biostratigraphy combined in correlation of the Oxfordian (Late Jurassic) formations of the Swiss Jura Range. Eclogae Geol. Helv., 79(2): 385-454.

Hallam, A., 1985. A review of Mesozoic climate. J. Geol. Soc. London, 142(3): 433-445.

Hallam, A., 2001. A review of the broad pattern of Jurassic sea-level changes and their possible causes in the light of current knowledge. Palaeogeogr., Palaeoclimatol., Palaeoecol., 167(1-2): 23-37.

Haq, B.U., Hardenbol, J. and Vail, P.R., 1988. Mesozoic and Cenozoic chronostratigraphy and cycles of sea-level change. In: K. Wilgus Cheryl et al. (Editors), Sea-level changes; an integrated approach. Soc. Econ. Paleonto. Mineralo., Special Publication. SEPM (Society for Sedimentary Geology), Tulsa, OK, United States, pp. 72-108.

Hautevelle, Y., 2005. Géochimie organique des série argilo-carbonatées du Callovo-Oxfordien de l'Est du bassin de Paris et d'Angleterre. Variabilités et implications paléoenvironnementales. Ph. D. Thesis Thesis, Université Henri Poincaré, Nancy.

Hayes, J.M., Strauss, H., Kaufman, A.J. and Canadian Institute for Advanced Research, s., 1999. The abundance of (super 13) C in marine organic matter and isotopic fractionation in the global biogeochemical cycle of carbon during the past 800 Ma. In: J. Veizer (Editor), Earth system evolution; geochemical perspective. Chem. Geol., pp. 103-125.

Hotinski, R.M. and Toggweiler, J.R., 2003. Impact of a Tethyan circumglobal passage on ocean heat transport and "equable" climates. Paleoceanography, 18(1): 7.

Hsu, K.J., 1975. Paleoceanography of the Mesozoic Alpine Tethys. Geology, 3(6): 347-348.

Hsu, K.J., 1976. Paleoceanography of the Mesozoic Alpine Tethys. GSA, Special Paper, 170.

Isern, A.R. et al., 2001. Sites 1196 and 1199. Correlation of deep sea sediments and forereef carbonates in the Red Sea; an important clue for basin analysis. The Marion plateau carbonates (NE Australia); a platform-slope-shelf edifice shaped by sea level change and ocean currents. In: R. Isern Alexandra et al. (Editors), Proceedings of the Ocean Drilling Program; initial reports; constraining Miocene sea level change from carbonate platform evolution, Marion Plateau, Northeast Australia; covering Leg 194 of the cruises of the drilling vessel JOIDES Resolution, Townsville, Australia, to Apra Harbor, Guam, sites 1192-1199, 3 January-2 March 2001. Mar. Geol., pp. 255-267.

Jacquin, T., Dardeau, G., Durlet, C., de, G.P.C. and Hantzpergue, P., 1998. The North Sea cycle; an overview of 2nd-order transgressive/ regressive facies cycles in Western Europe. In: C. de Graciansky Pierre, J. Hardenbol, T. Jacquin and R. Vail Peter (Editors), Mesozoic and Cenozoic sequence stratigraphy of European basins. Soc. Sed. Geol., Special Publication, pp. 445-466.

James, N.P., Bone, Y., Collins, L.B. and Kyser, T.K., 2001. Surficial sediments of the Great Australian Bight; facies dynamics and oceanography on a vast cool-water carbonate shelf. J. Sediment. Res., 71(4): 549-567.

Jenkyns, H.C., Jones, C.E., Groecke, D.R., Hesselbo, S.P. and Parkinson, D.N., 2002. Chemostratigraphy of the Jurassic system; applications, limitations and implications for palaeoceanography. J. Geol. Soc. London, 159 Part 4: 351-378.

Jones, C.E., Jenkyns, H.C., Coe, A.L. and Hesselbo, S.P., 1994. Strontium isotopic variations in Jurassic and Cretaceous seawater. Geochim. Cosmochim. Acta, 58(14): 3061-3074.

Kugler, C., 1987. Die Wildegg Formation im Ostjura und die Schilt-Formation um oestlichen Helvetikum; ein Vergleich. Ph. D. thesis Thesis, ETH Zurich, Zurich, Switzerland, 209 pp.

Leinfelder, R.R., Schmid, D.U., Nose, M. and Werner, W., 2002. Jurassic reef patterns; the expression of a changing globe. In: W. Kiessling, E. Fluegel and J. Golonka (Editors), Phanerozoic reef patterns. Soc. Sediment. Geol. (SEPM). Tulsa, US.

Louis-Schmid, B., 2006. Feedback mechanisms between carbon cycling, climate and oceanography: a combined geochemical, sedimentological and modeling approach. Ph. D. thesis Thesis, ETH Zurich, Zurich.

Louis-Schmid, B. et al., in press. Detailed record of the mid-Oxfordian (Late Jurassic) positive carbon-isotope excursion in two hemipelagic sections (France and Switzerland): a plate tectonic trigger? Palaeogeogr., Palaeoclimatol., Palaeoecol.

Lécuyer, C. et al., 2003. Thermal evolution of Tethyan surface waters during the Middle-Late Jurassic: Evidence from ∂ 18O values of marine fish teeth. Paleoceanography, 18(3): 1076.

Martin, E.E. and Haley, B.A., 2000. Fossil fish teeth as proxies for seawater Sr and Nd isotopes. Geochim. Cosmochim. Acta, 64(5): 835-847.

Martin, E.E. and Scher, H.D., 2004. Preservation of sea water Sr and Nd isotopes in fossil fish teeth; bad news and good news. Earth Planet. Sci. Lett., 220(1-2): 25-39.

Martire, L., 1992. Sequence stratigraphy and condensed pelagic sediments; an example from the Rosso Ammonitico Veronese, northeastern Italy. Palaeogeogr., Palaeoclimatol., Palaeoecol., 94(1-4): 169-191.

McArthur, J.M., Howarth, R.J. and Bailey, T.R., 2001. Strontium isotope stratigraphy; LOWESS Version 3; best fit to the marine Sr-isotope curve for 0-509 Ma and accompanying look-up table for deriving numerical age. J. Geol., 109(2): 155-170.

Mohr, H., 1992. Der helvetische Schelf der Ostschweiz am Ueberganng vom späten Jura zur frühen Kreide, Universität Zurich, 221 pp.

Moore, G.T., Hayashida, D.N., Ross, C.A. and Jacobson, S.R., 1992a. Paleoclimate of the Kimmeridgian/ Tithonian (Late Jurassic) world; I, Results using a general circulation model. Palaeogeogr., Palaeoclimatol., Palaeoecol., 93(1-2): 113-150.

Moore, G.T., Sloan, L.C., Hayashida, D.N. and Umrigar, N.P., 1992b. Paleoclimate of the Kimmeridgian/ Tithonian (Late Jurassic) world; II, Sensitivity tests comparing three different paleotopographic settings. Palaeogeogr., Palaeoclimatol., Palaeoecol., 95(3-4): 229-252.

Morgans, B.H.S. et al., 2001. Integrated stratigraphy of the Kimmeridge Clay Formation (Upper Jurassic) based on exposures and boreholes in South Dorset, UK. Geol. Magazine, 138(5): 511-539.

Muttoni, G., Erba, E., Kent, D.V. and Bachtadse, V., 2005. Mesozoic Alpine facies deposition as a result of past latitudinal plate motion. Nature, 434: 59-62.

Ogg, J.G., 1981. Middle and Upper Jurassic sedimentation history of the Trento Plateau (northern Italy). In: A. Farinacci and S. Elmi (Editors), Rosso Ammonitico symposium., pp. 479-503.

Padden, M., Weissert, H., Funk, H., Schneider, S. and Gansner, C., 2002. Late Jurassic lithological evolution and carbon-isotope stratigraphy of the western Tethys. Eclogae Geol. Helv., 95: 333-346.

Pagani, M., 2002. The alkenone-CO (sub 2) proxy and ancient atmospheric carbon dioxide. In: R. Groecke Darren and M. Kucera (Editors), Understanding climate change; proxies, chronology and ocean-atmosphere interactions.

Paillard, D., Labeyrie, L. and Yiou, P., 1996. Macintosh program performs time-series analysis. EOS Trans. AGU, 77: 379.

Parrish, J.T., 1993. Climate of the supercontinent Pangea. J. Geol., 101(2): 215-233.

Pavia, G., Benetti, A. and Minetti, C., 1987. Il Rosso Ammonitico dei Monti Lessini Veronesi (Italia NE), faune ad ammoniti e discontinuita stratigrafiche nel Kimmeridgiano inferiore. Boll. Soc. Paleonto. Italiana, 26(1-2): 63-92.

Picard, S. et al., 1998. delta (super 18) O values of coexisting brachiopods and fish; temperature differences and estimates of paleo-water depths. Geology, 26(11): 975-978.

Piepgras, D.J., Wasserburg, G.J. and Dasch, E.J., 1979. The isotopic composition of Nd in different ocean masses. Earth Planet. Sci. Lett., 45(2): 223-236.

Price, G.D. and Sellwood, B.W., 1997. "Warm" palaeotemperatures from high Late Jurassic palaeolatitudes (Falkland Plateau); ecological, environmental or diagenetic controls? Palaeogeogr., Palaeoclimatol., Palaeoecol., 129(3-4): 315-327.

Rais, P., Louis-Schmid, B., Bernasconi, S.M. and Weissert, H., Submitted-a. Links between the Late Jurassic radiolarite to limestone transition in the southern Alpine Tethys and the sedimentary evolution on the northern margin.

Rais, P., Louis-Schmid, B., Bernasconi, S.M. and Weissert, H., submitted-b. Paleoceanographic and paleoclimatic reorganization around the Middle-Late Jurassic transition. Palaeogeogr., Palaeoclimatol., Palaeoecol.

Ramanampisoa, L. and Disnar, J.R., 1994. Primary control of paleoproduction on organic matter preservation and accumulation in the Kimmeridge rocks of Yorkshire (UK). Organic Geochem., 21(12): 1153-1167.

Riboulleau, A. et al., 1998. Evolution de la paleotemperature des eaux de la plate-forme russe au cours du Jurassique superieur. C.R. Acad. Sci., Ser II, 326(4): 239-246.

Riccardi, A.C., 1991. Jurassic and Cretaceous marine connections between the Southeast Pacific and Tethys. In: E.T. Channell James, L. Winterer Edward and F. Jansa Lubomir (Editors), Palaeogeography and paleoceanography of Tethys. Palaeogeogr., Palaeoclimatol., Palaeoecol., pp. 155-189.

Rioult, M. et al., 1991. Outcrop sequence stratigraphy of the Anglo-Paris Basin, Middle to Upper Jurassic (Normandy, Maine, Dorset). Bull. Cent. Rech. Explor. Prod. Elf-Aquitaine, 15(1): 101-194.

Roth, P.H., 1989. Ocean circulation and calcareous nannoplankton evolution during the Jurassic and Cretaceous. In: L. Eicher Don and R. Diner (Editors), Biological paleoceanography; plankton, productivity and carbon in ancient marine systems, a selection of papers presented at the Fourth North American paleontological convention. Palaeogeogr., Palaeoclimatol., Palaeoecol., pp. 111-126.

Royer, D.L., in press 2006. CO2-forced climate thresholds during the Phanerozoic. Geochim. Cosmochim. Acta.

Saelen, G., Doyle, P. and Talbot, M.R., 1996. Stable-isotope analyses of belemnite rostra from the Whitby Mudstone Formation, England; surface water conditions during deposition of a marine black shale. Palaios, 11(2): 97-117.

Schneider, B. and Schmittner, A., 2006. Simulating the impact of the Panamanian seaway closure on ocean circulation, marine productivity and nutrient cycling. Earth Planet. Sci. Lett., 246(3-4): 367-380.

Scotese, C.R., 2001. Atlas of Earth History. Paleogeography, 1. PALEOMAP Project, Arlington, Texas, 52 pp.

Seguret, M., Moussine, P.A., Gabaglia, G.R. and Bouchette, F., 2001. Storm deposits and storm-generated coarse carbonate breccias on a pelagic outer shelf (South-East Basin, France). Sedimentology, 48(2): 231-254.

Smith, A.G. and Pickering, K.T., 2003. Oceanic gateways as a critical factor to initiate icehouse Earth. J. Geol. Soc. London, 160(3): 337-340.

Spaeth, C., Hoefs, J. and Vetter, U., 1971. Some aspects of isotopic composition of belemnites and related paleotemperatures. Geol. Soc. Am. Bull., 82(11): 3139-3150.

Stampfli, G.M. and Borel, G.D., 2002. A plate tectonic model for the Paleozoic and Mesozoic constrained by dynamic plate boundaries and restored synthetic oceanic isochrons. Earth Planet. Sci. Lett., 196(1-2): 17-33.

Steinmann, M. and Stille, P., 1997. Rare earth element behavior and Pb, Sr, Nd isotope systematics in a heavy metal contaminated soil. Applied Geochemistry, 12(5): 607-623.

Stille, P. et al., 2006. The impact of vegetation on REE fractionation in stream waters of a small forested catchment. Geochim. Cosmochim. Acta, 70: 3217-3230.

Stille, P., Steinmann, M. and Riggs, S.R., 1996. Nd isotope evidence for the evolution of the paleocurrents in the Atlantic and Tethys oceans during the past 180 Ma. Earth Planet. Sci. Lett., 144(1-2): 9-19.

Thierry, J. et al., 2000. Peri-Tethys atlas; palaeogeographical maps; explanatory notes.

Tribovillard, N.P., 1988. Geochimie organique et minerale dans les Terres Noires calloviennes et oxfordiennes du bassin dauphinois (France SE); Mise en evidence de cycles climatiques. Bull. Soc. Geol. Fr., Huitieme Serie, 4(1): 141-150.

Veizer, J. et al., 1999. 87Sr/86Sr, ∂ 13C and ∂ 18O evolution of Phanerozoic seawater. In: J. Veizer (Editor), Earth system evolution; geochemical perspective. Chem. Geol. Elsevier, Amsterdam, Netherlands, pp. 59-88.

Vennemann, T., Hegner, E. and Cliff, G., 1998. Oxygen, strontium and neodymium isotope geochemistry of shark teeth as proxies for paleoclimatology and paleooceanography; examples from Recent and Miocene teeth. In: H. Schroeder Johannes, G. Holl Heinz and A. Brunsmann (Editors), Geowissenschaften in Ekonomie und Ekologie; das System Erde. Terra Nostra (Bonn), pp. V376.

Voros, A., 1993. Jurassic microplate movements and brachiopod migrations in the western part of the Tethys. In: M.O. Mancenido (Editor), Brachiopod and molluscan biogeography, palaeoecology and stratigraphy; a tribute to Derek Ager. Palaeogeogr., Palaeoclimatol., Palaeoecol. Elsevier, Amsterdam, Netherlands, pp. 125-145.

Vrielynck, B. and Bouysse, P., 2003. The changing face of the earth: the break-up of Pangaea and continental drift over the past 250 million years in ten steps, Commission for the Geological Map of the World, Paris.

Weissert, H. and Channell, J.E.T., 1989. Tethyan carbonate carbon isotope stratigraphy across the Jurassic-Cretaceous boundary; an indicator of decelerated global carbon cycling? Paleoceanography, 4(4): 483-494.

Weissert, H. and Mohr, H., 1996. Late Jurassic climate and its impact on carbon cycling. Palaeogeogr., Palaeoclimatol., Palaeoecol., 122(1-4): 27-43.

Winterer, E.L. and Bosellini, A., 1981. Subsidence and sedimentation on Jurassic passive continental margin, Southern Alps, Italy. AAPG Bulletin, 65(3): 394-421.

Ziegler, P.A., 1988. Evolution of the Arctic-North-Atlantic and the western Tethys. AAPG Memoir, 43. American Association of Petroleum Geologists, Tulsa, OK, United States, 198 pp.

CHAPTER 5

Distribution of authigenic albites in a limestone succession of the Helvetic Domain, eastern Switzerland.

Abstract

A new occurrence of authigenic albite was found in a Jurassic sedimentary succession of the Glarus Nappe near Walenstadt (eastern Switzerland). The euhedral shape and the chemical purity of these albites are evidence for their authigenic origin. The crystals are irregularly distributed in the sediment, highlighting the importance of the host rock composition for albite authigenesis. The crystals occur exclusively in limestones with a carbonate content higher than 80 wt-%. A diagenetic or hydrothermal origin of albite authigenesis is discussed for the studied region. Clay mineral transformation appears to be an important source of ions for albite formation.

Keywords:
Authigenic albite, Glarus Nappe, diagenetic processes

Submitted to Eclogae Geologicae Helvetiae as: P. Rais, B. Louis-Schmid, S. M. Bernasconi, E. Reusser and H. Weissert. Distribution of authigenic albites in a limestone succession of the Helvetic Domain, eastern Switzerland.

1. Introduction

Authigenic albites grow during the low-temperature burial of sedimentary rocks. They differ from detrital albites by their euhedral crystal shape, their high chemical purity, and their uncommon crystallographic properties (Füchtbauer, 1948). The occurrence of these albites is scarce and the exact processes controlling their formation remain unclear.

The specific features and the growth conditions of authigenic albites in carbonates were summarized by Kastner & Siever (1979), and more recently by Spoetl et al. (1999). They showed that authigenic albites preferentially grow in carbonate rocks, forming well-crystallized grains, with a common size of 60 to 120 μm. Their size increases with increasing burial temperature, and can reach up to 10 mm in rocks that experienced epizonal conditions (Richter, 1978; Brauckmann, 1984; Spoetl et al., 1999). Contrary to albites of igneous origin, authigenic albites show a peculiar twinning called "Roc Tourné", which is a combination of X-Carlsbad and albite twins (Rose, 1865; Füchtbauer, 1948).

Electron microprobe analyses show that authigenic albites tend to be nearly pure end-members of the plagioclase feldspar series with only very low anorthite and orthoclase component (Kastner and Siever, 1979). This high chemical purity is responsible for the lack of light emission in cold cathodoluminescence microscopy. However, by using a hot-cathode equipment, Richter et al. (2002) were able to show a weak luminescence emission, due to the activation of Mn^{2+} and Fe^{3+}.

In this study, we document for the first time the occurrence of authigenic albite in a Jurassic limestone of the Glarus Nappe (eastern Swiss Alps). We describe the albite distribution from a regional to a thin section scale, and we discuss a possible diagenetic or hydrothermal origin of these albites.

2. Geological setting

Authigenic albites were found in two sections situated in the Lüsis Slice (Glarus Nappe s. l.), which belongs to the Helvetic Domain of the eastern Swiss Alps (Herb and Franks-Dollfus, 2003)(Fig. 1). This study focuses on the section Nissibach, situated near the town of Walenstadt (Swiss coordinates: 742.930/221.940). The second section, Milchbach, is located along a stream, 2.8 kilometers east of Nissibach (744.940/219.880).

The Nissibach and Milchbach sections are composed of sediments accumulated along the northern Tethyan margin during the Jurassic. The sediment succession containing albite starts in the Middle Jurassic with Bajocian limestones and ends with the deposition of Oxfordian marlstones (Late Jurassic) (Fig. 2). The age of the sections is well constrained by ammonite- (Kugler, 1987) and carbon isotope stratigraphy (Padden et al., 2002; Rais et al., submitted).

The sediments were deposited on the continental shelf, in an open marine environment episodically affected by strong oceanic currents (Rais et al., submitted).
During alpine orogeny, the studied part of the Glarus Nappe experienced deep burial diagenesis to low-grade metamorphism. The burial history of the region was reconstructed by Wang et al. (1996) using illite crystallinity, the presence of index minerals, and the ordering of illite/smectite. In the studied area, clay mineral assemblages indicate deep burial diagenesis close to the anchizone boundary, suggesting burial temperatures around 200 °C (Merriman and Frey, 1999).

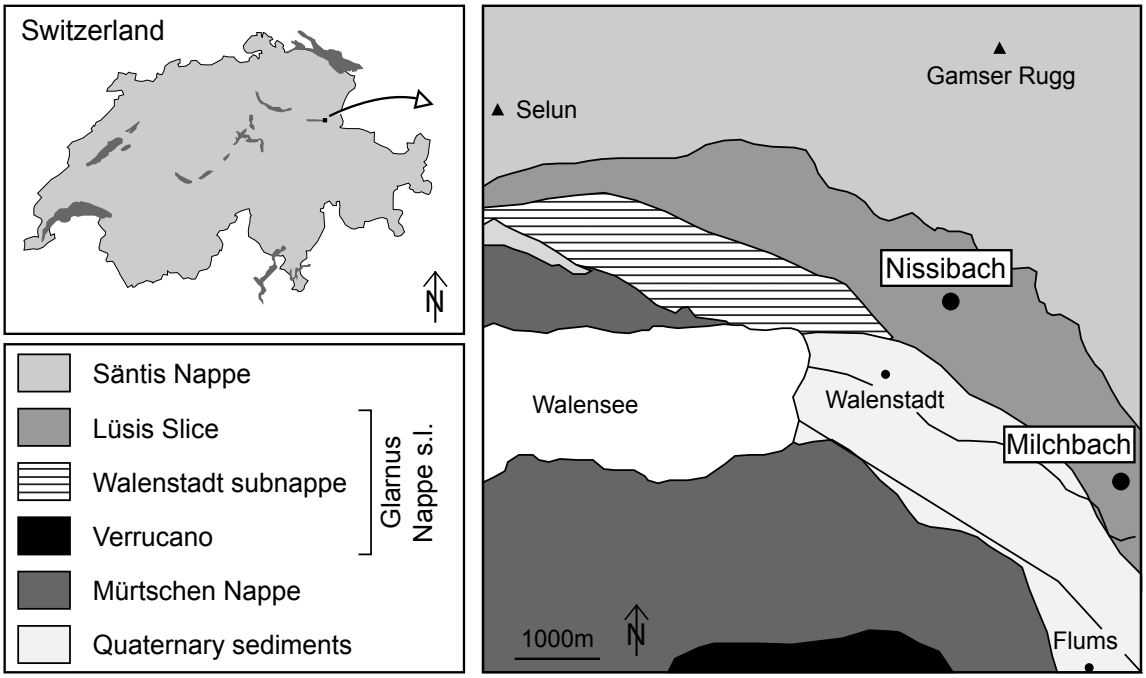

Figure 1:
Location of Nissibach and Milchbach on the tectonic map of Walensee, Switzerland (after Herb and Franks-Dollfus, 2003).

3. Methods

Albites were studied using a combination of optical microscopy, cathodoluminescence microscopy, back-scattered electron microscopy, and electron microprobe analysis.
The counting of albite crystals was carried out on a 6.25 mm^2 surface of thin-sections under the optical microscope. Albite concentration is expressed in number of albite crystals per square centimeter (Ab/cm^2). Cathodoluminescence analyses were carried out on a cold-cathode device, using polished thin-sections.

The elemental composition was determined using a JEOL-JXA 8200 electron microprobe. Analytical conditions were 15 kV acceleration voltage at a current of 20 nA. The spatial resolution attained is about 2 µm. Standard used were synthetic and natural oxides and silicates.

The carbon content was measured with a UIC CM5012 Coulometer. Powders were extracted from the slab used for thin-section preparation by using a micro-drill. The inorganic carbon was obtained by dissolution of the sample in perchloric acid, and total carbon by combustion at 950 °C. Organic carbon contents were calculated by difference and are expressed in wt-%. Inorganic carbon results are expressed in wt-% carbonate. Analytical precision is ±0.1 % for carbonate carbon and ±0.3 % for organic carbon.

4. Albite crystal distribution

Albite crystals found in the studied sections are of authigenic origin, as indicated by the euhedral shape and the chemical purity of the crystals. To assess the influence of the host rock composition on the development of authigenic albites, their distribution is described from a regional to a thin-section scale.

Regional scale

The difference in albite abundance in the two studied sections indicates important regional variations. The section of Nissibach contains abundant crystals of large size (200 µm in average), whereas at Milchbach they are smaller (max 130 µm and 80 µm in average) and only occur in the 2 m-thick limestone bed of the Schilt-Kalk. The presence of authigenic albite is not reported in previous studies of the region (Kugler, 1987; Wang et al., 1996), suggesting a geographically very restricted occurrence.

Outcrop scale

The Nissibach section is described in more detail because of the numerous and well developed authigenic albites. The section is 9 m-thick and comprises four lithologies (Fig. 2). The “Reischiben-Serie” is a grainstone of Bathonian to Bajocian age mainly composed of echinoderm fragments with minor amounts of serpulids, shell fragments, quartz grains and reworked clasts of micritic limestone. The Reischiben-Serie contains only few albites.

The “Blegi-Oolite” is a 80 cm-thick hardground of Callovian to Early Oxfordian age consisting of an iron-rich micritic limestone. It is a mudstone to packstone containing iron-

ooids and bioclasts (cephalopods, echinoderms, sponges, and microfauna). This bed does not contain albite.

The "Schilt-Kalk" is a Middle Oxfordian member of the Schilt Formation. It is composed of a 6.2 m-thick succession of micritic nodular limestones containing a typical pelagic fauna (ammonites, belemnites) surrounded by a micritic to microsparitic matrix (Fig. 3D). Between the nodules, bioclasts are scarce and usually unidentifiable. The nodules have been interpreted to be the result of reworking of early-cemented mud pebbles at the sea floor

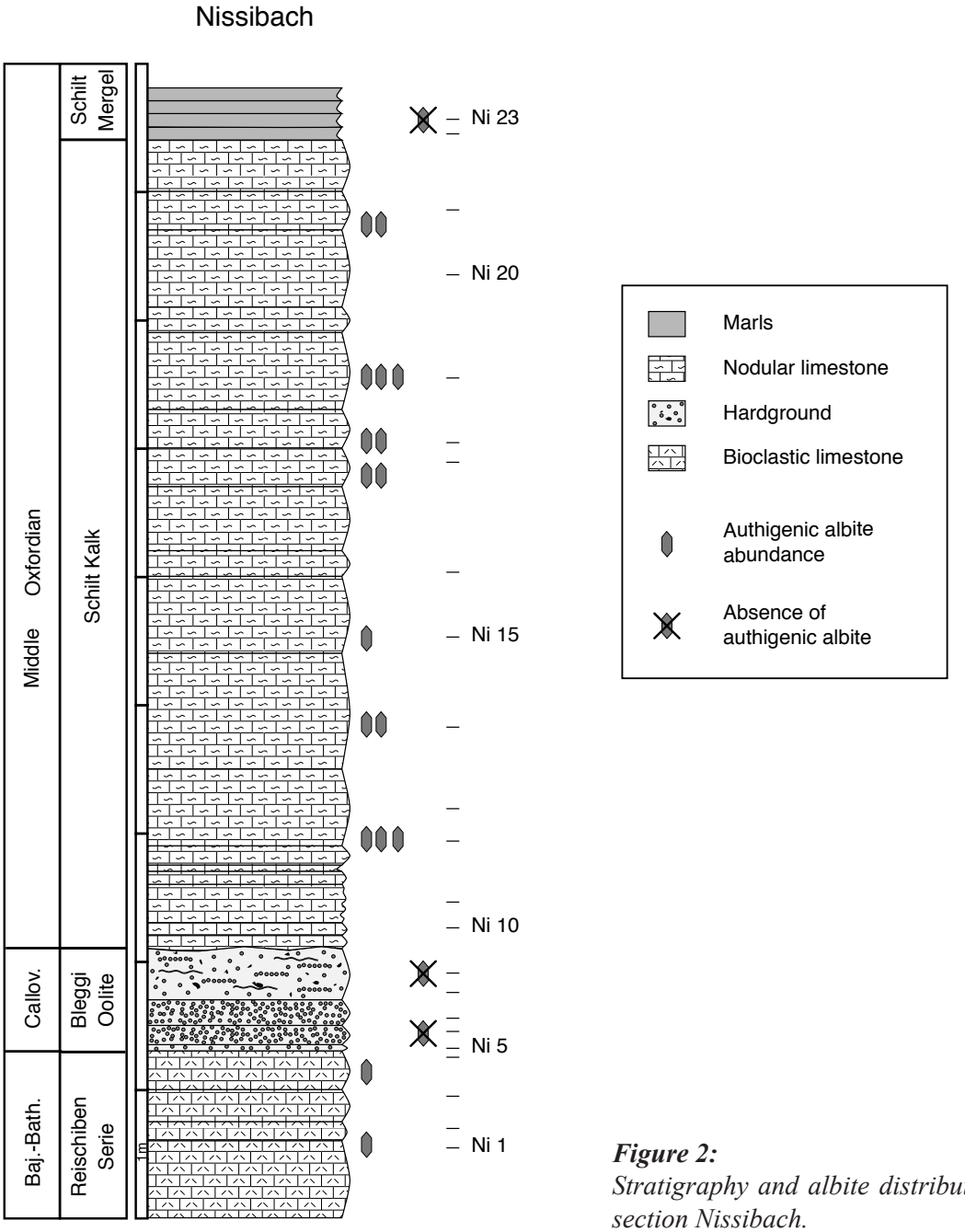

Figure 2:
Stratigraphy and albite distribution of the section Nissibach.

(Kugler, 1987; Rais et al., submitted). In the Schilt-Kalk, albites are large and abundant, but crystals only occur in the nodules (see below).
The "Schilt-Mergel" is a succession of monotonous grey to beige marls containing rare fragments of cephalopods, sponges or echinoderms. The detrital fraction consists of clay, and no quartz crystals or authigenic albites were observed.

Bed scale

At Nissibach, the amount of albite is variable from bed to bed (see Fig. 2). The variation is random, with no systematic increase or decrease along the section. The maximum concentration is reached in samples Ni 12 and Ni 19 with respectively 624 Ab/cm^2 and 656 Ab/cm^2. In contrast, sample Ni 15 has a maximum of 96 Ab/cm^2.

Thin-section scale

Thin-section observations of the Reischiben-Serie and the Schilt-Kalk reveal that authigenic crystals growth is limited to specific zones. In the Reischiben-Serie, albites are especially abundant in the micritic clasts (up to 400Ab/cm^2). In the grainstones, they occur mostly between bioclasts, only a few grew on bioclasts. Albites are less abundant in the grainstone (in average 200 Ab/cm^2) than in the micritic clasts, but they are larger (up to 400µm).
In the Schilt-Kalk, the albites are confined to the nodules. In most of the samples, the crystals are scattered throughout the nodules in a regular pattern, and are not concentrated at the edge of the nodule, and rarely along joints or veins. Albites never occur in veins. Some crystals appear to be cut at the limit between nodule and matrix (Fig. 3E). Overgrowth of albite in the matrix has not been observed.
The amount of albite varies from a nodule to another within the same sample. For example, the albite concentration in the sample Ni 19 varies between 656 Ab/cm^2 and 368 Ab/cm^2.

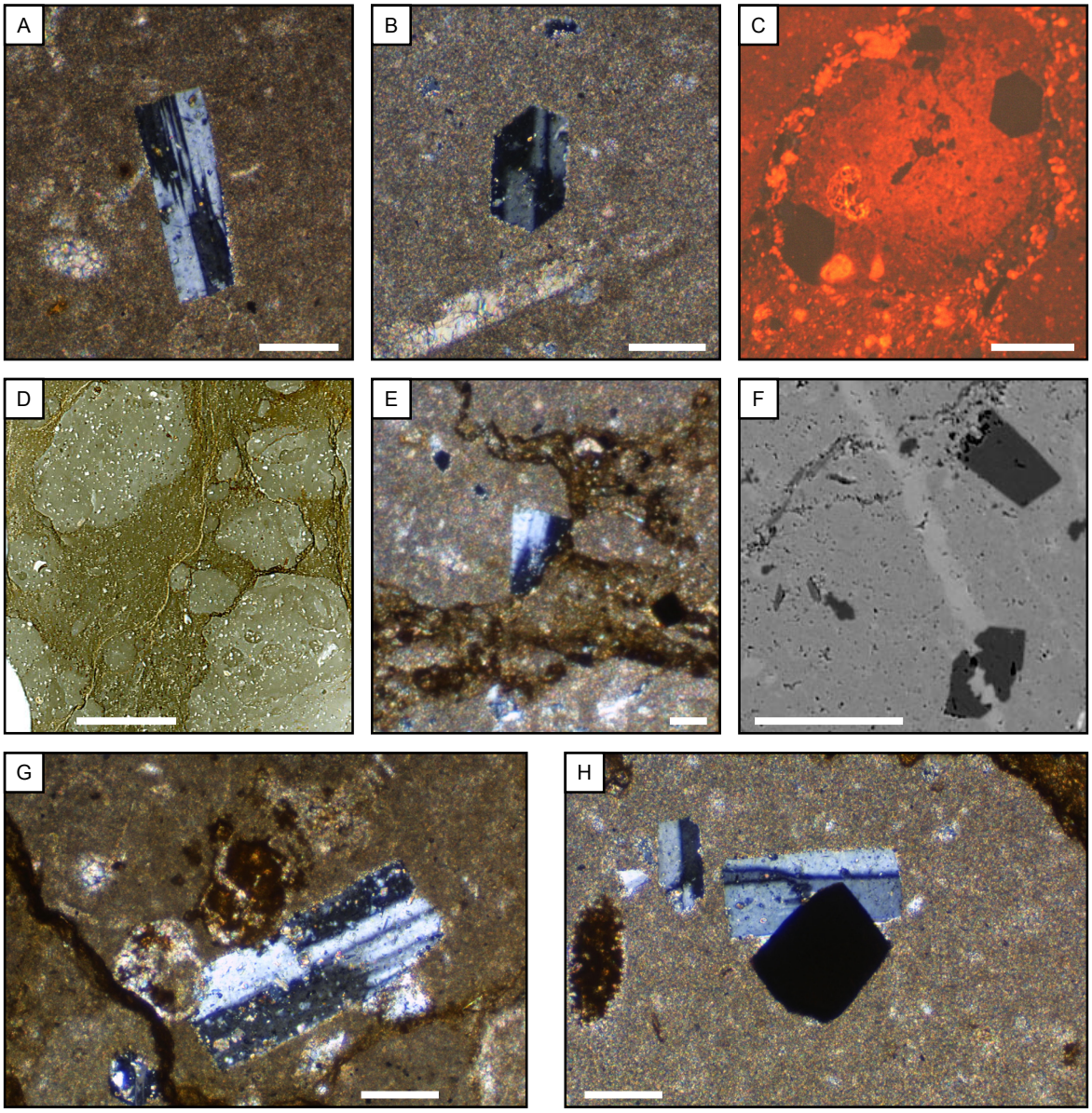

Figure 3:
(A,B) Euhedral authigenic albites. Roc Tourné and polysynthetic twinning (Thin-section, crossed polars) (C) Cathodoluminescence. The nonluminescent albites contrast with the dark orange micritic nodule and the bright orange color of the surrounding matrix. (D) Picture of a thin-section from the Schilt-Kalk: the albites are concentrated in the nodules. (E) Cut albite crystal at the edge of a nodule (Thin-section, crossed polars). (F) The top albite is reduced by pressure solution, and the lower albite is cut by a calcite vein (electron microprobe back-scatter image). (G) Albite growth is disturbed at the contact with a bioclast (Thin-section, crossed polars). (H) Intergrowth between authigenic albite and pyrite (Thin-section, crossed polars) Scales: A,B,C,E,F,G,H: 100µm. D: 5mm.

5. Petrography and geochemistry

Authigenic albites are euhedral and on average 200 µm long (range from 50 µm to 400 µm). The crystals show Roc Tourné twinning (Füchtbauer, 1948; Füchtbauer, 1950) (Figs. 3A,B,G,H) and contain varying amounts of solid and fluid inclusions which are mostly residues of the host rock (calcite, dolomite, clay). Unfortunately the scarcity and small size (4 to 5 µm in average) of fluid inclusions exclude an analysis of crystallization temperatures and fluid compositions. Under cold-cathodoluminescence microscope, albite crystals are nonluminescent (Fig. 3C), where the dark albites contrast with the bright orange of the surrounding carbonate.

The relation of the albites with other components of the sediment provides information on their genesis. Whereas bioturbation structures do not have an impact on crystal formation, the presence of a bioclast slightly disturbs their growth (Figs. 3C,G). Albites never grew beyond the border of the nodules, and in many cases, the crystals are clearly cut by dissolution seams (Figs. 3E,C). Dissolution seams are commonly observed around or within nodules, as shown in Figure 3F, where the upper albite crystal is dissolved on one side by pressure solution. Some albites formed across a first generation of calcite veins, whereas in other places late generation calcite veins cut trough them (Fig. 3F). Figure 3H shows a late-diagenetic pyrite crystal, intergrown with albite.

Microprobe analyses show that albites are nearly pure, with on average 98.4 mol% albite component (Table 1, Fig. 4). Very little variations were observed between the center and the rim of a crystal, indicating the absence of a detrital core as nucleation center. No detrital feldspars were found in the samples.

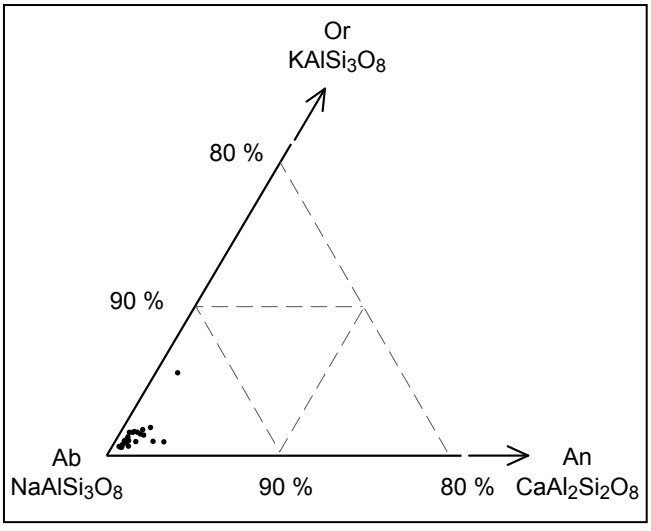

Figure 4:
Ternary diagram of the plagioclase feldspar series. The authigenic albites are almost pure end-members (ΔPlot program from John (2004)).

Sample	SiO2	Al_2O_3	Na_2O	K_2O	CaO	Total	Ab	Or	An	Comments
			(wt %)			(wt %)		(mol %)		
Ni 10	69.21	19.43	11.33	0.08	0.10	100.15	99.05	0.48	0.47	1 Centre
Ni 10	68.44	19.31	11.07	0.27	0.29	99.38	97.07	1.53	1.40	2 Centre
Ni 10	67.65	20.09	10.63	0.92	0.23	99.52	93.57	5.30	1.13	3 Edge of 2
Ni 10	68.78	19.54	11.22	0.21	0.10	99.85	98.30	1.20	0.50	4
Ni 10	69.19	19.50	11.29	0.15	0.08	100.21	98.74	0.89	0.37	5
Ni 10	69.29	19.16	11.22	0.09	0.08	99.83	99.12	0.51	0.38	6 Centre
Ni 10	68.74	19.56	11.10	0.24	0.21	99.85	97.61	1.38	1.01	7 Edge of 6
Ni 10	68.30	19.38	11.06	0.21	0.16	99.10	98.02	1.21	0.77	8
Ni 10	68.44	19.36	11.26	0.10	0.42	99.58	97.40	0.57	2.03	9
Ni 15	69.24	19.30	11.38	0.11	0.08	100.11	98.97	0.64	0.38	11
Ni 15	69.51	19.39	11.36	0.10	0.21	100.57	98.44	0.56	1.01	12
Ni 15	69.37	19.08	11.45	0.03	0.07	99.99	99.53	0.15	0.31	13
Ni 15	69.21	19.33	11.23	0.10	0.09	99.96	98.98	0.59	0.44	14
Ni 15	69.29	19.39	11.25	0.12	0.07	100.12	98.96	0.68	0.36	15
Ni 15	69.06	19.45	11.23	0.11	0.11	99.96	98.83	0.63	0.54	16
Ni 15	69.76	19.13	11.44	0.03	0.08	100.44	99.46	0.18	0.36	17 Centre
Ni 15	69.69	19.30	11.08	0.09	0.09	100.25	99.01	0.54	0.45	18 Edge of 17
Ni 15	69.17	19.38	10.91	0.17	0.25	99.88	97.74	1.01	1.25	19 Small
Ni 15	68.65	19.44	10.92	0.21	0.12	99.34	98.18	1.25	0.58	20 Small
Ni 20	69.28	19.50	11.16	0.21	0.06	100.21	98.50	1.20	0.30	21 Centre
Ni 20	70.01	19.20	11.31	0.04	0.15	100.71	99.04	0.24	0.72	22 Edge of 21
Ni 20	69.75	19.35	11.31	0.08	0.08	100.57	99.15	0.47	0.38	23
Ni 20	69.71	19.34	11.14	0.06	0.06	100.31	99.34	0.35	0.31	25
Ni 20	68.79	18.99	11.16	0.10	0.56	99.60	96.77	0.54	2.69	27
Ni 20	70.11	19.22	11.45	0.04	0.04	100.86	99.60	0.22	0.17	28
Ni 20	69.56	19.34	11.16	0.10	0.06	100.22	99.10	0.61	0.29	29
Ni 20	69.63	19.39	11.32	0.19	0.21	100.74	97.91	1.08	1.01	30
	69.18	19.36	11.20	0.15	0.15	100.05	98.38	0.89	0.73	Average

Table 1:
Results of electron microprobe analyses of authigenic albites. Albite (Ab), orthoclase (Or), and anorthite (An) percentages were calculated using the general formula $NaAlSi_3O_8$ for albite.

6. Albite abundance and carbonate content

The variation of albite abundance from one lithology to another indicates that the chemical composition of the host rock is determinant for albite authigenesis. In contrast the presence of authigenic crystals in micritic and sparitic limestone suggests that the texture of the host rock does not significantly influence albite formation.

A plot of carbonate content vs. the relative abundance of albite crystals (Fig. 5) shows that albite only occurs in sediments with more than 87 wt-% carbonate, whereas no albite was observed when the carbonate content is lower than 80 wt-%. Above 87 wt-% carbonate, albite abundance is not correlated to carbonate content. Organic carbon contents were lower than 0.1 % in all samples.

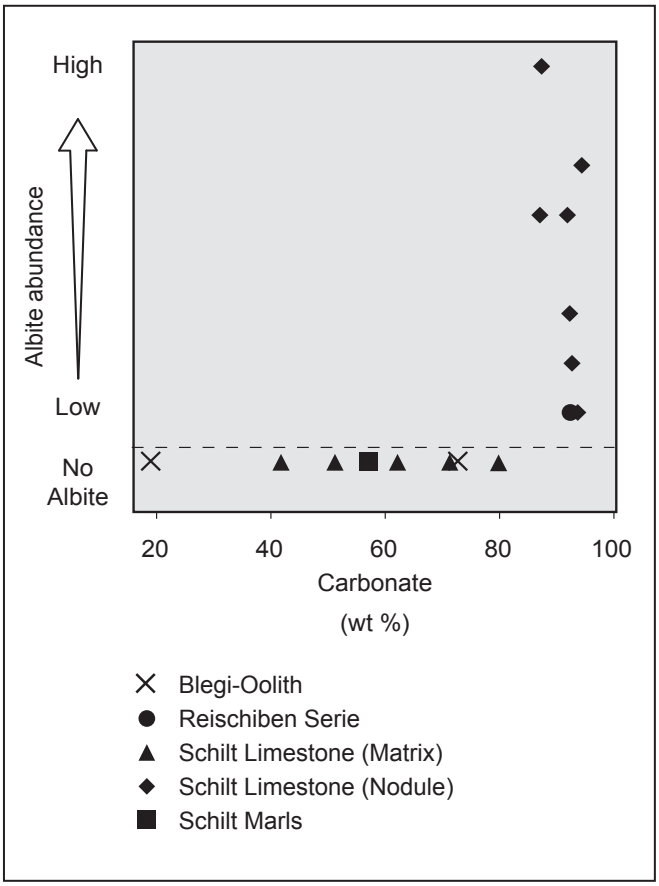

Figure 5:
Relation between carbonate content and albites abundance. Authigenic albites occur in sediment with a carbonate content higher than 87 wt-%.

7. Discussion

Albite characteristics and growth environment

The euhedral shape, the Roc-Tourné twinning and the chemical composition of the studied albites testify of their authigenic origin. The 98.4 mol% albite content is consistent with other occurrences where compositions mostly above 99 mol% were reported (Spoetl et al., 1999; Richter et al., 2002). The lack of chemical zoning in Nissibach samples (Table 1) indicates that albite growth initiated without a preexisting core, in contrast to authigenic albites developing as overgrowths around detrital plagioclases described by Turner et al. (1982). The growth of albites across bioturbation structures, and their interrupted growth at the contact with a bioclast are also in agreement with an authigenic origin.

The nodular structure of the “Schilt-Kalk”, is related to reworking of mud pebbles at the sediment surface (Kugler, 1987; Rais et al., submitted), and must predate albite authigenesis. The texture of the limestone does not influence the albite development, whereas the strong correlation between albite abundance and carbonate content suggests that the chemistry of the host rock is an important control. This relation is surprising as the difference of carbonate

content between sediments containing albite and those without albite seems to be too low to create extremely different chemical conditions.

Distinctive features of the albites from Nissibach

Kastner & Siever (1979) estimated that most authigenic albites fall in the 60 to 120 µm range. In Nissibach, crystals range from 50 to 400 µm with an average of 200 µm. Previous studies have shown that the size of the albite crystals is closely linked to the maximum thermal grade of the host rock (Richter, 1978; Brauckmann, 1984). Thus, the albites from Nissibach are relatively large compared to other occurrences of similar burial grade. Brauckmann (1984) reported authigenic albites from Bramsche and Vlotho (Germany) of a few micrometers to 294 µm. In the northern England Pendleside Formation albites size is of 120 to 150 µm in average in packstones, and up to 400 µm in grainstones. Authigenic albites can reach several millimeters in sediments which experienced epizonal conditions, like in Triassic dolostones of Crete (up to 3.5 mm) (Kastner and Siever, 1979), or in Roches des Amoureux and Roten Turra (up to 10 mm) (Rose, 1865; Jakob and Neher, 1951).
The albites from Nissibach have the typical nearly-pure chemical composition of authigenic albites, although the albite component is slightly lower than previous reports, with values ranging from 96.77 to 99.60 mol% (except 93.57 mol% measured on the edge of a crystal), and an average of 98.36 mol%. Richter et al. (2002) reported albite contents of 98.78 to 99.87 mol% (99.35 in average) from outcrops in Germany and Greece, whereas Spoetl et al. (1999) concluded that most of authigenic albites have an albite content typically above 99 mol%. They also showed that, in contrary to crystal size, albite composition is not related to the grade of thermal alteration of the host rock.

Albite formation models

Two principal models have been proposed to explain the provenance of the chemical components required for albite authigenesis: a model based on isochemical transformations (Kastner and Siever, 1979), and a model including migration of deep saline fluids (Kastner and Siever, 1979; Schedl et al., 1992; Spoetl et al., 1996).
The isochemical transformation model is a simple but pertinent model, where all the components necessary for albite authigenesis are supplied by the host rock. Sodium is concentrated in seawater trapped in the sediment pores or can be released by clay mineral transformation during diagenesis. Silica can also be supplied by clay minerals, or by the dissolution of biogenic siliceous fossils (sponge spicules, diatoms, etc). Aluminum can be

released by the decomposition of Al-rich smectite (montmorillonite), which is a common detrital constituent of hemipelagic sediments.

The deep-brine migration model proposes a chemical exchange between the components of the host rock and migrating saline fluids. The chemical composition of the brines depends on their origin (meteoric, seawater, or hydrothermal), and on the lithology of the rocks through which they have passed. According to Kastner and Siever (1979), the most likely origin of these brines are hydrothermal waters, which migrate upward carrying high concentrations of H_4SiO_4 and Na^+. In this model, aluminum species, which are hardly soluble, are supplied directly from the sediment.

The albite formation model applied to the studied sediments has to be consistent with the geological history of the region. The components required for albite formation according to the isochemical model, are present in the sediments of Nissibach and Milchbach. Moreover, deep burial transformations of the clay minerals during Alpine orogenesis (Wang et al., 1996) could have provided the chemical components for albite authigenesis. However, this model does not explain the restricted occurrence of authigenic albite in the region and its general scarcity. If clay diagenesis in limestones were the only requirements for its formation, albite would be expected to be a common mineral of these rocks. Contrary to the isochemical model, the brine migration model could explain the local occurrence of authigenic albite, forming along fluid migration paths, and evidence for hydrothermal fluid migration is reported from the Gonzen Mountain, situated a few kilometers away from Nissibach. Fluids having a temperature of about 100 °C migrated through a Jurassic fault system affecting the continental basement and overlying sediments. They generated a massive Fe-Mn ore body deposited in alternation with Early Kimmeridgian limestones (Pfeifer et al., 1988). This model implies an albite formation approximately 5 Ma after sediment deposition, whereas in the isochemical model, albite grew under deep diagenetic burial conditions during Alpine orogenesis. Therefore, the burial conditions at which albite formed are a key to the understanding of albite origin.

Constraining the depth of authigenesis

The textural relation of the albites with other components of the rock gives insight on the relative sequence of the events (Fig. 6). In Nissibach, albites grew after a first generation of calcite-filled veins and in association with secondary pyrite (Spoetl et al., 1999). Albite and calcium carbonate are dissolved at the edge of nodules by pressure solution (Kastner and Waldbaum, 1968; Frey et al., 1973; Beach, 1979), indicating that pressure solution processes were still active after albite formation. A last generation of calcite veins cut through the albite crystals. These observations support a formation of albite during deep burial diagenesis.

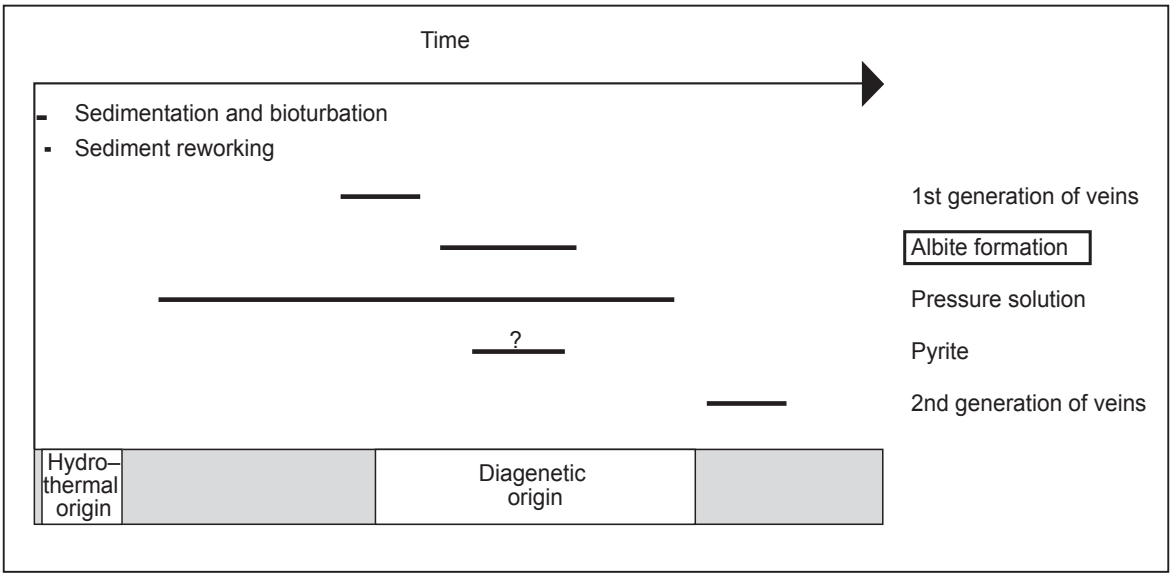

Figure 6:
Relative sequence of the sedimentologic and diagenetic events.

Another argument in favor of a diagenetic origin is that the maximum burial rate of the host rock has an effect on the size of the crystals, which suggests a continuous albite growth during burial diagenesis (Richter, 1978; Brauckmann, 1984; Spoetl et al., 1999). In Nissibach, the crystal size varies around 200 μm, which is consistent with deep diagenetic burial conditions.

8. Conclusions

The albites found in the sedimentary rocks of the Glarus Nappe are of authigenic origin. The chemical composition of the host sediment is determinant in albite formation, as illustrated by the irregular distribution of albites in the Nissibach section. Albite crystals apparently formed during deep burial diagenesis conditions, in association with other diagenetic processes. Clay mineral transformation is a potential important source of ions for albite growth. The apparent local distribution of albite remains enigmatic and would deserve further investigation.

Acknowledgements:

This project was supported by the Swiss Science Foundation, grant No. 2-77549-04. We thank Thomas Pettke for the interesting discussion on fluid inclusions. We thank PD Dr. Glasmacker and Prof. Dr. Richter for constructive reviews.

References:

Beach, A., 1979. Pressure solution as a metamorphic process in deformed terrigenous sedimentary rocks. Lithos 12, 51-58.

Brauckmann, F.J., 1984. Hochdiagenese im Muschelkalk der Massive von Bramsche und Vlotho. Bochumer Geologische und Geotechnische Arbeiten 14, 1-195.

Frey, M., Hunziker, J.C., Roggwiller, P. and Schindler, C., 1973. Progressive niedriggradige Metamorphose glaukonitfuehrender Horizonte in den helvetischen Alpen der Ostschweiz. Contributions to Mineralogy and Petrology 39, 185-218.

Füchtbauer, H., 1948. Einige Beobachtungen an authigenen Albiten. Schweizerische Mineralogische und Petrographische Mitteilungen = Bulletin Suisse de Mineralogie et Petrographie 28, 709-716.

Füchtbauer, H., 1950. Die nichtkarbonatischen Bestandteile des Goettinger Muschelkalkes mit besonderer Beruecksichtigung der Mineralneubildungen. Beitraege zur Mineralogie und Petrologie 2, 235-254.

Herb, R. and Franks-Dollfus, S., 2003. Geologischer Atlas der Schweiz: 1134 Walensee.

Jakob, J. and Neher, J., 1951. Einige Analysen von authigenem Albit aus Sedimenten. Schweiz. Miner. Petrogr. Mitteil. 31, 528-534.

John, C.M., 2004. Plotting and analyzing data trends in ternary diagrams made easy. EOS 85, 158.

Kastner, M. and Waldbaum, D.R., 1968. Authigenic albite from Rhodes. American Mineralogist 53, 1579-1602.

Kastner, M. and Siever, R., 1979. Low temperature feldspars in sedimentary rocks. American Journal of Science 279, 435-479.

Kugler, C., 1987. Die Wildegg Formation im Ostjura und die Schilt-Formation um oestlichen Helvetikum; ein Vergleich. Unpublished PhD thesis, Universitaet Zuerich, 209 pp.

Merriman, R.J. and Frey, M., 1999. Patterns of very low-grade metamorphism in metapelitic rocks. In: Frey, M. and Robinson, D. (Eds.), Low-grade metamorphism. Blackwell Science, Oxford, 60-107.

Padden, M., Weissert, H., Funk, H., Schneider, S. and Gansner, C., 2002. Late Jurassic lithological evolution and carbon-isotope stratigraphy of the western Tethys. Eclogae Geologicae Helvetiae 95, 333-346.

Pfeifer, H.R., Oberhaensli, R. and Epprecht, W., 1988. Geochemical evidence for a synsedimentary hydrothermal origin of Jurassic iron-manganese deposits at Gonzen (Sargans, Helvetic Alps, Switzerland). Marine Geology 84, 257-272.

Rais, P., Louis-Schmid, B., Bernasconi, S.M. and Weissert, H., submitted. Paleoceanographic and paleoclimatic reorganization around the Middle-Late Jurassic transition. Palaeogeography, Palaeoclimatology, Palaeoecology.

Richter, D., 1978. Very low grade metamorphism in Middle Triassic red limestones from Hydra. In: Closs, H., Roeder, D. and Schmidt, K. (Eds.), Alps, Apennines, Hellenides., 477-479.

Richter, D.K., Goette, T. and Habermann, D., 2002. Cathodoluminescence of authigenic albite. Sedimentary Geology 150, 367-374.

Rose, G., 1865. Ueber die Krystallform des Albits von dem Roc Tourné und von Bonhomme in Savoyen und des Albits im Allgemeinen. Annalen Physik Chemie 125, 457-468.

Schedl, A., McCabe, C., Montanez, I.P., Fullagar, P.D. and Valley, J.W., 1992. Alleghenian regional diagenesis; a response to the migration of modified metamorphic fluids derived from beneath the Blue Ridge-Piedmont thrust sheet. Journal of Geology 100, 339-352.

Spoetl, C., Kralik, M. and Kunk, M.J., 1996. Authigenic feldspar as an indicator of paleo-rock/ water interactions in Permian carbonates of the northern Calcareous Alps, Austria. Journal of Sedimentary Research 66, 139-146.

Spoetl, C., Longstaffe, F.J., Ramseyer, K. and Ruedinger, B., 1999. Authigenic albite in carbonate rocks; a tracer for deep-burial brine migration? Sedimentology 46, 649-666.

Turner, P., Ashworth, J.R. and Iskenderian, F.A., 1982. Authigenic albite in the Pendleside Formation (Dinantian) of northern England. Geological Magazine 119, 395-404.

Wang, H., Frey, M. and Stern, W.B., 1996. Diagenesis and metamorphism of clay minerals in the Helvetic Alps of eastern Switzerland. Clays and Clay Minerals 44, 96-112.

CHAPTER 6

Conclusions

To better understand the causes and consequences of the paleoceanographic and paleoclimatic changes during the Late Jurassic, the present study investigated the sedimentological and geochemical variations of different paleoenvironments from the Alpine Tethys. An accurate stratigraphy was established by using carbon isotopes as a correlation tool between the sections. By combining sedimentological and geochemical analyses, this study worked out the following conclusions:

1) An accelerated hydrothermalism associated with the fragmentation of Pangea during the Jurassic is reflected in the lowest Mesozoic $^{87}Sr/^{86}Sr$ values, measured within Middle Oxfordian belemnites. This fragmentation resulted in the opening of the Hispanic Corridor, connecting the western Tethys to the Pacific. The continuous widening and deepening of the Hispanic Corridor modified the global ocean circulation pattern and triggered the Late Jurassic changes in oceanography and climate.
2) Evidence for changes in oceanic currents was found in the Alpine Tethys. Sedimentological analyses on the hardgrounds from the northern Tethyan shelf indicate that they formed under intense oceanic current activity. The decline of these strong shelf currents triggered the end of sediment condensation during the Middle Oxfordian (Plicatilis ammonite zone). The situation is more complex in the Trento Plateau, however changes in ocean dynamics appear to have occurred during the same period.
3) The opening of the Hispanic Corridor and the related reorganization of ocean currents influenced global climate. $\delta^{18}O$ measurements on belemnites indicate a very small sea-surface temperature increase at low latitudes, whereas at higher latitudes, belemnites record an increase of several degrees. These variations, reflecting a decrease of latitudinal temperature gradients, are consistent with model simulation of the onset of a circum-equatorial ocean circulation through the Hispanic Corridor.
4) The transition from carbonate-poor to carbonate rich sediments, in the Middle Oxfordian, indicates that the establishment of new climatic and oceanic conditions was favorable for

calcareous organisms. The homogenization of sea-surface temperatures, aridization of the climate, and rising sea level offered ideal conditions for the development of the Late Jurassic carbonate world.
These findings contribute significantly to the understanding of Late Jurassic oceanographic and climatic changes, and emphasize the role of tectonics in oceanography. Additionally, detailed stratigraphic analyses allow us to date the onset of circum-equatorial ocean circulation as Middle Oxfordian.

In addition to the paleoceanographic study, we describe the discovery of a new occurrence of albites within the sedimentary rocks of the Glarus Nappe (Swiss Alps). These albites are of authigenic origin and formed during deep burial diagenesis conditions. The chemical composition of the host sediment is determinant in albite formation, as illustrated by the irregular distribution of albites in the studied sections.

APPENDIX

List of the studied sections

Date	Section	Main reference	Swiss coordinates	Sample name	Number of samples
Nov-02	Auenstein	Padden (2002)	653.825/252.725	A	5
Mar-03	Churztal	Gygi (2000)	682.100/286.850		2
Mar-03	Räckholterenbuck (SH)	Gygi (2000)	680.975/287.175		5
May-03	Auenstein	Padden (2002)	653.825/252.725	AU	38
Jul-03	Gantrisch	Furrer (1979)	600.440/173.000	GA	22
Jul-03	Musenalp	Felber (1984)	677.090/197.750	MU	11
Aug-03	Rotspitz	Felber (1984)	648.750/186.480	RO	2
Aug-03	Stanserhorn	Felber (1984)	668.670/198.000	ST	2
Aug-03	Nissibach	Padden (2002), Kugler (1987)	742.980/221.940	Ni	23
Aug-03	Erzegg	Tröhler (1966)	665.300/178.050	Er	27
Sep-03	Musenalp	Felber (1984)	677.090/197.750	Mu	2
Sep-03	Milchbach	Kugler (1987)	744.940/219.880	Mi	22
Sep-03	Auenstein	Padden (2002), Kugler (1987)	653.825/252.725	AU 1xx	28
Sep-03	Mönthal	Kugler (1987)	651.710/264.070	MO	6
Sep-03	Torre de Busi (I)	Baumgartner field guide		TB	170
May-04	Auenstein	Padden (2002)	653.825/252.725	AUB	9
Jun-04	Madonna della Coronna	Baumgartner field guide		MC	30
Jun-04	Kaberlaba	Martire (1996)		KA	25
Jun-04	Ponte Serra	Baumgartner field guide		PS	39
Sep-04	Gantrisch 2	Furrer (1979)	600.440/173.000	GS	81
Oct-04	Weiach	Matter (1988)	Core NAGRA	W	157
Nov-05	San Giorgio	Pavia (1987)		SG	44
Nov-05	Ponte Serra 2	Cobianchi (2002)		PS-	43
Nov-05	Val Miela	Benigni (1982)		VM	37

Main sections with samples position

Key to lithologies

Limestone

Thin bedded limestone

Limestone with scarce chert nodules

Limestone/Marl alternation

Marl/Marly limestone alternation

Hardground

Siliceous limestone

Nodular limestone (no or scarce cherts)

Nodular limestone with few cherts

Nodular limestone with many cherts

Radiolarite

Organic-rich clays

Weiach

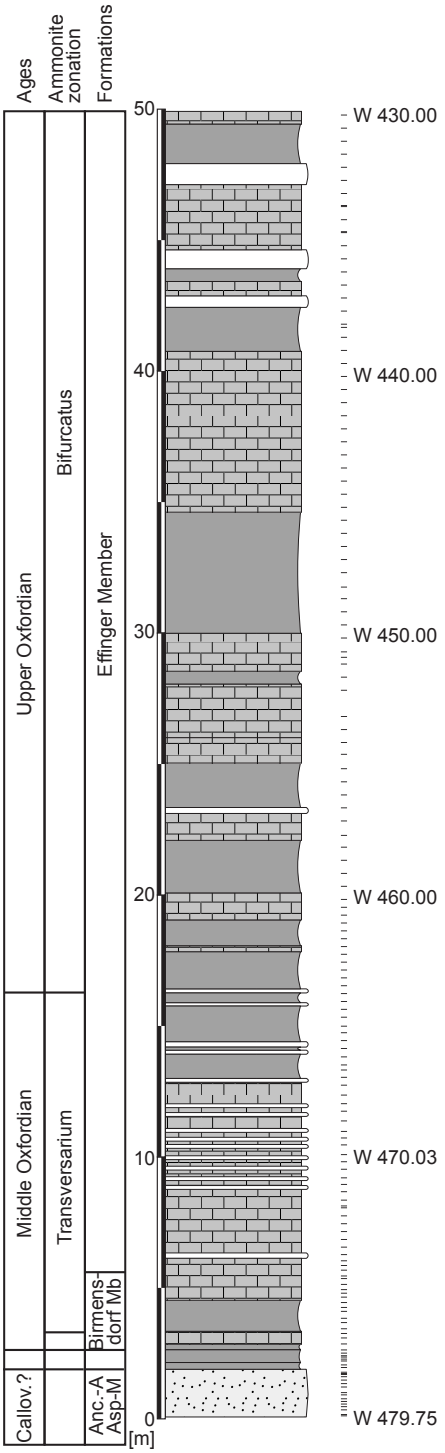

Main sections with samples position

Auenstein

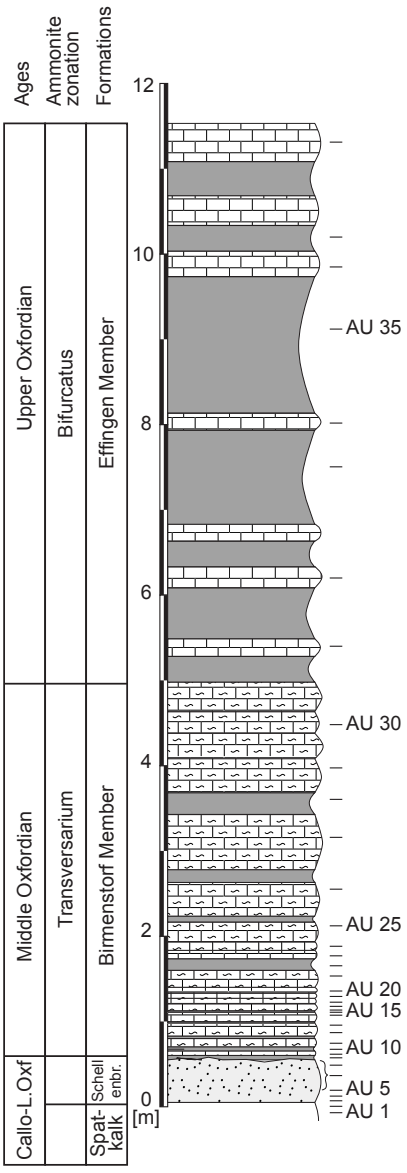

Mönthal

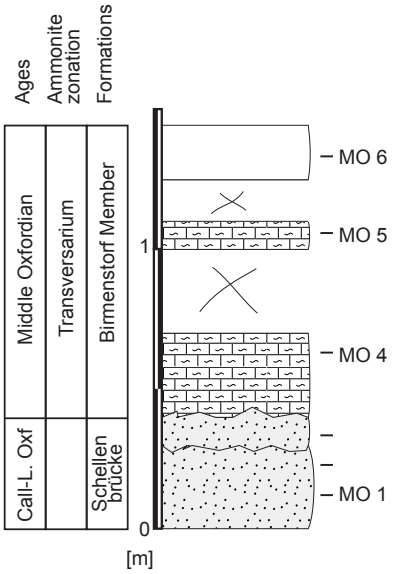

Main sections with samples position

Nissibach

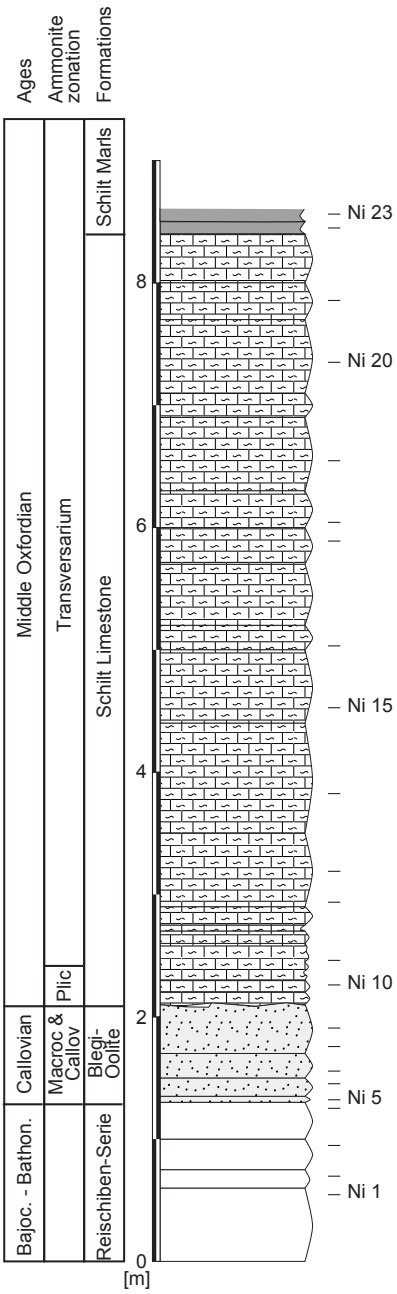

Milchbach

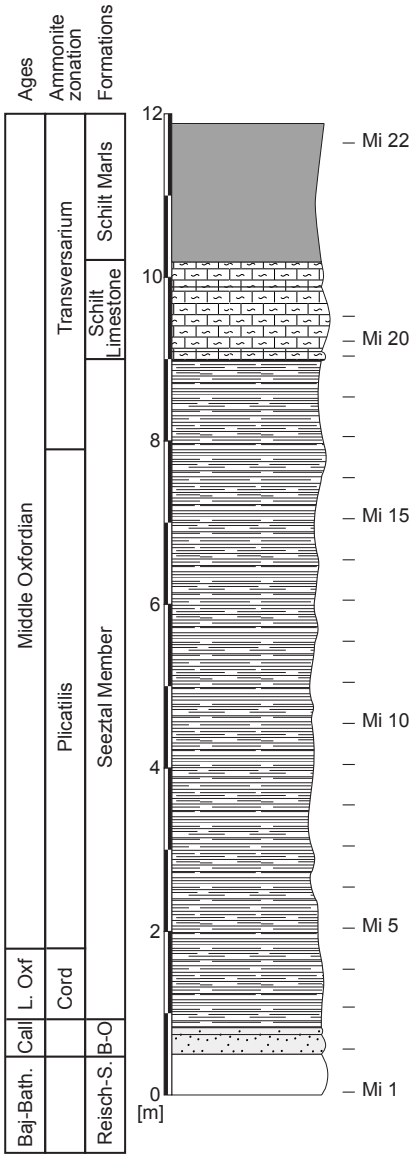

Main sections with samples position

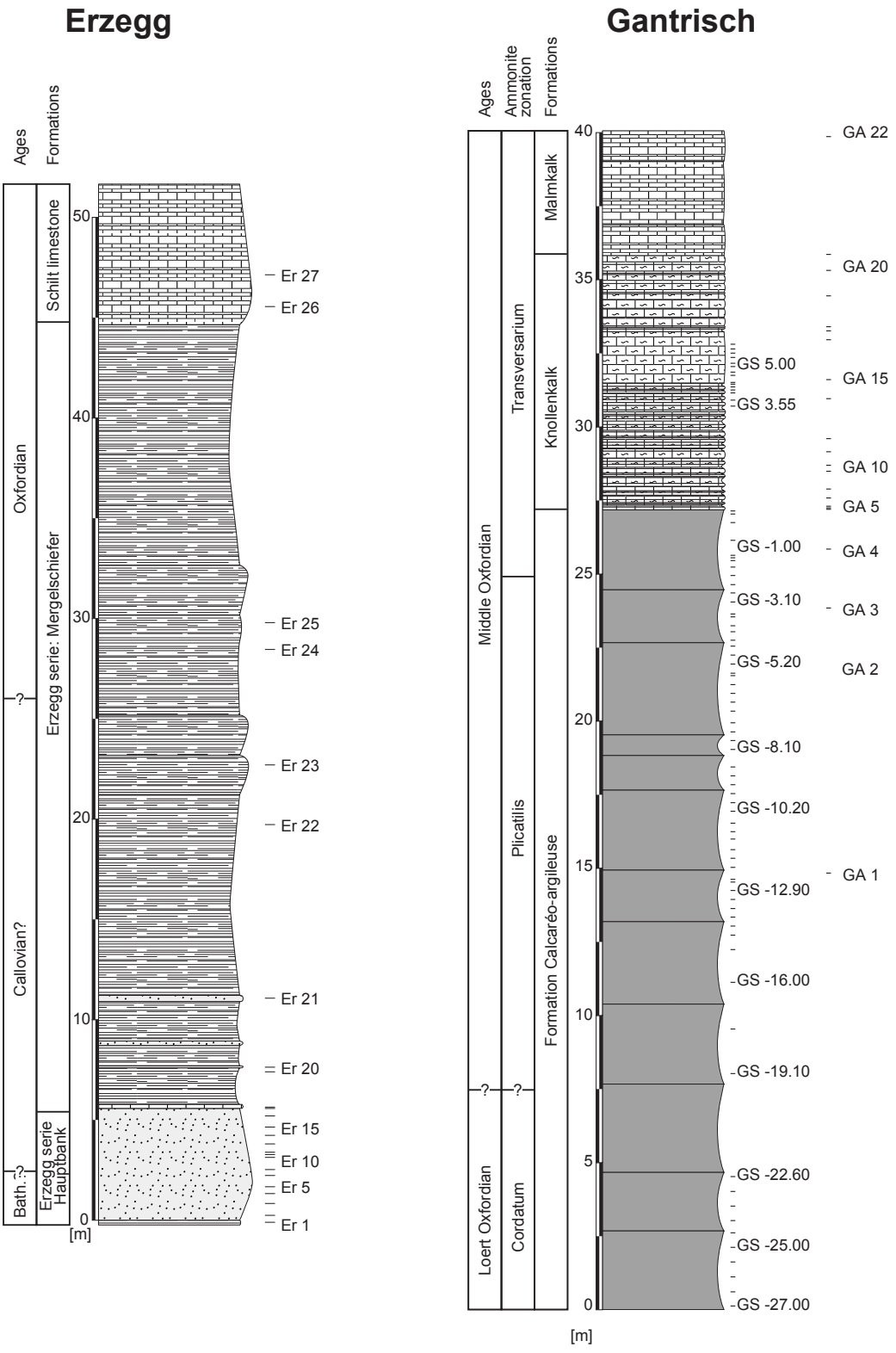

Main sections with samples position

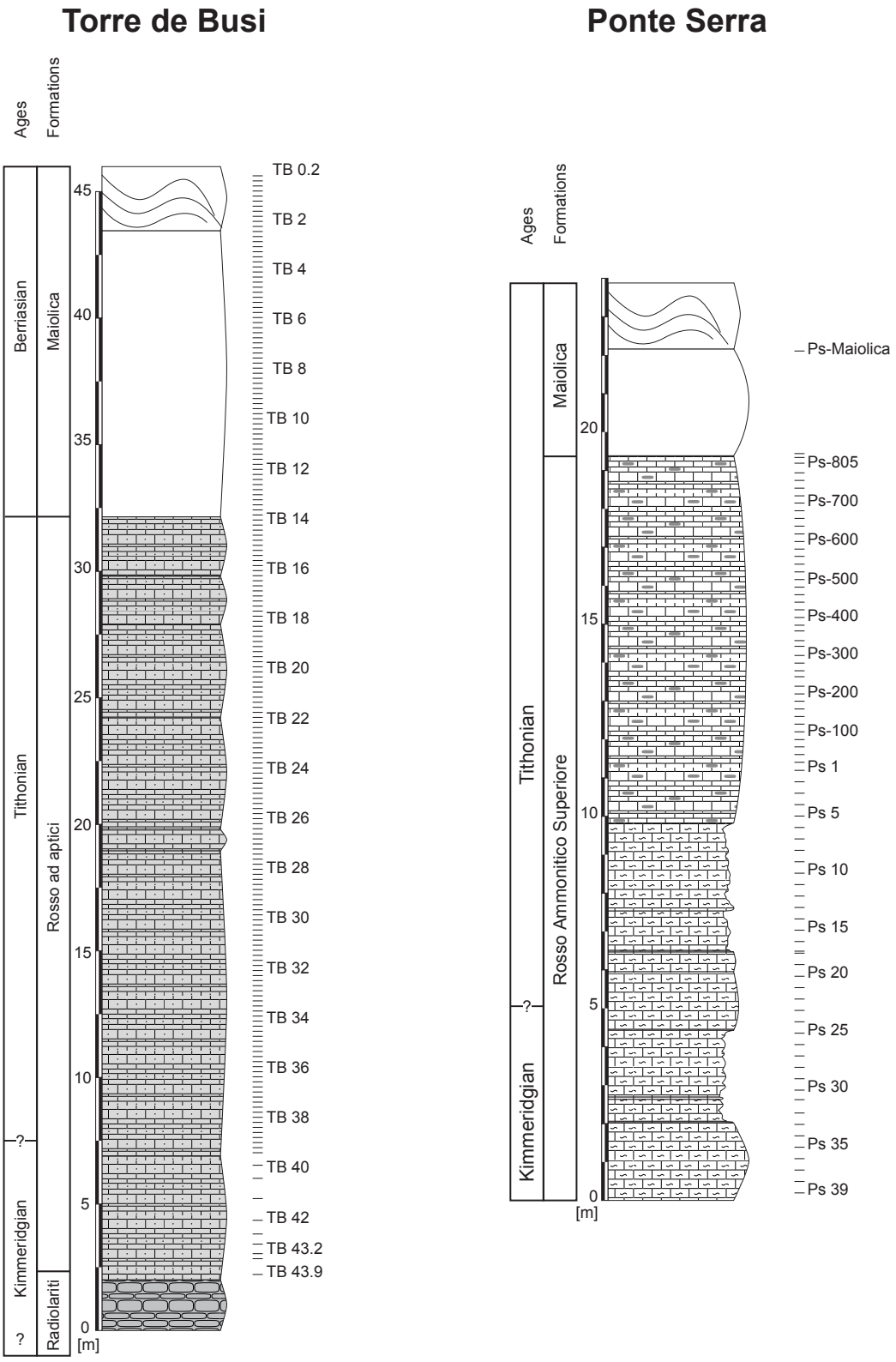

Main sections with samples position

Spiazzi

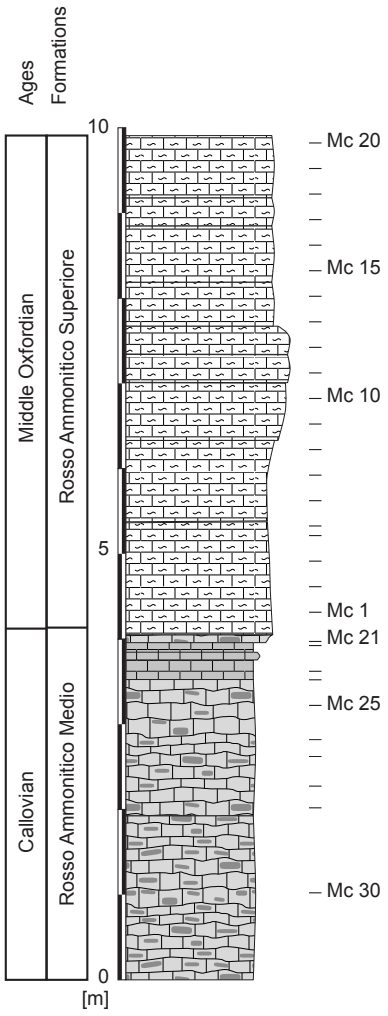

San Giorgio

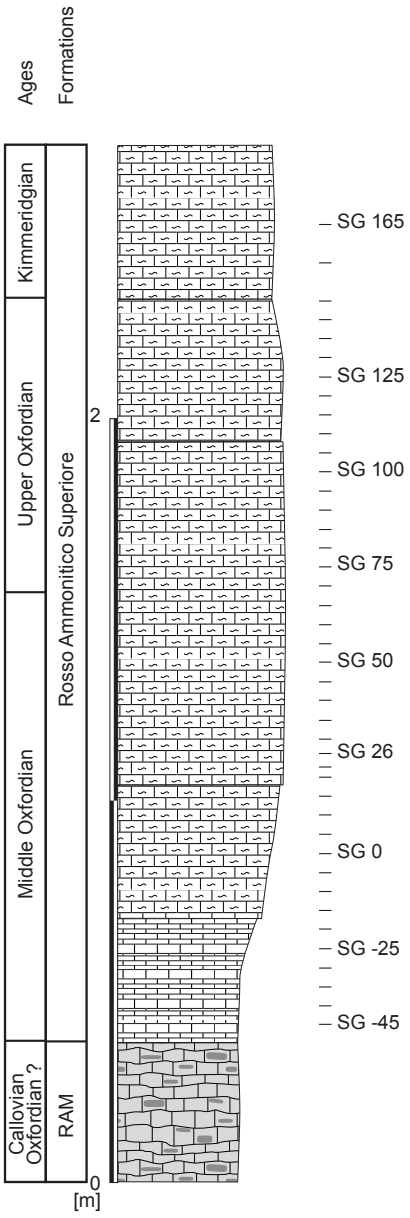

Main sections with samples position

Kaberlaba

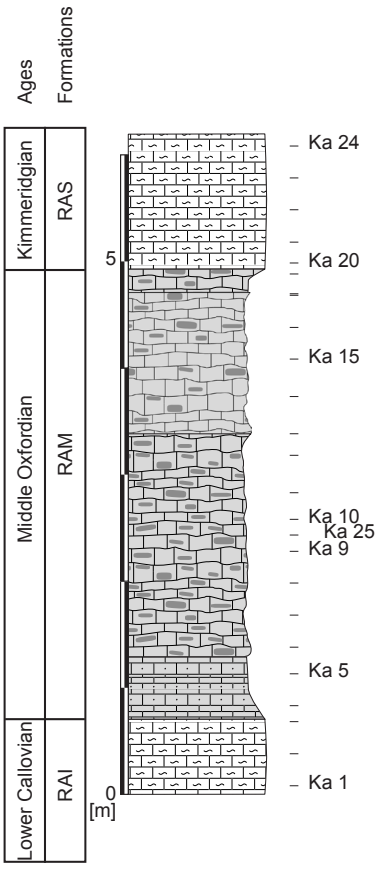

Val Miela

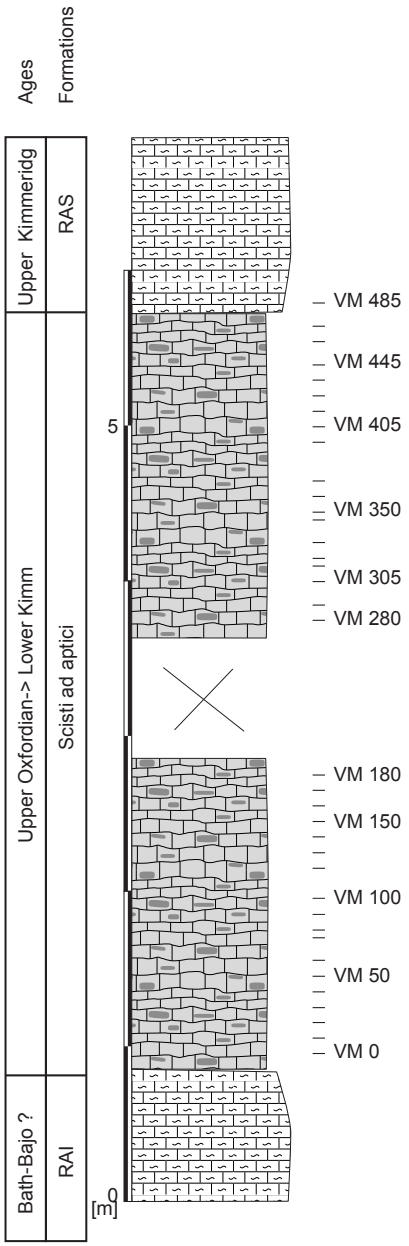

Auenstein,
complement to Padden (2002)

Sample	High (m)	$\delta^{13}C$	$\delta^{18}O$	Sample	High (m)	$\delta^{13}C$	$\delta^{18}O$
AU 04	0.27	1.79	-1.66	AU 26	3.57	2.90	-2.97
AU 07	0.76	1.65	-0.33	AU 27	4.39	2.56	-4.35
AU 08	0.88	2.12		AU 28	4.99	2.76	-2.36
AU 09	0.93	3.08	-1.78	AU 29	5.49	2.79	-2.78
AU 11	1.11	3.03	-1.42	AU 30	6.18	2.43	-2.94
AU 12	1.28	2.90	-2.01	AU 31	7.43	2.65	-1.54
AU 14	1.55	2.91	-1.85	AU 32	8.52	2.51	-2.63
AU 18	1.77	2.69	-3.66	AU 33	10.29	2.47	-1.68
AU 20	1.94	2.64	-2.69	AU 34	10.99	2.51	-1.71
AU 21	2.18	3.05	-1.81	AU 35	12.48	2.56	-1.33
AU 23	2.5	2.94	-2.29	AU 36	13.48	2.64	-2.09
AU 25	2.98	2.58	-2.43	AU 38	15.46	2.63	-1.34

Gantrisch

Sample	High (m)	$\delta^{13}C$	$\delta^{18}O$	Sample	High (m)	$\delta^{13}C$	$\delta^{18}O$
GA22	12.70	2.90	-0.52	GA02	-5.50	2.83	-2.15
GA21	8.70	3.51	-0.65	GS-5.60	-5.60	2.92	-2.08
GA20	8.15	3.32	-2.28	GS-5.90	-5.90	3.01	-1.57
GA19	7.30	3.55	-0.96	GS-6.20	-6.20	2.73	-1.81
GA18	6.25	3.62	-0.74	GS-6.50	-6.50	2.80	-1.66
GA17	6.10	3.29	-2.45	GS-6.80	-6.80	2.79	-2.26
GS+5.80	5.80	3.51	-1.09	GS-7.20	-7.20	2.84	-1.82
GA16	5.80	3.69	-0.34	GS-7.50	-7.50	2.92	-2.16
GS+5.65	5.65	3.43	-0.90	GS-7.80	-7.80	2.91	-2.06
GS+5.00	5.00	3.29	-2.20	GS-8.10	-8.10	2.87	-1.89
GS+4.70	4.70	3.25	-2.36	GS-8.70	-8.70	2.65	-1.71
GA15	4.35	2.10	-2.52	GS-9.00	-9.00	2.63	-2.36
GA14	3.75	3.62	-3.11	GS-9.3	-9.30	2.52	-1.92
GS+3.55	3.55	3.44	-1.97	GS-9.60	-9.60	2.50	-1.87
GS+3.35	3.35	3.43	-1.54	GS-9.90	-9.90	2.48	-1.84
GA13	2.45	3.73	-1.14	GS-10.20	-10.20	2.39	-1.62
GA12	2.00	3.59	-0.58	GS-10.60	-10.60	2.26	-2.44
GA11	1.55	3.39	-2.44	GS-10.90	-10.90	2.42	-1.86
GA10	1.35	3.70	-1.08	GS-11.15	-11.15	2.38	-2.49
GA09	0.75	3.43	-2.01	GS-11.50	-11.50	2.48	-1.58
GA08	0.45	3.68	-0.96	GS-11.80	-11.80	2.43	-1.89
GA07	0.15	3.42	-1.77	GS-12.10	-12.10	2.34	-1.85
GA06	0.10	3.44	-1.33	GS-12.30	-12.30	2.29	-1.86

GS+0.05	0.05	3.48	-1.79
GA05	-0.00	3.60	-2.03
GS-0.10	-0.10	3.45	-2.35
GS-0.40	-0.40	3.43	-2.15
GS-0.70	-0.70	3.30	-2.21
GS-1.30	-1.30	3.47	-2.40
GA04	-1.50	3.49	-1.65
GS-1.60	-1.60	3.25	-1.81
GS-1.90	-1.90	3.40	-2.19
GS-2.20	-2.20	3.22	-1.98
GS-2.50	-2.50	3.22	-1.57
GS-2.80	-2.80	3.12	-2.16
GS-3.10	-3.10	3.01	-2.16
GS-3.30	-3.30	3.16	-2.04
GA03	-3.50	3.10	-1.82
GS-3.60	-3.60	3.01	-2.51
GS-3.90	-3.90	3.03	-2.51
GS-4.10	-4.10	2.93	-2.21
GS-4.40	-4.40	2.71	-2.16
GS-4.60	-4.60	2.78	-2.23
GS-4.90	-4.90	2.42	-2.96
GS-5.20	-5.20	2.50	-2.93
GA01	-12.50	2.41	-1.76
GS-12.60	-12.60	2.22	-2.26
GS-12.90	-12.90	2.24	-1.75
GS-13.2	-13.20	2.33	-1.99
GS-13.80	-13.80	2.33	-2.30
GS-14.10	-14.10	2.37	-2.17
GS-14.40	-14.40	2.34	-1.58
GS-14.90	-14.90	2.32	-1.80
GS-16.00	-16.00	2.28	-2.16
GS-17.60	-17.60	2.31	-2.03
GS-19.10	-19.10	2.36	-2.17
GS-22.60	-22.60	2.35	-1.50
GS-23.10	-23.10	2.35	-2.76
GS-23.60	-23.60	2.36	-2.00
GS-24.10	-24.10	2.43	-1.43
GS-24.50	-24.50	2.37	-1.59
GS-25.00	-25.00	2.29	-2.34
GS-25.50	-25.50	2.41	-1.72
GS-26.00	-26.00	2.29	-3.01
GS-26.50	-26.50	2.15	-1.82
GS-27.00	-27.00	2.34	-1.51

Milchbach

Sample	High (m)	$\delta^{13}C$	$\delta^{18}O$
MI1	0	1.20	-6.04
MI2	50	1.05	-6.06
MI3	100	1.73	-5.04
MI4	150	1.72	-5.15
MI5	200	1.81	-4.86
MI6	250	1.83	-5.23
MI7	300	1.91	-5.59
MI8	350	1.88	-5.38
MI9	400	1.28	-6.28
MI10	450	1.74	-4.03
MI11	500	0.47	-6.92
MI12	550	0.48	-6.35
MI13	600	1.46	-6.13
MI14	650	1.62	-6.50
MI15	700	1.30	-6.27
MI16	750	1.64	-6.30
MI17	800	1.31	-6.26
MI18	850	2.63	-6.27
MI19	900	2.78	-6.24
MI19n	900	2.84	-6.17
MI20	920	2.25	-6.30
MI21	950	2.54	-6.49
MI22	1160	2.68	-6.18

Nissibach, complement to Padden (2002)

Sample	High (m)	$\delta^{13}C$	$\delta^{18}O$	Sample	High (m)	$\delta^{13}C$	$\delta^{18}O$
Ni 04	125	2.01	-4.65	Ni 14	380	2.93	-4.88
Ni 05	132	1.79	-4.79	Ni 15	450	2.74	-4.73
Ni 06	145	1.93	-5.23	Ni 16	500	2.62	-4.83
Ni 07	155	1.42	-5.71	Ni 17	585	2.11	-5.43
Ni 08	175	1.83	-4.62	Ni 18	610	2.13	-4.96
Ni 09	190	1.60	-5.47	Ni 19	650	2.46	-4.74
Ni 10	225	2.71	-5.35	Ni 20	730	2.58	-4.90
Ni 11	245	2.73	-5.13	Ni 21	780	2.53	-4.65
Ni 12	290	2.87	-4.90	Ni 22	835	1.19	-6.70
Ni 13	320	2.84	-4.91	Ni 23	850	1.45	-5.65

Weiach

Sample	High (m)	$\delta^{13}C$	$\delta^{18}O$	Sample	High (m)	$\delta^{13}C$	$\delta^{18}O$
W430.00	430.00	2.61	-2.73	W463.60	463.60	2.35	-2.86
W430.50	430.50	2.56	-2.86	W463.90	463.90	2.34	-2.80
W431.00	431.00	2.74	-2.65	W464.20	464.20	2.58	-2.65
W431.50	431.50	2.65	-2.69	W464.50	464.50	2.51	-2.76
W432.00	432.00	2.60	-3.05	W464.85	464.85	2.58	-2.56
W432.50	432.50	2.48	-2.84	W465.10	465.10	2.53	-2.60
W433.00	433.00	2.55	-2.85	W465.40	465.40	2.32	-2.75
W433.50	433.50	2.41	-2.57	W465.70	465.70	2.15	-2.71
W434.00	434.00	2.42	-2.80	W466.02	466.02	2.45	-2.56
W434.50	434.50	2.78	-3.02	W466.33	466.33	2.49	-2.48
W435.00	435.00	2.83	-2.97	W466.52	466.52	2.33	-2.46
W435.50	435.50	2.42	-3.27	W466.80	466.80	2.53	-2.58
W436.00	436.00	2.66	-2.93	W467.10	467.10	2.45	-2.58
W436.50	436.50	2.50	-2.56	W467.48	467.48	2.51	-2.74
W437.00	437.00	2.49	-2.76	W467.81	467.81	2.60	-2.92
W437.50	437.50	2.81	-2.56	W468.10	468.10	2.57	-2.80
W438.00	438.00	2.95	-2.68	W468.47	468.47	2.61	-2.88
W438.50	438.50	3.00	-2.62	W468.87	468.87	2.55	-2.84
W439.00	439.00	2.98	-2.98	W469.12	469.12	2.70	-3.03
W439.50	439.50	2.94	-2.89	W469.39	469.39	2.88	-3.16
W440.00	440.00	2.88	-2.77	W469.76	469.76	2.61	-3.03
W440.50	440.50	2.98	-3.02	W470.03	470.03	2.58	-2.95
W441.00	441.00	2.82	-3.10	W470.32	470.32	2.36	-3.14
W441.50	441.50	2.97	-2.83	W470.65	470.65	2.37	-2.88

W442.00	442.00	3.14	-2.67
W442.50	442.50	3.05	-2.72
W443.00	443.00	3.07	-2.66
W443.50	443.50	2.92	-2.73
W444.00	444.00	3.08	-2.78
W444.50	444.50	2.94	-2.90
W445.00	445.00	2.59	-3.07
W445.50	445.50	2.12	-3.44
W446.00	446.00	2.62	-3.76
W446.50	446.50	2.91	-2.98
W447.00	447.00	2.64	-3.46
W447.50	447.50	2.76	-3.11
W448.05	448.05	2.60	-2.90
W448.50	448.50	2.53	-3.23
W449.00	449.00	2.58	-2.11
W449.50	449.50	2.53	-2.80
W450.00	450.00	2.53	-2.68
W450.53	450.53	2.85	-2.92
W451.00	451.00	2.48	-3.02
W451.50	451.50	2.71	-2.51
W452.00	452.00	2.87	-2.58
W452.50	452.50	2.68	-2.52
W453.00	453.00	2.94	-2.74
W453.50	453.50	3.01	-2.71
W454.00	454.00	2.85	-2.60
W454.45	454.45	2.70	-3.03
W455.00	455.00	2.76	-2.51
W455.50	455.50	2.72	-2.46
W456.00	456.00	2.83	-2.53
W456.50	456.50	3.04	-2.49
W457.00	457.00	2.66	-2.79
W457.55	457.55	2.77	-2.69
W458.00	458.00	2.85	-2.52
W458.50	458.50	2.87	-2.53
W459.00	459.00	2.92	-2.54
W459.50	459.50	2.64	-2.76
W460.00	460.00	2.74	-2.57
W460.30	460.30	2.64	-2.66
W460.60	460.60	2.49	-2.68
W460.90	460.90	2.62	-2.64
W461.20	461.20	2.72	-2.52
W461.50	461.50	2.40	-2.71
W461.80	461.80	2.54	-2.56
W462.10	462.10	2.52	-2.58
W462.40	462.40	2.35	-2.67
W462.70	462.70	2.30	-2.81
W463.00	463.00	2.38	-2.77
W463.30	463.30	2.44	-2.87
W470.90	470.90	2.62	-2.69
W471.18	471.18	2.50	-2.48
W471.50	471.50	2.82	-2.88
W471.72	471.72	2.81	-2.80
W472.10	472.10	2.91	-2.67
W472.40	472.40	3.01	-2.22
W472.70	472.70	2.46	-2.82
W473.00	473.00	2.43	-2.60
W473.58	473.58	2.84	-3.33
W473.82	473.82	3.01	-3.12
W474.00	474.00	3.08	-3.32
W474.18	474.18	2.94	-3.38
W474.40	474.40	3.14	-3.14
W474.50	474.50	2.94	-3.35
W474.72	474.72	3.16	-2.98
W474.92	474.92	3.03	-3.21
W475.21	475.21	3.14	-2.96
W475.42	475.42	3.10	-3.01
W475.60	475.60	3.30	-3.03
W475.75	475.75	3.12	-3.15
W476.02	476.02	2.98	-3.06
W476.18	476.18	2.97	-3.17
W476.42	476.42	3.09	-2.84
W476.60	476.60	2.84	-3.02
W477.00	477.00	2.71	-3.74
W477.23	477.23	2.73	-3.54
W477.35	477.35	2.53	-3.77
W477.45	477.45	2.51	-3.94
W477.50	477.50	2.61	-3.80
W477.58	477.58	1.67	-4.12
W477.65	477.65	2.08	-3.60
W477.80	477.80	2.20	-3.78
W477.90	477.90	2.17	-3.39
W478.13	478.13	1.97	-3.06
W478.17	478.17	1.41	-4.08
W478.25	478.25	1.68	-1.79
W478.38	478.38	1.44	-2.73
W478.52	478.52	1.48	-0.66
W478.86	478.86	1.67	-3.65
W478.95	478.95	1.28	-1.25
W479.10	479.10	1.56	-1.56
W479.20	479.20	1.39	-2.49
W479.30	479.30	1.32	-1.78
W479.40	479.40	1.00	-1.84
W479.52	479.52	1.28	-3.26
W479.70	479.70	1.17	-2.50
W479.75	479.75	1.35	-1.84

Kaberlaba

Sample	High (m)	$\delta^{13}C$	$\delta^{18}O$	Sample	High (m)	$\delta^{13}C$	$\delta^{18}O$
KA 1	-0.60	2.74	-1.88	KA 13	2.70	2.91	-1.31
KA 2	-0.30	2.62	-1.97	KA 14	3.05	3.05	-1.16
KA 3	0.00	2.65	-1.91	KA 15	3.40	2.97	-1.52
KA 4	0.15	3.39	-1.06	KA 16	3.70	3.03	-1.54
KA 5	0.45	3.05	-0.85	KA 17	4.00	2.92	-1.94
KA 6	0.70	2.99	-0.87	KA 19	4.20	3.01	-1.53
KA 7	1.00	2.91	-1.48	KA 20	4.30	2.75	-1.74
KA 8	1.30	2.98	-1.63	KA 21	4.50	2.88	-1.18
KA 9	1.60	2.95	-2.07	KA 22	4.80	2.93	-1.36
KA 10	1.90	2.77	-1.31	KA 23	5.10	2.83	-0.93
KA 11	2.15	2.92	-1.15	KA 24	5.40	2.92	-1.33
KA 12	2.50	2.84	-1.81				

Ponte Serra

Sample	High (m)	$\delta^{13}C$	$\delta^{18}O$	Sample	High (m)	$\delta^{13}C$	$\delta^{18}O$
PS MAI	1100	1.33	-0.68	PS 1	0	1.73	-0.83
PS-830	830	1.42	-1.09	PS 2	-30	1.88	-0.35
PS-820	820	1.47	-0.17	PS 3	-60	1.82	-0.11
PS-805	805	1.40	-0.27	PS 4	-90	1.81	-0.65
PS-780	780	1.44	-0.43	PS 5	-120	1.83	-0.24
PS-760	760	1.45	-0.11	PS 6	-150	1.82	-0.52
PS-740	740	1.46	-0.88	PS 7	-180	1.94	-0.20
PS-720	720	1.44	-0.64	PS 8	-210	2.01	-0.27
PS -700	700	1.50	-0.19	PS 9	-240	1.86	-0.87
PS -680	680	1.46	-0.63	PS 10	-270	1.90	-0.47
PS -660	660	1.47	-0.25	PS 11	-300	1.89	-0.96
PS -640	640	1.57	-0.03	PS 12	-330	1.94	-0.02
PS -620	620	1.53	-0.07	PS 13	-360	2.03	-0.03
PS -580	580	1.53	-0.65	PS 14	-390	1.90	0.15
PS -540	540	1.38	-0.56	PS 15	-420	2.01	-0.39
PS -520	520	1.51	-0.34	PS 16	-450	1.98	-0.16
PS -480	480	1.58	-0.75	PS 17	-475	2.03	-0.26
PS -460	460	1.56	-0.51	PS 18	-480	1.96	-0.45
PS -440	440	1.65	-0.59	PS 19	-510	1.97	-0.18
PS -420	420	1.64	-1.04	PS 20	-540	2.07	-0.33
PS -400	400	1.64	-0.22	PS 21	-570	2.12	-0.40
PS -380	380	1.63	0.12	PS 22	-600	2.14	0.27
PS -365	365	1.62	-0.44	PS 23	-630	2.21	0.20
PS -340	340	1.64	-0.42	PS 24	-660	2.14	0.14
PS -325	325	1.63	-0.37	PS 25	-690	2.40	0.00
PS -300	300	1.69	-0.16	PS 26	-720	2.32	-0.31

PS -280	280	1.69	-0.34
PS -260	260	1.72	-0.11
PS -245	245	1.69	-0.42
PS -220	220	1.64	-0.83
PS -200	200	1.66	-0.40
PS -180	180	1.65	-0.57
PS -160	160	1.64	-0.72
PS -140	140	1.72	-0.01
PS -120	120	1.71	-0.45
PS -100	100	1.75	-0.57
PS -80	80	1.76	-0.61
PS -60	60	1.70	-0.51
PS -40	40	1.65	-0.52
PS -20	20	1.63	-0.48
PS 27	-750	2.16	-0.26
PS 28	-780	2.06	-0.87
PS 28b	-810	2.32	-0.20
PS 29	-810	2.07	-0.82
PS 30	-840	1.97	-1.34
PS 32	-900	2.29	-0.67
PS 33	-930	2.28	-1.93
PS 34	-960	2.34	-1.21
PS 35	-990	2.27	-1.11
PS 36	-1020	2.34	-1.39
PS 37	-1050	2.29	-1.89
PS 38	-1080	2.27	-1.36
PS 39	-1110	2.19	-2.06

San Giorgio

Sample	High (m)	$\delta^{13}C$	$\delta^{18}O$
SG 165	165	3.22	-0.50
SG 155	155	3.01	-0.76
SG 145	145	2.82	-0.92
SG 140	140	3.18	-0.29
SG 135	135	3.01	-0.47
SG 130	130	2.84	-2.46
SG 125	125	2.76	-0.36
SG 120	120	2.63	-0.26
SG 115	115	2.79	-0.14
SG 110	110	2.97	-0.26
SG 105	105	2.86	-2.57
SG 100	100	3.03	-0.30
SG 95	95	3.14	0.09
SG 90	90	2.83	-2.23
SG 85	85	3.14	-0.01
SG 80	80	3.36	0.26
SG 75	75	3.13	-0.05
SG 70	70	3.24	-0.06
SG 65	65	3.18	-0.00
SG 60	60	3.07	0.09
SG 55	55	3.01	-0.27
SG 50	50	2.90	0.04

Sample	High (m)	$\delta^{13}C$	$\delta^{18}O$
SG 45	45	3.04	-0.25
SG 40	40	3.15	0.03
SG 35	35	3.39	-0.02
SG 30	30	3.24	-0.96
SG 26	26	3.31	-2.88
SG 22.5	22.5	3.01	-2.02
SG 20	20	3.30	-1.61
SG 15	15	3.24	-1.13
SG 10	10	3.38	-0.52
SG 5	5	3.35	-1.24
SG 0	0	3.33	-0.52
SG -5	-5	3.25	-1.73
SG -10	-10	3.23	-1.43
SG -15P	-15	3.18	-1.38
SG -15S	-15	3.21	-1.24
SG -20P	-20	3.23	-0.58
SG -20S	-20	3.19	-1.05
SG -25	-25	3.07	-1.56
SG -30	-30	3.13	-2.00
SG -35	-35	3.18	-1.94
SG -40	-40	3.28	-1.51
SG -45	-45	3.32	-1.41

Spiazzi

Sample	High (m)	$\delta^{13}C$	$\delta^{18}O$
MC 30	-3	2.92	-1.07
MC 29	-2	2.69	-1.26
MC 28	-1.75	2.96	-0.80
MC 27	-1.4	2.92	-1.20
MC 26	-1.2	3.14	-0.92
MC 25	-0.8	2.79	-1.64
MC 23	-0.4	3.13	-0.78
MC 22	-0.1	3.35	-0.83
MC 21	-0.05	3.26	-0.92
MC1	0.3	3.13	-0.85
MC2	0.6	3.01	0.69
MC3	0.9	2.76	0.64
MC4	1.2	3.22	0.13
MC5	1.3	3.13	-0.38
MC6	1.6	2.80	0.03

Sample	High (m)	$\delta^{13}C$	$\delta^{18}O$
MC7	1.9	2.88	0.32
MC8	2.2	2.74	0.34
MC9	2.5	2.67	0.24
MC10	2.8	2.56	0.39
MC11	3.1	2.57	0.43
MC12	3.4	2.64	-0.49
MC13	3.7	2.43	0.44
MC14	4	2.37	0.36
MC15	4.3	2.38	0.03
MC16	4.6	2.21	0.26
MC17	4.9	2.28	0.41
MC18	5.2	2.23	0.46
MC 19	5.5	2.06	0.07
MC 20	5.8	1.89	-0.14

Torre de Busi

Sample	High (m)	$\delta^{13}C$	$\delta^{18}O$
TB0.00	0.00	1.13	-1.75
TB0.20	0.20	1.23	-1.49
TB0.40	0.40	1.13	-3.03
TB0.60	0.60	1.31	-1.38
TB0.80	0.80	1.12	-1.90
TB1.00	1.00	1.20	-1.76
TB1.20	1.20	1.17	-2.41
TB1.40	1.40	1.19	-1.53
TB1.60	1.60	1.00	-2.09
TB1.80	1.80	0.96	-2.52
TB2.00	2.00	1.09	-1.71
TB2.40	2.40	0.97	-2.20
TB2.60	2.60	0.80	-2.52
TB2.80	2.80	0.82	-2.22
TB3.00	3.00	1.06	-2.60
TB3.20	3.20	1.27	-2.29
TB3.40	3.40	0.94	-1.97
TB3.60	3.60	1.01	-2.01
TB3.80	3.80	1.12	-2.44
TB4.00	4.00	1.20	-1.98
TB4.20	4.20	1.20	-1.88
TB4.40	4.40	1.26	-2.09

Sample	High (m)	$\delta^{13}C$	$\delta^{18}O$
TB17.80	17.80	1.38	-2.35
TB18.00	18.00	1.11	-3.26
TB18.35	18.35	1.67	-1.58
TB18.80	18.80	1.40	-1.32
TB19.00	19.00	1.64	-2.83
TB19.30	19.30	1.24	-2.79
TB19.50	19.50	1.49	-2.52
TB19.60	19.60	1.83	-1.82
TB19.80	19.80	1.75	-2.09
TB20.00	20.00	1.42	-1.95
TB20.20	20.20	1.68	-2.34
TB20.40	20.40	1.61	-2.58
TB20.60	20.60	1.53	-2.97
TB20.80	20.80	1.66	-2.64
TB21.40	21.40	1.63	-4.04
TB21.60	21.60	1.62	-2.39
TB21.80	21.80	1.77	-2.56
TB22.00	22.00	1.81	-2.34
TB22.20	22.20	1.86	-2.41
TB22.40	22.40	1.27	-2.06
TB23.00	23.00	1.55	-4.00
TB23.20	23.20	1.67	-3.34

TB4.80	4.80	0.75	-3.41	TB23.40	23.40	1.55	-3.40
TB4.80	4.80	1.06	-2.52	TB23.60	23.60	1.88	-2.77
TB5.00	5.00	1.38	-1.60	TB24.00	24.00	1.60	-2.74
TB5.20	5.20	1.26	-2.03	TB24.20	24.20	1.85	-2.97
TB5.40	5.40	1.20	-1.98	TB24.40	24.40	1.68	-2.26
TB5.60	5.60	1.32	-1.42	TB24.60	24.60	1.80	-2.39
TB6.00	6.00	1.29	-2.04	TB25.00	25.00	1.68	-3.00
TB6.20	6.20	1.33	-2.68	TB25.20	25.20	1.89	-1.57
TB6.40	6.40	1.28	-1.84	TB25.40	25.40	1.93	-2.84
TB6.60	6.60	1.20	-1.94	TB25.60	25.60	1.33	-3.38
TB6.80	6.80	1.32	-1.90	TB25.80	25.80	2.22	-2.90
TB7.00	7.00	1.32	-2.01	TB25.80	25.80	2.09	-3.19
TB7.20	7.20	1.31	-1.90	TB26.00	26.00	2.01	-2.89
TB7.35	7.35	1.39	-2.11	TB26.80	26.80	2.24	-2.50
TB7.40	7.40	1.15	-3.09	TB27.00	27.00	2.26	-2.78
TB7.60	7.60	1.12	-2.86	TB27.20	27.20	2.23	-2.29
TB7.80	7.80	1.24	-2.47	TB27.40	27.40	1.83	-3.65
TB8.00	8.00	1.13	-2.99	TB27.60	27.60	1.95	-2.84
TB8.20	8.20	1.02	-3.94	TB27.80	27.80	1.95	-2.90
TB8.40	8.40	1.09	-2.71	TB28.00	28.00	2.03	-3.04
TB8.60	8.60	1.14	-2.92	TB28.20	28.20	2.04	-3.23
TB8.80	8.80	0.59	-3.11	TB28.40	28.40	2.05	-2.93
TB9.00	9.00	0.96	-2.74	TB28.60	28.60	1.99	-2.76
TB9.20	9.20	0.81	-2.73	TB30.00	30.00	2.07	-2.09
TB9.40	9.40	1.20	-2.20	TB30.20	30.20	1.41	-2.06
TB9.60	9.60	0.95	-2.37	TB30.40	30.40	2.13	-2.38
TB9.80	9.80	0.64	-2.79	TB30.60	30.60	2.20	-1.99
TB10.00	10.00	1.05	-2.28	TB30.80	30.80	1.80	-2.20
TB10.20	10.20	0.81	-2.74	TB31.00	31.00	2.25	-2.06
TB10.40	10.40	1.05	-2.90	TB31.20	31.20	2.20	-2.91
TB10.60	10.60	1.01	-1.95	TB31.40	31.40	2.35	-2.06
TB10.60	10.60	0.96	-2.00	TB31.60	31.60	2.16	-2.40
TB10.80	10.80	0.81	-2.79	TB31.80	31.80	2.08	-3.02
TB11.00	11.00	0.85	-2.76	TB32.20	32.20	2.18	-3.31
TB11.20	11.20	1.03	-2.81	TB32.50	32.50	2.01	-2.92
TB11.40	11.40	0.76	-3.12	TB32.80	32.80	2.08	-2.28
TB11.60	11.60	1.01	-2.73	TB33.30	33.30	2.17	-1.73
TB12.00	12.00	1.04	-3.08	TB33.40	33.40	2.25	-2.54
TB12.20	12.20	0.54	-3.46	TB33.60	33.60	2.19	-3.45
TB12.40	12.40	0.96	-3.09	TB34.00	34.00	2.22	-3.47
TB12.60	12.60	1.21	-3.45	TB34.20	34.20	2.26	-3.18
TB13.00	13.00	1.31	-2.12	TB34.60	34.60	2.19	-3.42
TB13.20	13.20	1.43	-2.01	TB35.40	35.40	2.21	-2.89
TB13.40	13.40	1.54	-1.78	TB35.60	35.60	2.35	-3.12
TB13.60	13.60	1.53	-1.96	TB35.95	35.95	2.55	-3.17
TB13.60	13.60	1.48	-1.98	TB36.20	36.20	2.10	-3.01
TB13.80	13.80	1.51	-1.57	TB36.60	36.60	2.06	-3.17
TB14.00	14.00	1.57	-1.61	TB36.80	36.80	2.29	-2.86
TB14.20	14.20	1.44	-1.62	TB37.00	37.00	1.92	-2.60

TB14.40	14.40	1.48	-1.63	TB37.20	37.20	1.63	-2.92
TB14.60	14.60	1.57	-1.68	TB37.40	37.40	2.30	-2.37
TB14.80	14.80	1.54	-1.66	TB37.60	37.60	2.19	-3.18
TB15.00	15.00	1.54	-1.79	TB37.80	37.80	2.21	-2.79
TB15.20	15.20	1.55	-1.77	TB38.30	38.30	2.12	-2.18
TB15.40	15.40	1.32	-3.18	TB38.60	38.60	2.32	-2.98
TB15.80	15.80	1.51	-1.90	TB38.80	38.80	2.33	-2.96
TB16.20	16.20	1.47	-2.31	TB42.00	42.00	2.65	-2.22
TB16.40	16.40	1.43	-2.14	TB42.40	42.40	2.34	-3.19
TB16.60	16.60	1.33	-3.37	TB42.80	42.80	2.49	-2.36
TB16.80	16.80	1.60	-1.95	TB43.20	43.20	2.73	-2.04
TB17.10	17.10	1.47	-1.47	TB43.40	43.40	2.85	-2.19
TB17.30	17.30	0.91	-2.87	TB43.40	43.40	2.70	-2.41
TB17.50	17.50	1.45	-2.27	TB43.90	43.90	2.57	-2.63

Torre de Busi

Sample	High (m)	$\delta^{13}C$	$\delta^{18}O$	Sample	High (m)	$\delta^{13}C$	$\delta^{18}O$
VM0	0	2.47	-1.28	VM 280	280	2.56	-1.80
VM 10	10	2.46	-0.46	VM 290	290	2.61	-2.10
VM20	20	2.63	-1.02	VM 305	305	2.49	-2.12
VM30	30	2.58	-0.89	VM 315	315	2.45	-1.90
VM40	40	2.60	-1.38	VM 320	320	2.39	-2.18
VM50	50	2.70	-1.65	VM 330	330	2.58	-2.49
VM60	60	2.57	-1.35	VM 345	345	2.55	-1.99
VM75	75	2.47	-1.40	VM 350	350	2.60	-1.46
VM80	80	2.93	-2.02	VM 360	360	2.46	-1.70
VM 90	90	2.92	-1.43	VM 370	370	2.54	-1.71
VM 100	100	2.97	-2.47	VM 380	380	2.52	-1.81
VM 110	110	2.93	-1.83	VM 395	395	2.61	-2.46
VM 120	120	2.73	-2.35	VM 415	415	2.73	-1.14
VM 130	130	3.18	0.09	VM 425	425	2.68	-2.38
VM 140	140	3.23	-1.33	VM 435	435	2.90	-0.26
VM 150	150	3.40	0.23	VM 445	445	2.56	-1.71
VM 160	160	2.74	-0.58	VM 460	460	2.44	-1.25
VM 170	170	2.96	-0.80	VM 470	470	2.41	-1.64
VM 180	180	2.85	-2.62	VM 485	485	2.40	-1.73

Late Jurassic $\delta^{13}C$ compilation curve

Age	$\delta^{13}C$	Age	$\delta^{13}C$	Age	$\delta^{13}C$	Age	$\delta^{13}C$
144.50	0.87	150.80	2.58	155.81	1.94	156.04	2.33
144.71	1.43	150.91	1.94	155.81	1.86	156.05	2.57
144.75	1.33	150.98	2.24	155.82	1.87	156.05	2.57
144.92	1.3	151.19	2.16	155.82	2.17	156.05	2.57
145.00	1.27	151.28	2.04	155.83	2.39	156.06	2.61
145.05	1.1	151.37	2.21	155.83	2.28	156.06	2.62
145.14	1.13	151.54	1.94	155.83	2.16	156.07	2.42
145.20	1.43	151.73	2.22	155.84	2.14	156.07	2.41
145.23	1.14	151.74	2.52	155.84	1.93	156.07	2.63
145.29	1.16	151.80	2.75	155.85	2.06	156.08	2.54
145.32	1.13	152.00	2.67	155.85	1.78	156.08	2.53
145.32	1.11	152.07	2.79	155.85	1.75	156.09	2.67
145.40	0.81	152.13	2.58	155.86	2.12	156.09	2.63
145.42	1.35	152.32	2.64	155.86	2.17	156.10	2.57
145.43	1.39	152.36	2.53	155.87	2.12	156.10	2.51
145.44	0.98	152.49	2.27	155.87	2.31	156.20	2.605
145.46	1.19	152.58	2.31	155.88	2.18	156.23	2.559
145.49	1.41	152.73	2.3	155.88	2.16	156.25	2.744
145.50	1.54	152.88	2.48	155.88	2.27	156.28	2.646
145.87	1.35	152.91	2.72	155.89	2.35	156.31	2.604
146.15	1.5	153.01	2.52	155.89	2.55	156.34	2.484
146.45	1.4	153.04	2.35	155.90	2.26	156.37	2.55
147.02	1.6	153.10	2.56	155.90	2.18	156.40	2.405
147.32	1.24	153.12	2.61	155.90	2.25	156.42	2.422
147.48	1.55	153.15	2.63	155.91	2.23	156.45	2.775
147.74	2.07	153.22	2.37	155.91	2.18	156.48	2.828
147.80	1.5	153.27	2.48	155.92	2.4	156.51	2.418
147.88	1.44	153.30	2.63	155.92	2.29	156.54	2.657
148.14	1.75	153.32	2.03	155.92	2.23	156.57	2.5
148.30	1.74	153.37	2.62	155.93	2.31	156.59	2.494
148.41	1.84	153.38	2.39	155.93	2.22	156.62	2.808
148.58	1.98	153.42	2.41	155.94	2.33	156.65	2.951
148.89	1.85	153.46	2.58	155.94	2.11	156.68	2.999
149.40	1.96	153.46	2.22	155.94	2.37	156.71	2.977
149.45	1.96	153.48	2.13	155.95	2.11	156.74	2.942
149.49	2.03	153.49	2.31	155.95	2.28	156.76	2.88
149.54	2.04	153.52	2.31	155.96	2.33	156.79	2.98
149.63	1.68	153.60	2.13	155.96	2.48	156.82	2.82
149.63	2.03	154.17	2.44	155.96	2.6	156.85	2.97
149.68	1.91	154.94	2.55	155.97	2.46	156.88	3.14
149.73	1.99	155.70	2.48	155.97	2.45	156.91	3.05
149.77	1.96	155.72	2.28	155.98	2.5	156.93	3.07
149.82	2.05	155.73	2.17	155.98	2.37	156.96	2.92
149.87	2.02	155.75	2.38	155.99	2.54	156.99	3.08
149.91	2.03	155.75	2.06	155.99	2.26	157.02	2.94
149.95	2.06	155.76	2.1	155.99	2.5	157.05	2.59
149.96	2.07	155.76	2.23	156.00	2.33	157.08	2.12
150.01	2.07	155.77	2.44	156.00	2.32	157.10	2.623
150.05	2.12	155.77	2.32	156.01	2.26	157.13	2.911
150.15	2.01	155.77	1.96	156.01	2.37	157.16	2.636
150.33	2.11	155.78	1.94	156.01	2.24	157.19	2.764
150.42	2.05	155.79	1.96	156.02	2.68	157.22	2.597
150.43	2.18	155.79	1.96	156.02	2.37	157.25	2.526
150.53	2.18	155.79	2.16	156.03	2.49	157.27	2.58
150.61	2.15	155.80	2.03	156.03	2.44	157.30	2.528
150.62	2.32	155.80	1.98	156.03	2.46	157.33	2.529
150.71	2.33	155.81	2.01	156.04	2.41	157.36	2.85

Age	$\delta^{13}C$	Age	$\delta^{13}C$	Age	$\delta^{13}C$	Age	$\delta^{13}C$
157.39	2.483	158.27	2.108	158.63	2.874	159.00	2.511
157.42	2.714	158.28	1.836	158.64	2.583	159.00	2.638
157.44	2.869	158.28	2.487	158.65	0.941	159.01	2.306
157.47	2.677	158.29	1.977	158.65	2.91	159.01	2.614
157.50	2.942	158.29	1.663	158.66	2.725	159.02	2.278
157.53	3.095	158.29	2.331	158.67	2.849	159.03	1.863
157.56	2.851	158.30	1.752	158.67	3.01	159.04	1.667
157.58	2.702	158.31	1.654	158.68	2.8275	159.04	2.334
157.62	2.759	158.31	2.525	158.69	2.648	159.05	2.075
157.64	2.716	158.31	1.915	158.69	2.46	159.05	1.411
157.67	2.831	158.32	2.019	158.69	2.9375	159.06	1.876
157.70	3.038	158.33	2.447	158.71	2.631	159.06	2.132
157.73	2.657	158.34	1.892	158.71	2.43	159.07	1.362
157.76	2.771	158.34	2.11	158.71	3.0095	159.08	1.737
157.79	2.854	158.35	2.505	158.73	1.78	159.08	1.274
157.81	2.869	158.37	2.137	158.74	2.2235	159.09	2.444
157.84	2.919	158.38	1.653	158.75	2.84	159.09	1.791
157.87	2.64	158.38	2.603	158.76	2.351	159.09	2.199
157.90	2.736	158.39	1.314	158.77	3.1	159.10	2.214
157.92	2.644	158.39	2.281	158.78	3.08	159.10	2.137
157.93	2.493	158.40	2.569	158.78	2.077	159.11	2.117
157.95	2.618	158.40	2.198	158.79	2.94	159.11	1.993
157.97	2.718	158.41	2.244	158.79	2.102	159.12	2.267
157.98	2.404	158.42	2.235	158.80	3.139	159.12	2.171
158.00	2.535	158.42	2.613	158.80	3.14	159.12	1.859
158.02	2.516	158.43	2.223	158.81	2.413	159.13	2.236
158.03	2.349	158.43	2.414	158.81	2.94	159.13	1.821
158.05	2.295	158.44	2.498	158.82	3.143	159.14	2.259
158.07	2.384	158.45	2.552	158.82	3.16	159.15	1.943
158.09	2.438	158.45	2.46	158.83	1.846	159.15	1.748
158.10	2.354	158.46	2.148	158.84	3.03	159.16	1.429
158.10	2.153	158.46	2.702	158.84	3.092	159.16	2.313
158.11	2.123	158.47	1.989	158.86	3.14	159.17	1.38
158.12	2.344	158.47	1.689	158.86	3.049	159.17	1.703
158.12	1.947	158.48	2.877	158.87	3.1	159.18	1.589
158.13	1.818	158.48	1.887	158.87	2.648	159.18	1.974
158.14	2.575	158.49	2.173	158.88	3.3	159.18	2.003
158.14	1.831	158.50	2.068	158.89	3.007	159.19	1.288
158.15	1.93	158.50	2.608	158.89	3.12	159.19	1.409
158.15	2.09	158.51	1.653	158.90	2.358	159.19	1.226
158.16	1.933	158.52	2.642	158.91	2.98	159.20	2.185
158.16	2.513	158.52	2.583	158.91	2.96	159.21	1.677
158.17	1.757	158.52	1.089	158.92	2.97	159.21	1.464
158.17	1.745	158.53	1.672	158.93	2.113	159.22	1.631
158.18	1.293	158.54	2.361	158.93	3.09	159.22	1.644
158.18	2.582	158.54	2.386	158.94	1.854	159.23	1.845
158.18	1.96	158.55	2.119	158.95	2.844	159.23	1.763
158.19	1.604	158.55	2.778	158.95	2.435	159.24	1.683
158.20	2.529	158.56	1.936	158.96	2.981	159.24	1.311
158.20	1.429	158.56	2.369	158.96	1.4295	159.24	1.439
158.21	2.092	158.57	1.89	158.97	2.635	159.25	1.265
158.22	2.324	158.58	2.62	158.97	2.828	159.25	1.766
158.22	1.624	158.59	1.557	158.97	2.711	159.26	1.703
158.23	2.46	158.59	2.504	158.98	1.5705	159.26	1.739
158.24	2.149	158.60	0.149	158.98	2.163	159.27	2.068
158.24	2.315	158.61	1.822	158.99	2.733	159.28	1.491
158.25	2.132	158.62	2.82	158.99	2.58	159.28	1.477
158.26	2.384	158.62	0.773	158.99	1.433	159.29	1.451
158.26	2.446	158.63	2.81	159.00	2.528	159.29	1.561

Age	$\delta^{13}C$	Age	$\delta^{13}C$	Age	$\delta^{13}C$	Age	$\delta^{13}C$
159.30	1.529	159.54	1.578	160.00	1.001	161.07	1.603
159.30	2.18	159.55	0.942	160.01	0.807	161.09	1.051
159.31	2.207	159.55	1.642	160.02	0.736	161.10	0.88
159.31	2.062	159.55	1.706	160.03	1.355	161.12	0.945
159.32	1.917	159.56	1.59	160.04	1.216	161.13	1.899
159.32	1.519	159.57	1.441	160.05	0.757	161.17	1.794
159.33	2.034	159.57	0.89	160.06	1.377	161.17	1.363
159.33	2.144	159.59	1.169	160.06	1.339	161.19	0.838
159.34	2.269	159.60	1.58	160.07	1.101	161.22	0.645
159.34	2.039	159.60	1.349	160.08	1.416	161.22	0.176
159.35	2.055	159.60	1.417	160.09	1.394	161.24	0.757
159.35	1.286	159.62	1.657	160.10	1.273	161.26	1.414
159.35	2.167	159.62	1.509	160.11	1.522	161.29	1.863
159.36	1.967	159.63	1.662	160.12	1.32	161.30	1.663
159.36	2.118	159.64	1.144	160.13	1.344	161.31	1.657
159.37	1.673	159.64	1.237	160.14	0.982	161.32	1.801
159.37	1.962	159.65	1.513	160.14	1.153	161.33	1.849
159.38	1.441	159.65	1.808	160.15	1.286	161.35	1.514
159.38	1.946	159.66	1.715	160.16	1.307	161.36	1.849
159.39	1.94	159.66	1.546	160.17	1.318	161.36	1.768
159.39	1.291	159.67	2.051	160.20	1.204	161.37	1.728
159.39	1.28	159.67	1.735	160.60	0.271	161.40	1.858
159.39	2.26	159.68	1.834	160.61	0.653	161.41	0.851
159.40	2.111	159.68	1.983	160.62	1.313	161.41	1.664
159.41	2.194	159.69	2.072	160.63	1.32	161.44	1.438
159.41	1.983	159.70	1.94	160.63	1.136	161.45	1.733
159.41	1.801	159.70	2.015	160.64	0.662	161.46	1.62
159.42	1.89	159.71	1.815	160.65	0.832	161.46	1.621
159.42	1.556	159.72	1.924	160.66	0.898	161.48	1.072
159.42	1.443	159.73	1.791	160.67	0.565	161.49	1.185
159.43	1.561	159.74	1.773	160.68	1.628	161.50	1.405
159.43	1.077	159.74	1.677	160.68	0.924		
159.44	1.33	159.75	1.592	160.70	1.628		
159.45	1.788	159.76	1.755	160.70	1.687		
159.45	1.764	159.77	1.788	160.71	1.444		
159.46	2.003	159.78	1.513	160.72	1.673		
159.46	1.392	159.79	0.868	160.73	1.628		
159.46	1.908	159.80	1.745	160.74	1.586		
159.47	1.907	159.81	1.454	160.75	1.597		
159.47	2.084	159.82	1.75	160.76	1.179		
159.48	2.034	159.82	1.323	160.77	1.762		
159.48	1.322	159.83	1.638	160.78	1.796		
159.48	1.77	159.84	1.744	160.83	1.94		
159.49	1.993	159.85	1.652	160.86	1.669		
159.49	1.84	159.86	1.761	160.86	2.01		
159.50	1.298	159.87	1.568	160.89	1.789		
159.51	1.27	159.88	1.427	160.92	1.744		
159.51	1.599	159.89	1.485	160.93	1.849		
159.51	1.002	159.90	1.014	160.93	1.772		
159.51	1.706	159.90	1.295	160.94	1.704		
159.51	1.73	159.91	1.24	160.95	1.804		
159.52	1.514	159.92	1.493	160.96	1.6		
159.52	1.695	159.93	1.469	160.97	1.688		
159.52	1.545	159.94	1.46	160.99	1.623		
159.53	1.497	159.95	1.463	161.00	1.808		
159.53	1.579	159.96	0.844	161.01	1.283		
159.53	1.352	159.97	1.318	161.03	1.806		
159.53	1.645	159.98	1.284	161.04	1.349		
159.54	1.406	159.98	1.199	161.05	1.317		
159.54	1.276	159.99	1.134	161.06	1.436		

Specific $\partial^{13}C$ analyses on nodular limestones

Nodules			Matrix		
Sample	$\delta^{13}C$	$\delta^{18}O$	Sample	$\delta^{13}C$	$\delta^{18}O$
N1AU21	2.84	-2.11	M1AU21	2.79	-3.58
N2AU21	2.97	-1.35	M2AU21	2.58	-4.17
N3AU21	2.92	-1.83			
N4AU21	3.11	-1.94			
NAU 29	2.60	-3.19	MAU 29	2.64	-3.85
NAU26	2.86	-3.58	MAU26	2.64	-4.27
N1NI13	2.78	-4.34	M1NI13	2.44	-5.06
N2NI13	2.62	-4.85	M1NI13	2.57	-5.01
N3NI13	2.72	-4.86			
NNi 17	2.50	-4.81	MNi 17	2.11	-5.43
NNI14	2.68	-4.94	MNI14	2.51	-5.16
N1GA8	3.57	-1.21	MGA8	3.61	-1.42
N2GA8	3.62	-1.09			
N3GA8	3.85	-0.59			
N4GA8	3.68	-0.96			
GA22	2.90	-0.52	MGA22	2.84	-1.69
NGA12	3.59	-0.72	MGA12	3.46	-1.87
NGA16	3.67	-0.81	MGA16	3.67	0.20
N1GA14	3.96	-1.65	MGA14	3.56	-2.61
N2GA14	3.89	-1.78			
N3GA14	3.56	-2.26			

Specific isotopic analyses on the hardground samples of Weiach

Sample	Material	$\delta^{13}C$	$\delta^{18}O$
WA 1	Gray micritic limestone	0.779	-0.798
WA 2	Middle of a dark bioturbation	0.98	-1.052
WA 3	Orange area around bioturbation	0.614	-0.923
WA 4	Gray micritic limestone	0.777	-0.968
WA 5	Zone with vertical cracks	1.11	-1.983
WA 6	Small shell fillings	0.713	-1.339
WA 7	Gray micritic limestone with iron ooids	1.017	-0.918
WA 8	Light gray zone	1.121	-0.904
WA 9	Vertical crack	0.972	-1.364
WA 10	Calcite filling horizontal crack	-1.141	-4.117
WB 1	Cavity infill (shell)	-0.631	-5.456
WB 2	Dark gray bioturbation	0.973	-1.038
WB 3	Gray micritic limestone	0.368	-1.55
WB 4	Zone with vertical cracks	1.017	-1.439
WB 5	Gray micritic limestone	0.911	-1.289
WB 6	Light gray zone	1.016	-1.147
WB 7	Light gray zone	0.95	-0.804
WC 1	Cavity infill, calcite from the center	0.143	-6.962
WC 2	Cavity infill, calcite from the edge	0.789	-0.047
WC 3	Gray micritic limestone	0.463	-1.299
WC 4	Gray micritic limestone	0.351	-1.463
WC 5	Gray micritic limestone	0.392	-1.476

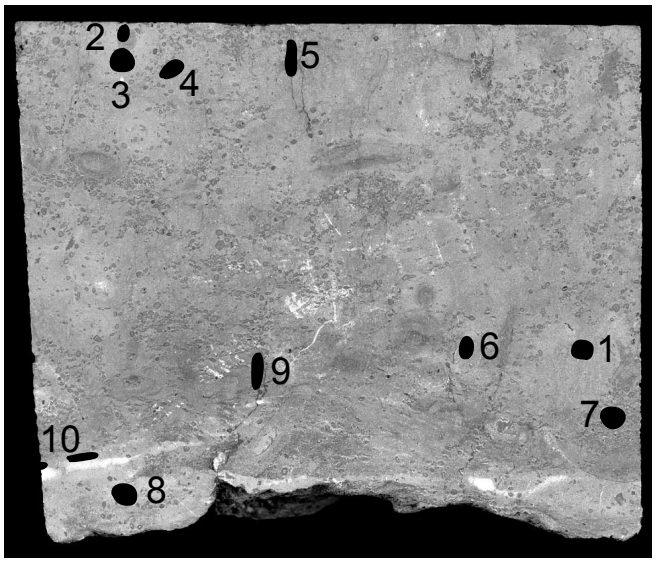
WA
2
3
4
5
6
1
9
7
10
8
2 cm

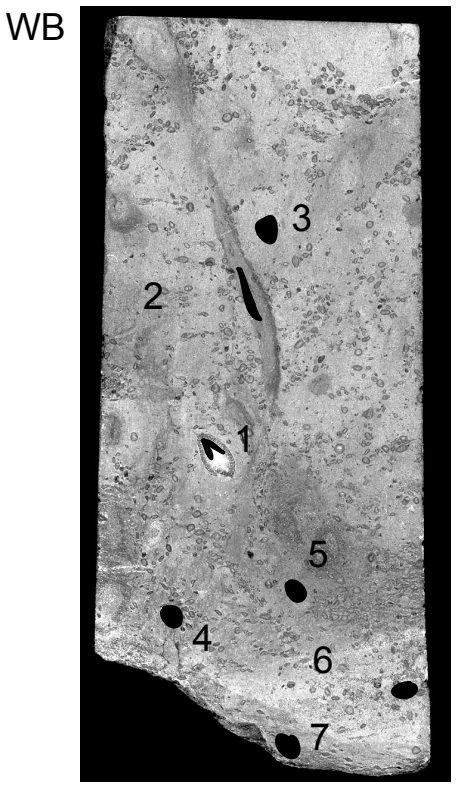
WB
3
2
1
5
4
6
7
1 cm


WC
1
2
3
4
5
1 cm

Specific isotopic analyses on the hardground samples of Auenstein

Sample	Material	$\delta^{13}C$	$\delta^{18}O$
ASA 1	Gray micritic limestone	1.505	-0.844
ASA 2	Gray limestone	1.661	-0.445
ASA 3	Gray micritic limestone inside a shell	1.627	-0.512
ASA 4	Gray limestone	1.651	-1.428
ASA 5	Greenish limestone	2.043	-0.142
ASA 6	Brownish limestone	1.464	-1.007
ASA 7	Greenish limestone	1.262	-2.618
ASA 8	Redish limestone	1.874	-0.479
ASA 9	Cavity infill	1.553	-6.228
ASA 10	Cavity infill	1.599	-6.88
ASA 11	Cavity infill	0.618	-7.229
ASA 12	Belemnite	0.245	-0.594
ASA 13	Belemnite	-1.331	0.172
ASA 14	Bryozoan	1.48	0.26
ASA 15	Serpulid	2.829	-0.13
ASA 16	Microbial mat	1.461	-4.189
ASB 1	Cavity infill, calcite from the center	1.598	-7.911
ASB 2	Cavity infill, calcite from the edge	1.743	-2.751
ASB 3	Cavity infill	1.46	-6.745
ASB 4	Calcite in glauconitic pebble	1.399	-7.552
ASB 5	Gray micritic limestone	1.234	-1.588
ASB 6	Gray limestone	1.248	-0.757

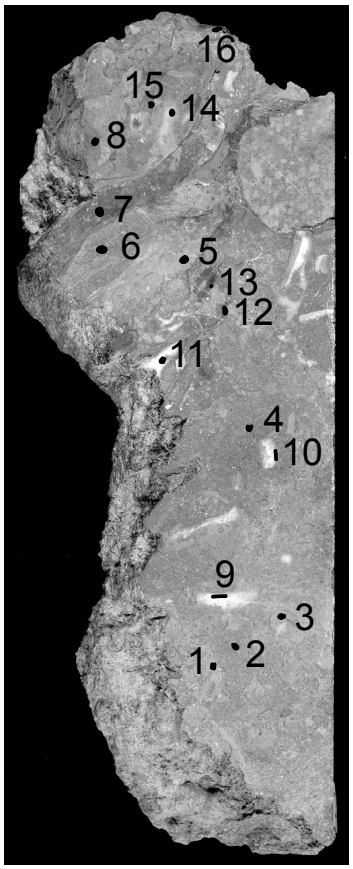
ASA
16
15
14
8
7
6
5
13
12
11
4
10
9
3
1
2
5 cm

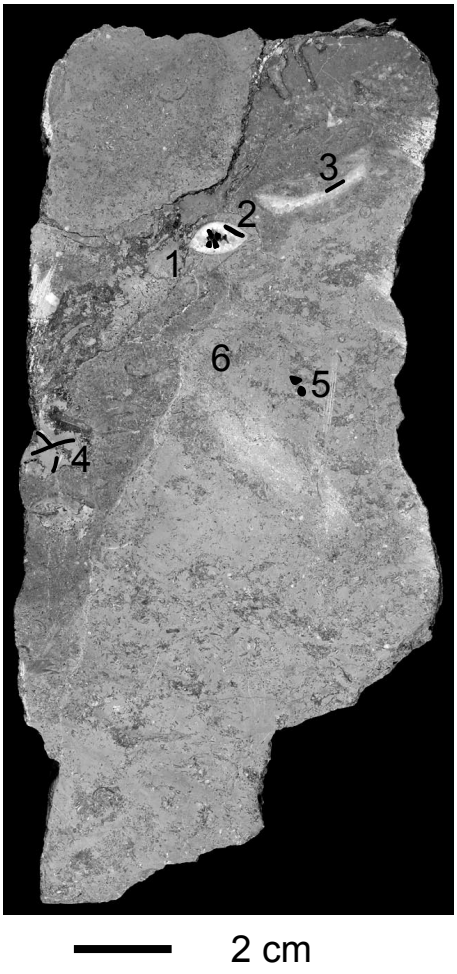
ASB
3
2
1
6
5
4
2 cm

Carbonate content, Weiach

Sample	TIC (wt %)	Sample	TIC (wt %)	Sample	TIC (wt %)
W 479.75	1.36	W 454.45	9.40	W 473.82	8.64
W 430.00	8.26	W 456.50	8.67	W 474.00	8.62
W 431.00	7.41	W 457.00	9.16	W 474.40	6.74
W 432.50	7.86	W 457.55	8.82	W 474.72	7.01
W 433.50	7.61	W 459.00	5.72	W 475.21	6.70
W 434.50	7.01	W 460.30	7.18	W 475.75	7.78
W 436.50	6.78	W 461.20	7.48	W 476.42	6.45
W 437.50	8.19	W 462.10	6.63	W 477.00	8.09
W 438.50	7.95	W 463.00	6.75	W 477.45	6.24
W 439.50	7.87	W 463.90	7.96	W 477.58	2.08
W 441.00	8.78	W 465.10	8.24	W 477.80	3.10
W 442.50	7.88	W 465.70	10.09	W 478.13	1.88
W 444.00	8.06	W 466.52	5.74	W 478.17	1.86
W 445.50	5.33	W 467.48	8.13	W 478.25	8.11
W 447.00	4.10	W 468.47	8.14	W 478.38	2.21
W 448.50	4.97	W 469.39	7.98	W 478.52	8.74
W 450.00	7.41	W 470.03	9.92	W 478.86	1.63
W 451.00	9.15	W 471.18	7.17	W 478.95	2.24
W 451.50	7.88	W 471.72	7.19	W 479.20	2.89
W 453.00	7.69	W 472.70	6.06	W 479.52	8.33

Compared carbonate content in nodules and matrix of the nodular limestones

Nodules			Matrix		
Sample	TIC (wt %)	TOC (wt %)	Sample	TIC (wt %)	TOC (wt %)
NMI16	10.748		MAU13	8.17	0.32
NAU13	10.85	0.17	MAU18	6.294	
NAU18	10.784		MAU26	10.189	
NAU26	11.356		MGA13	7.093	
NGA13A	10.925		MGA18	10.313	
NGA13B	10.462		MGA8	9.15	0.15
NGA18	10.608		MMI19	10.97	0.00
NGA8	10.93	0.14	MMI21	8.631	
NMI19	10.37	0.00	MNI12	5.01	0.25
NMI21	10.779		MNI16	6.144	
NNI12	11.02	0.04	MNI20	7.462	
NNI20	10.454				

Mircroprobe image

Auenstein
Schellenbrücke Bed
Mineral composition of the matrix

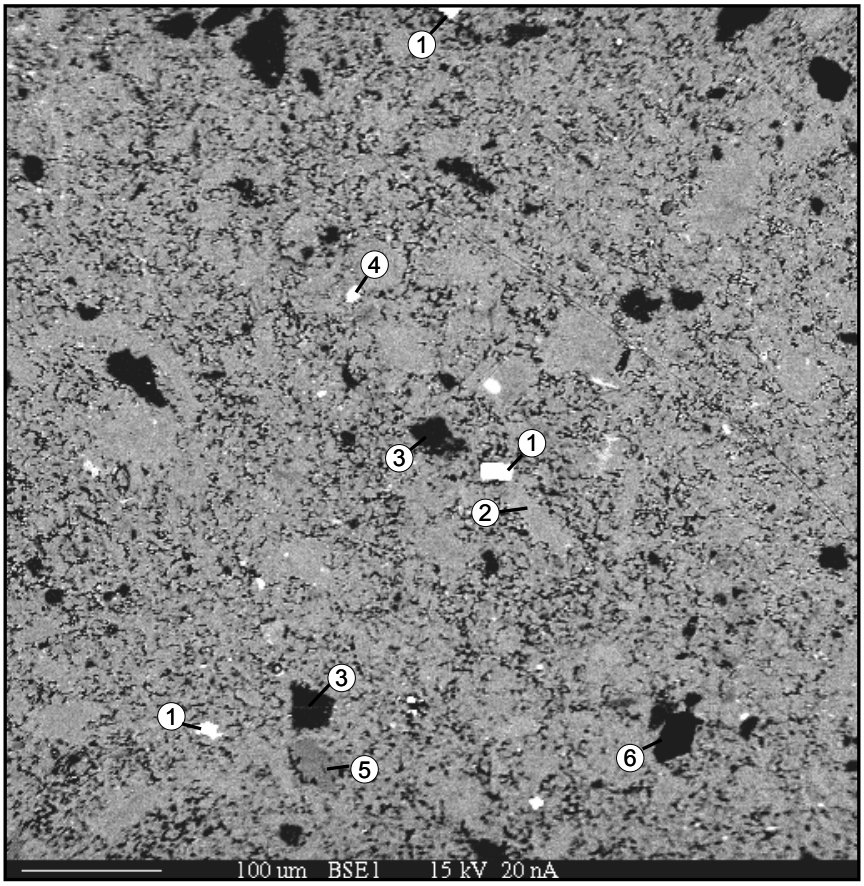

1 Pyrite
2 Calcite
3 Quartz
4 Detritic mineral with Ti (rutile?)
5 K-feldspar
6 Clay mineral, probably Monmorillonite

Mircroprobe image

Auenstein
Top of the Schellenbrücke Bed.
Greenish microbial mat with microboring structure

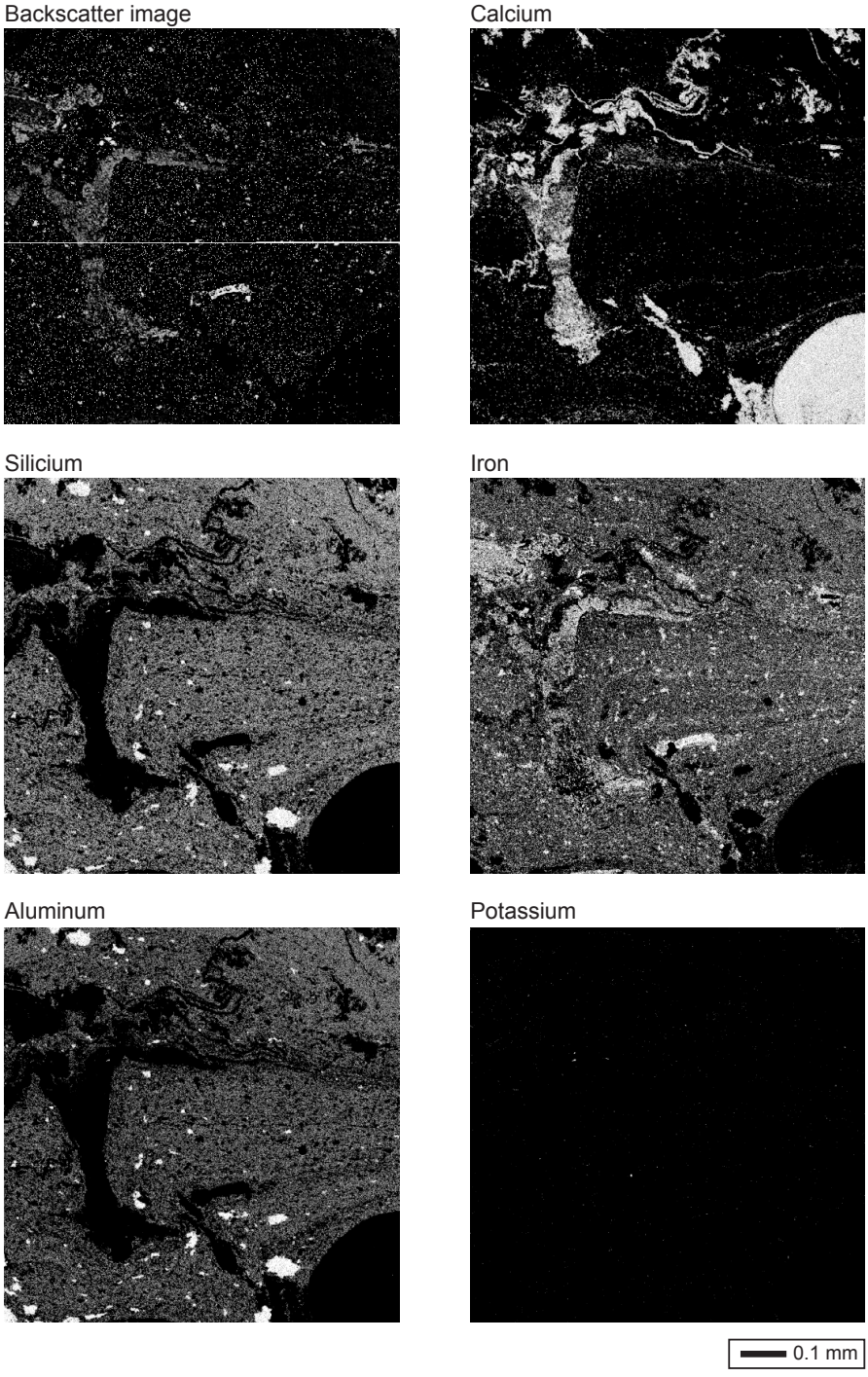

Mircroprobe image

Auenstein
Contact Schellenbrücke - Birmensdorf
Thin-laminated microbial mat

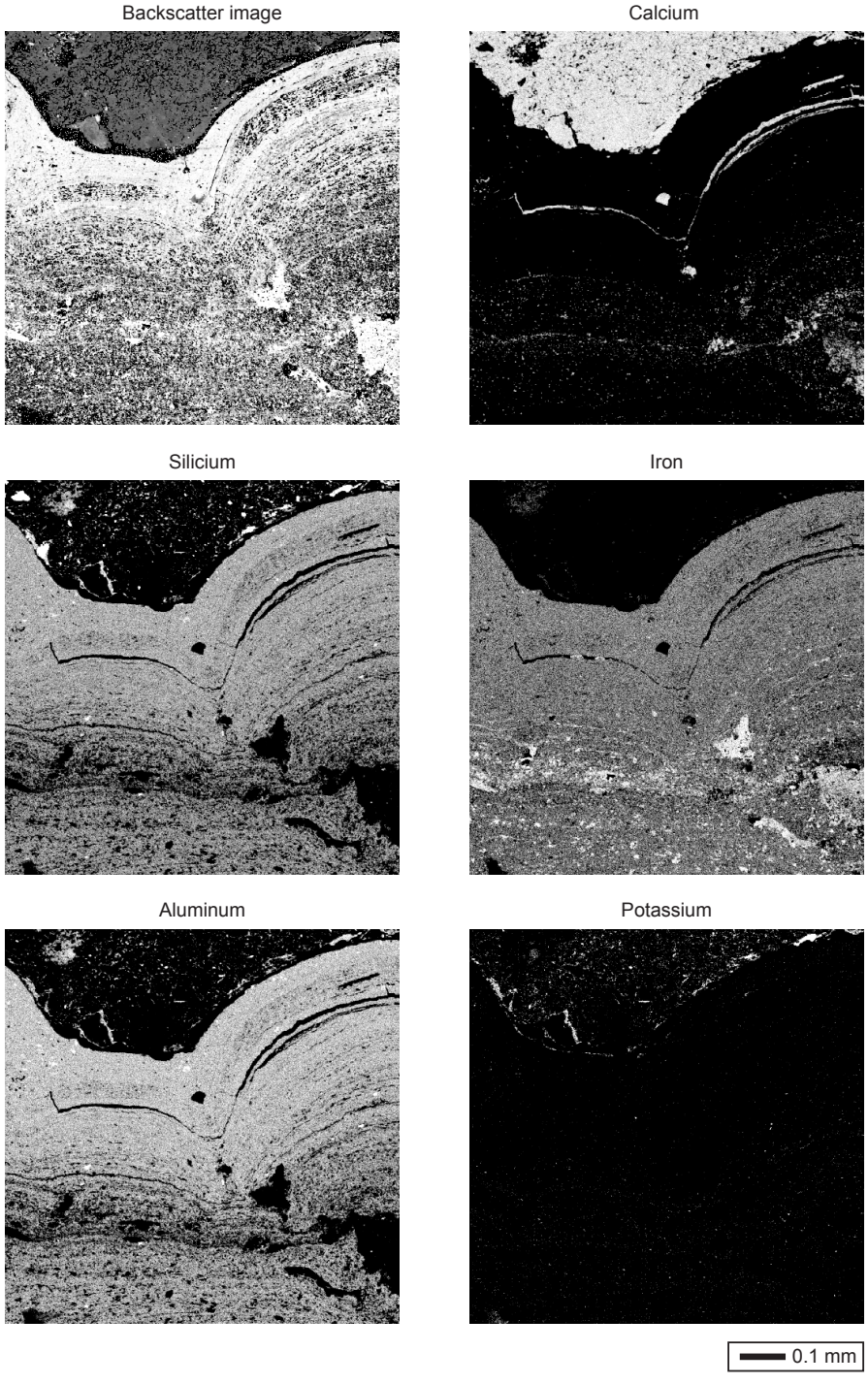

Mircroprobe image

Auenstein
Schellenbrücke Bed
Iron-ooid with a limestone core

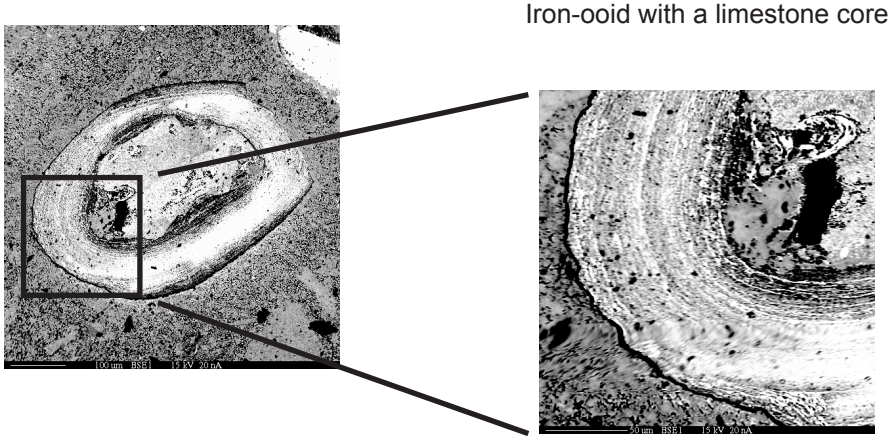

Calcium

Silicon

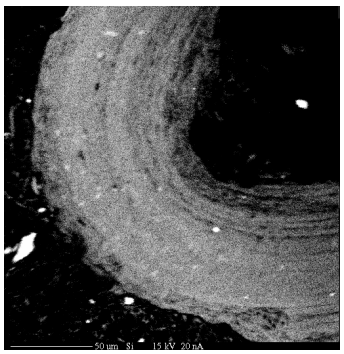

Aluminum

Iron

Potassium

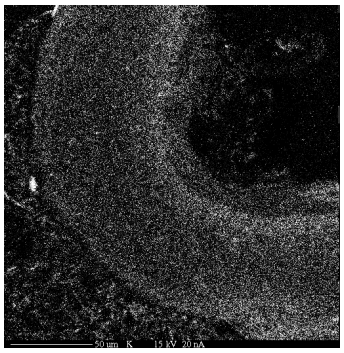

Magnesium

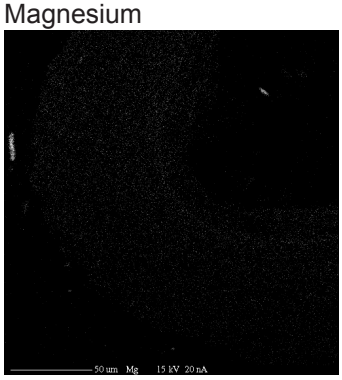

Sulfur

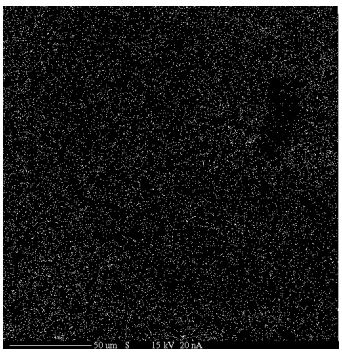

Sodium

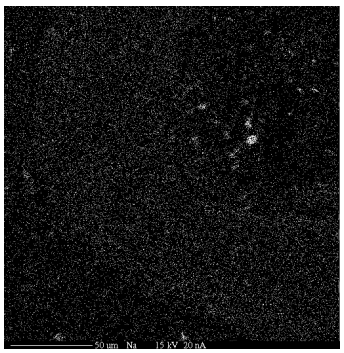

Manganese

Aknowledgements

I would like to thank all the people who supported me, shared their knowledge, helped me during this four years with ups and downs of my PhD.

First, I want to thank Helmi and Stefano, the two initiators of the Oxfordian project.

Helmi, you have been a motivating supervisor, amazingly available for “short questions” that always deserved very long answers. You always encouraged me to improve my scientific knowledge by going to summer schools and conferences. I also really appreciate scientific and non-scientific discussions we had in Zurich and during field trips.

Thank you Stefano for the motivation and inputs you gave me. Your “turbo corrections” and other reviews of my manuscripts helped to express things more clearly and your scientific and technical competences improved my thesis significantly. I will always remember your answer to “why is your French so fluent”: “well there was a guy, who came for one week in the lab and he was only speaking French, so... I had to practice.”

Beat, to answer you, yes, we are very different persons, and it was a pleasure for me to learn to know you. And from a scientific point of view... what a team! More efficient in the field than any other geologists! I also want to thank you for being patient enough to speak German with me.

Thank you Peter and Judy for interesting scientific discussions and for immediately agreeing on being my co-referees.

For technical assistance in the lab, my special thanks goes to Stefan Burla, Eric Reusser, Ellen Martin and Felix Oberli.

I also want to thank Andrea Cozzi, Wilfried Winkler, Flavio Anselmetti, Crisogono Vasconcelos, Thomas Pettke, Peter Hochuli, Karl Föllmi and Thierry Adatte for having shared constructive scientific discussions.

But of course, I also had fantastic life besides working hours during these four years and for that I would like to thank Léo, Erwan, Chris, Sam, Paola, Adélie, Marion, Estelle, Eliane, Fedi,

Manu, Monica, Tomaso, Thomas, Michi, Andy, the Vallejo family, Nele, France, Bouilhol, Seb, Jörgi, Marcus, Ansgar, Andrew, Christian, Zarina, Alex, Lena, Darrell, Maarten, Morten, Luca, Claudio, Weronika, Manuele, Giulio, Sonia, Miriam, Ashgar, Nick, Stephanie, Jessica, Anne, Marina, Benoît, Oli, Alice, all the Friday Beer crew, all the Adelboden crew.

Mais aussi: Gisou & Fan: vraiment merci pour tout ! Co, Phiston, Soph, Anne, Béné, Chris, Lala, Mich, Alex, Lei, Cristina, les routards s.l., les Fringeli.

Finally, I want to thank you Gérald, you are definitely the one that supports me (both French and English meaning) during the “downs”. I also want to thank you for the wonderful time we shared during these four years in Züri’.

Curriculum Vitae

Pauline Rais

Date of birth:	March 25, 1977
Place of birth:	Delémont, Switzerland
Place of origin:	Delémont
Nationality:	Swiss

Education:

2002-2006	Doctoral student and research assistant at the Geological Institute ETH Zurich, Switzerland. Ph.D. thesis: "Evidence for a major paleoceanographic reorganization during the Late Jurassic; Insights from sedimentology and geochemistry" Supervisors: Helmut Weissert and Stefano Bernasconi
2001-2002	Archeological technician and geologist in the "Section d'Archéologie et Paléontologie du Canton du Jura", Porrentruy
1996-2001	Diploma student at the Geological Institute University of Neuchâtel, Switzerland
1995-1996	Lycée Cantonal du Jura, Porrentruy
1992-1995	Ecole Supérieure de Commerce, Delémont
1987-1992	Ecole Secondaire, Collège Delémont
1983-1987	Ecole Primaire, Delémont